DOCTOR OF PHILOSOPHY

Quantum dot based semiconductor disk lasers

Butkus, Mantas

Award date:
2012

DOCTOR OF PHILOSOPHY

Quantum dot based semiconductor disk lasers

Mantas Butkus

2012

University of Dundee

UNIVERSITY OF DUNDEE

QUANTUM DOT BASED SEMICONDUCTOR DISK LASERS

By Mantas Butkus

A thesis submitted for the degree of

Doctor of Philosophy

In the

School of Engineering, Physics and Mathematics

April 2012

Table of contents

Table of contents 2

List of figures 6

List of tables 14

Acknowledgments 15

Declaration of Authorship 17

Abstract 18

List of publications 21

1. Introduction to quantum dot based semiconductor disk lasers 25

1.1. Development of semiconductor disk lasers 25

1.2. State of the art semiconductor disk lasers 30

1.2.1. High power semiconductor disk lasers and wavelength coverage 30

1.2.2. Tuneable semiconductor disk lasers 33

1.2.3. Mode-locked SDLs 35

1.2.4. Commercially available semiconductor disk lasers 37

1.3. Applications of semiconductor disk lasers 38

1.4. Operational principles of Semiconductor Disk Lasers 42

1.4.1. Semiconductor gain region 43

1.4.2. Distributed Bragg reflector 48

1.4.3. External cavity 51

1.5. Power scaling and thermal management in semiconductor disk lasers 55

1.6. Semiconductor quantum dots as the active medium 61

1.6.1. Quantum dots as an alternative to quantum well active region 61

1.6.2. The fabrication of Quantum Dots 65

1.6.3. Optical properties of quantum dots 69

1.7. Chapter conclusions 73

References 73

2. Design, fabrication and luminescence characterization of the SDL samples 95

2.1. Design of the semiconductor disk lasers 95

2.2. Growth of the SDL semiconductor part 101

2.2.1. Sample DO1845 growth (1040 nm) 101

2.2.2. Sample DO2251 growth (1180 nm) 102

2.2.3 Sample DO2254 growth (1260 nm) 103

2.3. Wafer inspection and characterisation 104

2.4. Chapter conclusions 115

References 116

3. Results in continuous wave regime 118

3.1. Sample preparation 118

3.2. Experimental setup 121

3.2. SDLs emitting at 1040 nm 122

3.3. SDLs at 1180 nm 127

3.4. SDLs at 1260 nm 130

3.5. Comparison between ground and excited states lasing 133

3.6. Second harmonic generation in quantum dot based semiconductor disk lasers. 135

3.6.1. Applications of frequency doubled semiconductor disk lasers 136

3.6.2. Intracavity second harmonic generation in semiconductor disk lasers..... 139

3.6.3. Experimental setups for SHG in QD SDLs 143

3.6.4. Second harmonic generation results 147

3.7. Wavelength tuneability..... 150

3.7.1. Wavelength tuning in semiconductor disk lasers 151

3.7.2. Wavelength tuning results in QD SDLs 153

3.8. Chapter conclusions 158

References 159

4. Quantum dot use in mode – locked semiconductor disk lasers 167

4.1. Principles of mode-locking semiconductor disk lasers 168

4.2. Properties of SESAMs..... 174

4.3. Design of the SESAMs..... 178

4.4. QD based SESAMs 181

4.5. Mode-locking results..... 184

4.6. Chapter conclusions 190

References 191

5. Electrically pumped VECSELs 198

5.1. Development of electrically pumped VECSELs 198

5.2. EP-VECSEL samples 203

5.3. Experimental testing of EP-VECSEL samples 204

5.3.1. Testing in CW regime 204

5.3.2. Mode-locking experiments 207

5.4. Chapter conclusions 210

References 212

6. Conclusions and future work 215

References 217

List of figures

1. Fig. 1.1. A radiative mirror concept as in [15]. 28
2. Fig. 1.2. Output powers and wavelength coverage by QW SDLs to date. Semiconductor compositions used for different spectral regions are also shown below 32
3. Fig. 1.3. QD SDLs with their output powers at different wavelengths demonstrated to date. Solid symbols show direct emission while open symbols demonstrate SHG. Circled data is presented in this work. 33
4. Fig. 1.4. Output power for different types of ultrafast lasers operating at GHz repetition rates [65]. 36
5. Fig. 1.5. Semiconductor disk laser family for visible spectral region offered by Coherent Inc. Picture from www.coherent.com. 38
6. Fig. 1.6. Extinction coefficient for water, melanin and HbO_2 at different wavelengths. 40
7. Fig. 1.7. Schematic drawing of the semiconductor disk laser with its main components in a straight cavity configuration. 43
8. Fig. 1.8. Schematic drawing of potential energy bands in typical SDL semiconductor gain mirror. Prepared using [18]. 45
9. Fig. 1.9. Standing electric field pattern for a) antiresonant and b) resonant cases of subcavity formed Fabry-Perot etalon. c and d show calculated Fabry-Perot etalon transmission, reflectivity of the structure and QD photoluminescence spectra of the same structures shown in a and b. 47
10. Fig. 1.10. a. Simulated spectra of DBR for different materials compsitions; b. DBR reflectivities at different N values. 50

11. Fig. 1.11.Various SDL cavity configurations. a - straight cavity configuration, b, c - V-shape cavity, d - Z-shape cavity, e - W-shape cavity with two gain chips, f - SDL with three gain chips. Here OPS - optically pumped semiconductor [37]..... 52
12. Fig. 1.12. Mode diameters in straight cavity laser configuration. An arrow indicates the operating point of SDL in our experiment. 54
13. Fig. 1.13. Schematic drawing of heat flow in SDL and different thermal management techniques: (a) unprocessed sample, (b) substrate removal, (c) intracavity heat spreader. The thicknesses of layers are not to scale. 57
14. Fig. 1.14. Maximum temperature rise in the active region of SDL using different thermal management techniques for different pump powers. Solid diamonds: thin-device soldered to a copper mount. Open circles: thin-device soldered to diamond and copper. Closed triangles: diamond heat spreader in a copper mount. Open squares: thin-device directly cooled at the bottom of the DBR [101]..... 60
15. Fig. 1.15. Density of states functions for semiconductor structures with different carriers' confinement configurations. Bulk - 3D, quantum well - 2D, quantum wire - 1D, quantum dot - 0D[109]. 63
16. Fig. 1.16. The reduction of threshold current density in laser diodes during the years using different semiconductor structures [112]..... 64
17. Fig. 1.17. A theoretical simulation of threshold current dependence on the temperature for different carrier confinement configurations [112]. 65
18. Fig. 1.18. (a) A TEM image of a single sheet of InAs quantum dots grown on GaAs. (b) A TEM image of a cross-section of a 25 layer thick stack of InGaAs quantum dots (thicker dark regions) grown on GaAs substrate (lighter area in the bottom of

the picture and surrounding the InGaAs layers). The QDs are connected within the layers by the wetting layers (thin dark regions). 68

19. Fig. 1.19. Schematic drawing of (a) Stranski-Krastanow and (b) Sub-monolayer grown quantum dots. 69
20. Fig. 1.20. Optical gain dependence on the pump current density in a QD based laser diode. Contributions from both ground and excited states are shown [108]. 71
21. Fig. 1.21. Density of states function in an (a) ideal and (b) real QDs. Density of states for self-assembled QD system is shown in (c) [108]. 72
22. Fig. 2.22. The design for 1040, 1180 and 1260 nm QD SDLs used in the research. Black line shows the profile of the potential energy in semiconductor structure. Red line represents the intensity pattern of the optical standing wave..... 100
23. Fig. 2.23. A cross section SEM image of DO1845 sample..... 102
24. Fig. 2.24. TencorSurfScan 4500 surface inspection system for evaluating the defect density in the surface of grown SDL wafers. 104
25. Fig. 2.25. A set of reflectivity spectra for different samples measured after the growth. Top photoluminescence spectra are also shown in red dashed lines. The arrows indicate operation points of different SDL samples. 106
26. Fig. 2.26. Examples of photoluminescence maps of DO2917 and DO2919 1180 nm samples. 107
27. Fig. 2.27. Experimental setup for edge and top photoluminescence measurements 109
28. Fig. 2.28. Calculated reflectivity spectra and measured normalized edge photoluminescence spectra of samples emitting at 1040, 1180 and 1260 nm. 110

29. Fig. 2.29. (a), (b) top and (c), (d) edge photoluminescence measurements from 1040 nm SDL sample. (a) and (c) show measurements at constant temperature while (d) and (d) show measurements at constant pump power..... 112
30. Fig. 2.30. Top and edge photolominescence measurements from DO2251, a 1040 nm SDL sample..... 114
31. Fig. 2.31. Top and edge photolominescence measurements from DO2254, a 1260 nm SDL sample..... 114
32. Fig. 2.32. Top and edge photolominescence measurements from DO2100, a 1260 nm SDL sample..... 115
33. Fig. 3.33. A synthetic diamond window for intracavity heat spreader use..... 119
34. Fig. 3.34. A cross section view of the diamond bonded to the SDL sample and mounted in a copper holder..... 120
35. Fig. 3.35. A photo of a SDL sample bonded to the diamond heat spreader and mounted to a copper heatsink..... 120
36. Fig.3.36. (a) straight and (b) V-shape cavity configurations for CW SDL operation. 122
37. Fig. 3.37. Pump - output power characteristics of the unprocessed DO1845 SDL sample. 123
38. Fig. 3.38. Pump - output power results for 1040 nm QD SDL sample at different heatsink temperatures. Inset shows measured beam profile at the focal spot..... 125
39. Fig. 3.39. Optical spectrum of the 1040 nm QD SDL sample..... 125
40. Fig. 3.40. Spatial beam profiles from SDLs without and with intracavity diamond heat spreader..... 127

41. Fig. 3.41. Pump - output power characteristics for DO2251 1180 nm SDL sample at different heatsink temperatures. 128
42. Fig. 3.42. Optical spectrum from DO2251 1180 nm sample. 128
43. Fig. 3.43. Pump - output power characteristics of DO2100 1260 nm sample. 131
44. Fig. 3.44. Pump - output power characteristics for DO2254 sample. 132
45. Fig. 3.45. Optical output spectrum of DO2254 sample at the highest output power. 132
46. Fig. 3.46. Output power characteristics from QD SDLs operating at GS and ES transitions. The inset shows a schematic picture of GS and ES energy levels in QD. 134
47. Fig. 3.47. Refractive indices for ordinary and extraordinary beams in uniaxial crystal [46]. 142
48. Fig. 3.48. A typical cavity configuration for intracavity second harmonic generation in QD SDLs.– 144
49. Fig. 3.49. Top view of frequency doubled green emitting QD based SDL. 145
50. Fig. 3.50. Frequency doubled red emitting QD based SDL. 145
51. Fig. 3.51. W-shape dual gain chip cavity configuration for SHG in 1180 nm QD SDL. 146
52. Fig. 3.52. Output spectra at different tuning points of second harmonic light from 1040 nm QD SDL. 149
53. Fig. 3.53. (a) Pump - output power characteristics of frequency doubled QD SDLs tested in our experiments. (b) Normalized optical spectra of fundamental and second harmonic light from tested devices. 150

54. Fig. 3.54. A schematic picture of spectral tuning principle in semicondcutor disk lasers by using an intracavity filter [65]. 153
55. Fig. 3.55. A Schematic drawing of V-shape cavity configuration for wavelength tuneable QD SDL 154
56. Fig. 3.56. Wavelength tuning curves of 1040 nm QD SDL sample using different output couplers 155
57. Fig. 3.57. Pump - output power characteristics of 1040 nm QD SDL with and without birefringent filter in the cavity. 155
58. Fig. 3.58. Wavelength tuning characteristics and output spectra of three different wavelength QD SDLs 157
59. Fig. 4.59. Pulse formation by interference of different number of phase locked modes in the laser cavity [2]. 169
60. Fig. 4.60. A schematic drawing of mode-locked mechanism in laser with saturable absorber. 170
61. Fig. 4.61. Pulse formation mechanisms using fast and slow saturable absorbers [11]. 172
62. Fig. 4.62. Typical nonlinear reflectivity curve of SESAM and its parameters [15]. 175
63. Fig. 4.63. Pump – probe measurement techniques for QD based saturable absorber [19]. 177
64. Fig. 4.64. Two sample structures of (a) antiresonant and (b) resonant type SESAMs [11]. 179
65. Fig. 4.65. Calculated group delay dispersion curves for resonant and antiresonant SESAMs. 181

66. Fig. 4.66. Quantum dots density dependence on the growth rate with fixed substrate temperature [19]. 182
67. Fig. 4.67. Bandgap profile of the QW SDL semiconductor part. 185
68. Fig. 4.68. A schematic structure of QD SESAM used in the experiments is shown in (a) part and reflectivity and luminescence spectra are shown in (b). 186
69. Fig. 4.69. Nonlinear reflectivity measurement of the SESAM used in the experiments [45]..... 186
70. Fig. 4.70. A scheme of the mode-locked SDL Z-shape cavity. 187
71. Fig. 4.71. Optical spectrum of the mode-locked SDL. RF spectrum trace is shown in the inset. 188
72. Fig. 4.72. Autocorrelation trace of the mode-locked laser pulses..... 188
73. Fig. 4.73. Calculated group delay dispersion values in the mode-locked SDL cavity. 189
74. Fig. 4.74. Dependence of pulse duration (symbol) and magnitude of GDD versus SESAM temperature 190
75. Fig. 5.75. A schematic cross section view of EP-VECSEL. 201
76. Fig.5.76. Near field elctroluminescence profile measurements of EP-VECSEL with different bottom contact diameters[11]. 202
77. Fig. 5.77. Schematic drawing of EP-VECSEL sample (top view). 204
78. Fig. 5.78. Current-light characteristics at different temperatures in cw for the 95_44 device from Philips. 206
79. Fig. 5.79. Current-light characteristics at different temperatures in cw for the 53_14 device from Philips. 206
80. Fig. 5.80. Optical spectrum of the 95_44 EP-VECSEL sample. 206

81. Fig. 5.81. Current-light characteristic in the CW regime from the device manufactured in Sheffield. 207

82. Fig. 5.82. Optical spectra of EP-VECSELs at different heatsink temperatures..... 207

83. Fig. 5.83. A schematic drawing of a cavity to mode-lock EP-VECSEL from Philips. 208

84. Fig. 5.84. Single line RF spectrum of the mode-locked device is shown in (a), and (b) shows the same spectrum with a few harmonics. 208

85. Fig. 5.85. Trace of the pulsed output from a mode-locked EP-VECSEL sample 94_44 showing pulse duration of 270 ps..... 209

86. Fig. 5.86. A schematic drawing of the Z-shape cavity configuration for a mode-locked EP-VECSEL. 209

87. Fig. 5.87. RF spectrum indicating pulsed operation of the device. The optical spectrum is shown in the inset. 210

List of tables

88. Table 1.1. Some of to date SDLs with widest wavelength tuning ranges at different spectral regions. QD SDLs presented in this thesis are shown in bold. 34

89. Table 1.2. Mode-locked SDLs' performance with incorporated quantum dots in gain, SESAM or both regions. 37

90. Table 1.3. Thermal conductivity values for different elements of an SDL chip and potential heat spreaders. 59

91. Table 2.4. Details of SDLs subcavities designed for the work presented in this thesis. Underlined numbers represent samples which provided best results in CW experiments. 98

92. Table 2.5. Surface defect density values for some of the samples 105

93. Table 3.6. The summary of presented QD SDL performance results in CW regime. All SDLs were tested using diamond heat spreaders unless otherwise stated. 135

94. Table 3.7. Summary of experimental setups used for SHG in QD SDLs 147

95. Table 4.8. Various expressions for laser pulse parameters. 170

96. Table 5.9. The list of best performing EP-VECSELs. 205

Acknowledgments

During the years of my studies towards the PhD degree, there were a number of people without whom all this work would not have been done. First and foremost I must thank my supervisor Prof. Edik U. Rafailov for providing me an opportunity to work in his group and guiding me during the years of my studies. He always was supportive with encouragement, new ideas, work and self-development opportunities. I also would like to thank all other current and former members of our Nanophotonics and Optoelectronics group, especially Dr. KseniaFedorovna, Dr. DaniilNikitichev, Dr. Maria Ana Cataluna and Dr. Svetlana Zolotovskaja for a nice atmosphere, their help and thoughtful discussions. I thank Ross Leyman and Dr. Rolf Birch for their help with preparation of this thesis.

Special thanks go to Dr. Keith Wilcox from Southampton University and Dr. Craig Hamilton from Solus Technologies Ltd. for teaching me the basics of semiconductor disk lasers and experimental skills required for my research. I also really appreciate the advices and suggestions these people gave to me. I thank JussiRautiainen and Prof. Oleg Okhotnikov from Tampere University of technology, Finland for thoughtful discussions and collaborative work.

I also would like to thank all administrative and technical staff at the Department of Electronic Engineering, Physics and Renewable Energy for all their help.

I also heartily thank all my relatives and friends and most of all – to my beloved wife Milda and our little daughter Fausta. They were really supportive and encouraging during all the time of my studies. Thank You!

The research leading to the results presented in this thesis has received funding from the European Community's Seventh Framework Programme (FAST-DOT) under grant agreement No: 224338.

Declaration of Authorship

I, Mantas Butkus, declare that the thesis entitled

QUANTUM DOT BASED SEMICONDUCTOR DISK LASERS

and the work presented in it are my own. I confirm that:

- this work was done wholly while in candidature for a research degree at this University;
- where any part of this thesis has previously been submitted for a degree or any other qualification at this University or any other institution, this has been clearly stated;
- where I have consulted the published work of others, this is always clearly attributed;
- where I have quoted from the work of others, the source is always given. With the exception of such quotations, this thesis is entirely my own work;
- I have acknowledged all main sources of help;
- where the thesis is based on work done by myself jointly with others, I have made clear exactly what was done by others and what I have contributed myself;
- parts of this work have been published (Please, see List of Publications).

Mantas Butkus

April 2012

Abstract

Since its first successful demonstration more than five decades ago [1], laser technology experienced a huge leap forward in terms of technological innovations and the understanding of underlying physical principles of operation. There were many efforts made by those in both the scientific and commercial communities who envisioned the potential of lasers. As a result, the laser now is a powerful scientific tool in many disciplines. It is widely used not only in physics, but also in chemistry, biology, medicine, engineering, environmental sciences, arts and their interdisciplinary fields. Moreover, it now has a vast number of applications in industry and everyday life whether it is light and matter interaction, communication and IT, healthcare and many other uses of this light source. By the same time, photonics comprises a market of multi-billion EUR value [2].

At every stage of development, different laser parameters were engineered to suit those to specific application with some other parameters usually being sacrificed. Together with this, things like compactness and cost were always an issue to consider. A huge impact to the field of photonics was made by the development of semiconductor based structures that could be used as a light amplifying medium. Semiconductor lasers not only allowed the miniaturization of many devices, but also provided new opportunities for laser scientists due to ability to engineer their bandgap properties and to confine the carriers in different dimensions.

The development of vertical external cavity surface emitting lasers (VECSELs), which are also known as optically pumped semiconductor lasers (OPSLs) or semiconductor disk lasers (SDLs) realized an important feature in semiconductor based lasers – high multi-Watt output power was combined with diffraction limited output beam profile.

This work is devoted to the development of semiconductor disk lasers based on novel quantum dot (QD) structures. QD structures were embedded in this type of laser recently and allowed a number of advantages compared with the widely used quantum well (QW) structure. These included new spectral region coverage at 1-1.3 µm, enhanced wavelength tuneability and ultrafast carrier dynamics, which potentially will improve mode locked operation. QDs were also used as a base for semiconductor saturable absorbers in mode-locking experiments.

During the time of these studies, QD SDLs at new spectral regions and record output power were demonstrated. Power scaling up to 6 W was achieved for 1040 nm, 2.25 W for 1180 nm and 1.6 W for 1260 nm devices. Excited state transition in QDs was shown to be more efficient for high power QD SDLs as compared with ground state transition. New spectral regions were covered by QD SDLs using frequency doubling into the visible region with green, orange and red light emission with output powers of 2 W, 2.5 W and 0.34 W respectively. The broad gain bandwidth of the quantum dot material was explored and wavelength tuneability up to 60 nm around 1040 nm, 69 nm around 1180 nm, and 25 nm around 1260 nm was demonstrated.

A QD based saturable absorber was used to mode-lock the quantum well SDL, resulting in the first such type of laser with sub-picosecond pulse widths. Pulses with duration of 870 fs at a repetition rate of 896 MHz and wavelength of 1028.5 nm were demonstrated. Pulses were 1.14 times Fourier limited and an average output power of 46 mW was achieved.

Finally, quantum well based VECSELs with electrical pumping schemes were tested. The devices were first tested in the cw configuration. Highest output powers up to 60 mW were achieved from such devices. Devices were then tested in mode-locking experiments. Pulsed

operation was observed and the measurements indicated 270 ps width pulses with 8 mW average output power at 1.9 GHz repetition rate. All devices operated at 980 nm.

This thesis consists of six chapters. In the introductory part of this work, QD based SDLs and their development and applications will be reviewed together with their operational principles. Chapter two will describe the growth, fabrication and preparation of SDL samples. Continuous wave and mode-locked operation results will be presented in chapters three and four. Electrically pumped devices will be presented in chapter five along with experimental results. Conclusions and future prospects will be given at the end of this work. The list of publications which were generated during the studies is included at the beginning of this work.

The work presented in thesis was done under the FAST-DOT project. This is a European FP 7 project targeted at the development of compact and low-cost novel quantum dot based laser sources for biophotonic applications.

List of publications

Publications in peer-reviewed journals:

1. A. Rantamäki, J. Rautiainen, L. Toikkanen, I. Krestnikov, M. Butkus, E. Rafailov, and O. Okhotnikov, “Flip Chip Quantum Dot Semiconductor disk laser at 1200 nm”, *IEEE Photonics Technology Letters*, vol. 24, pp. 12982-1294, 2012.

2. Svetlana A. Zolotovskaya, Mantas Butkus, Reto Häring, Andreas Able, Wilhelm Kaender, Igor L. Krestnikov, Daniil A. Livshits and Edik U. Rafailov, “*p-i-n* junction quantum dot saturable absorber mirror: electrical control of ultrafast dynamics”, *Optics Express*, Vol. 20, pp. 9038-9045, 2012.

3. M. Butkus, J. Rautiainen, O. G. Okhotnikov, C. J. Hamilton, G. P. A. Malcolm, S. S. Mikhrin, I. L. Krestnikov, D. A. Livshits, E. U. Rafailov, “Quantum Dot based semiconductor disk lasers for 1-1.3μm”, *IEEE Journal of Selected Topics in Quantum Electronics*, vol. 17, pp. 1763-1771, 2011.

4. M. Butkus, G. Robertson, G. Maker, G. P. A. Malcolm, C. J. Hamilton, A. B. Krysa, B. J. Stevens, R. A. Hogg, Y. Qiu, T. Walther, E. U. Rafailov, “High repetition rate Ti:Sapphire laser mode-locked by InP quantum-dot saturable absorber”, *IEEE Photonic Technology Letters*., vol. 23, pp. 1603-1605, 2011.

5. M. Butkus, C. J. Hamilton, J. Rautiainen, O. G. Okhotnikov, S.S. Mikhrin, I.L. Krestnikov, E. U. Rafailov, “Broadly Tunable 1250 nm Quantum Dot Based Semiconductor Disk Laser”, *IET Optoelectronics*, vol. 5, pp. 165-167, 2011.

6. J. Rautiainen, I. Krestnikov, M. Butkus, E. U. Rafailov, O. G. Okhotnikov, “Optically pumped semiconductor quantum dot disk laser operating at 1180 nm,” *Optics Letters*, vol. 35, pp. 694-696, 2010.

7. M. Butkus, K. G. Wilcox, J. Rautiainen, O. G. Okhotnikov, S. S. Mikhrin, I. L. Krestnikov, A. R. Kovsh, M. Hoffmann, T. Sudmeyer, U. Keller, and E. U. Rafailov, "High-power quantum-dot-based semiconductor disk laser," *Optics Letters*, vol. 34, pp. 1672-1674, 2009.

8. K. G. Wilcox, M. Butkus, I. Farrer, D. A. Ritchie, A. Tropper, and E. U. Rafailov, "Subpicosecond quantum dot saturable absorber mode-locked semiconductor disk laser," *Applied Physics Letters*, vol. 94, 251105, 2009.

Publication in peer-reviewed conferences:

1. J. Rautiainen, M. Butkus, I. Krestnikov, E. U. Rafailov, O. G. Okhotnikov, “High power quantum dot semiconductor disk lasers” (invited), SPIE Photonics West, San-Francisco, US, 2012.

2. J. R. Orchard, D. T. Childs, L. C. Lin, B. J. Stevens, D. M. Williams, R. A. Hogg, M. Butkus, E. U. Rafailov, S. Gronenborn, J. Kolb, H. Moench, M. Miller, M. Hoffmann, Y. Barbarin, W. P. Pallmann, D. H. Maas, P. Kreuter, B. Witzigmann, M. C. Golling, T. Sudmeyer, U. Keller “Development of EP-VECSELs for mode locking applications” (invited), SPIE Photonics West, San Francisco, US, 8242-11, 2012.

3. E. U. Rafailov, S.A. Zolotovskaya, M. Butkus, “QD-based saturable absorbers for utrafast lasers” (invited), SPIE Photonics West, San-Francisco, US, 7919-29, 2011.

4. M. Butkus, C. J. Hamilton, G. P. Malcolm, I. Krestnikov, D. Livshits, and E. U. Rafailov, "Wavelength tuning in quantum dot semiconductor disc lasers," IEEE International Semiconductor Laser Conference, Kyoto, Japan, 2010.

5. M. Butkus, J. Rautiainen, O. G. Okhotnikov, S. S. Mikhrin, I. L. Krestnikov, and E. U. Rafailov, "1270 nm quantum dot based semiconductor disk lasers " IEEE International Semiconductor Lasers Conference, Kyoto, Japan, 2010.

6. J. Rautiainen, M. Butkus, I. Krestnikov, E.U.Rafailov, O. G. Okhotnikov, “1170 nm optically-pumped quantum dot disk laser”, IEEE International Semiconductor Lasers Conference, Kyoto, Japan, 2010

7. M. Butkus, C. J. Hamilton, D. Jackson, G. P. A. Malcolm, I. Krestnikov, D. Livshits, and E. U. Rafailov, "Green second harmonic generation in quantum dot semiconductor disc lasers”, 14th International Conference "Laser Optics 2010", St. Petersburgh, Russia, 2010.

8. C. J. Hamilton, G. Robertson, D. Jackson, G. P. A. Malcolm, R. A. Hogg, Y. Qiu, T. Walther, B. J. Stevens, P. A. Houston, A.B. Krysa, M. Butkus, E. U. Rafailov, “Quantum dot SESAM for mode-locking operation of a Ti:Sapphire laser at 2 Ghz”, 14th International Conference "Laser Optics 2010", St.Petersburg, Russia, 2010.

9. M. Butkus, C. J. Hamilton, G. PA Malcolm, I. Krestnikov, D. Livshits, E. U. Rafailov, “Wavelength tuning in quantum dot semiconductor disc laser”, Laser Optics 2010, St Petersburg, Russia, 2010.

10. M. Butkus, J. Rautiainen, O. G. Okhotnikov, S.S. Mikhrin, I.L. Krestnikov, E. U. Rafailov, “Quantum dot semiconductor disk laser operating at 1270 nm”, 1st EOS Topical Meeting on Lasers, Capri, Italy, 2010.

11. J. Rautiainen, A. Rantamäki, M. Butkus, S.S. Mikhrin, I. L. Krestnikov, E. U. Rafailov, O. G. Okhotnikov, “1.2 µm quantum dot semiconductor disk laser with 0.5 W of output power”, 1st EOS Topical Meeting on Lasers, Capri, Italy, 2010.

12. M. Butkus, K. G. Wilcox, J. Rautiainen, O. G. Okhotnikov, S. S. Mikhrin, I. L. Krestnikov, A. R. Kovsh, M. Hoffmann, T. Südmeyer, U. Keller, E. U. Rafailov, “High-power quantum dot based semiconductor disk laser”, CLEO Europe, Munich, Germany, 2009.

13. Keith G. Wilcox, Mantas Butkus, Anne Tropper, Ian Farrer, David A. Ritchie, Edik U. Rafailov, “870-fs passively mode-locked quantum dot SESAM semiconductor disk laser”, ASSP, Denver, USA, 2009.

1. Introduction to quantum dot based semiconductor disk lasers

The first chapter of this thesis will review to date achievements in the area of semiconductor disk lasers with particular focus on devices based on quantum dot structures. It includes the main features and development of such laser sources, state of the art results, potential and existing applications and operational principles. Quantum dots as a gain medium and their properties are also discussed.

1.1. Development of semiconductor disk lasers

The first semiconductor lasers were successfully demonstrated in 1962 [3, 4] followed by the development of double heterostructures and room temperature operation in 1970 [5] and were extensively explored and developed since then, regarding materials, design, engineering and applications [6]. Semiconductor laser sources allowed the miniaturization, direct electrical pumping and wavelength versatility in a broad spectral region and enabled a vast amount of technological innovations. However, a high power single spatial mode semiconductor laser source was a challenge.

Semiconductor lasers usually come in two configurations: edge or surface emitters. In the edge emitting configuration, the light is confined in a stripe-shaped waveguide and a light beam is emitted at the edge of it being asymmetric and highly diverging. For a single transverse mode operation, waveguides of a few microns width are usually used. However, this results in a low output power as it is limited by heat dissipation and catastrophic optical damage. Output powers in the single-mode regime up to few hundreds of mW are typically achievable in such laser sources [7]. To increase the output power, wider waveguides must be used to improve the heat dissipation and to reduce the optical intensity at the surface of

material. With waveguide sizes of the order of 100 µm, output powers of tens of watts can be reached, however, the beams are highly multimode [8, 9]. For even higher output powers, stacks of edge emitters are used.

In the surface emitting configuration, the light is emitted through the circular aperture perpendicularly to the surface of the structure. This is a typical configuration for vertical cavity surface emitting lasers (VCSELs). For single transverse mode operation, apertures of the order of 10 µm can be used to produce output power of a few tens of mW [10]. The output power can be scaled to few hundreds of mW or even a few Watts [11] using wider apertures, however the beams become multimode as a uniform carrier injection through all gain region gets problematic. As dense stacks of these surface emitters can be fabricated, the output power can be scaled to hundreds of Watts, but again with multimode output beams [12].

To summarize, edge emitters are capable of producing high output power, however the beam quality and shape are the critical points. In the case of monolithic surface emitters, single transverse mode operation is possible, but with power limitations. Long term technological development has advanced both edge and surface emitting semiconductor lasers, enabling mass production and both types of lasers have found their niche applications. However, these configurations are typically not capable of producing a high multi-Watt output power with single transverse mode beam output.

A few concepts can be summarized which describe the principle of a high power single mode device:

- In order to achieve reasonable power scaling, the size of the emitting surface should be tens to hundreds of microns, which can be done in a surface emitting laser to maintain the circular shape of the outgoing beam.
- The size of the emitting surface being in the range of 100 µm, electrical pumping becomes difficult as a uniform carrier injection across a wide gain region becomes problematic. It requires a thick current spreading layer which provides additional losses and strongly decreases the performance of the device. As an alternative for it, external optical pumping can be used which can provide a uniform excitation over various sizes of gain area.
- To ensure fundamental transverse mode operation, external cavity control by additional optical elements is required. Such control ensures single mode operation as well as mode overlapping for the most efficient operation i.e. it keeps the diameter of the laser mode the same size as the emitting area.

The above defined concepts bring us to the idea of vertical external cavity surface emitting laser (VECSEL). Due to the cavity configuration and optical pumping, VECSELs have similarities with thin disk diode pumped solid state lasers (thin disk DPSSL) [13, 14]. The use of semiconductor based gain material enabled the engineering of desired properties of emission wavelengths and absorption. As VECSELs attracted attention from both semiconductor and solid state lasers communities, they also are known as semiconductor disk lasers (SDLs). This is how they are going to be named in the thesis. Alternatively they are also called optically pumped semiconductor lasers (OP-SL).

The first theoretical assumptions for such external cavity semiconductor lasers were mentioned by Basov et al in 1966 [15]. In their approach, a semiconductor layer with one surface fully reflecting, which they called a radiating mirror, could be irradiated by electron

or light beam and resonator could be formed by adding an external mirror. Fig. 1.1 shows a sketch of a concept presented in their work. However, at that time it was hard to achieve a reasonable output powers due to weakly amplifying media as the quality of the materials did not yet reach sufficient level and no heterostructures were yet fabricated.

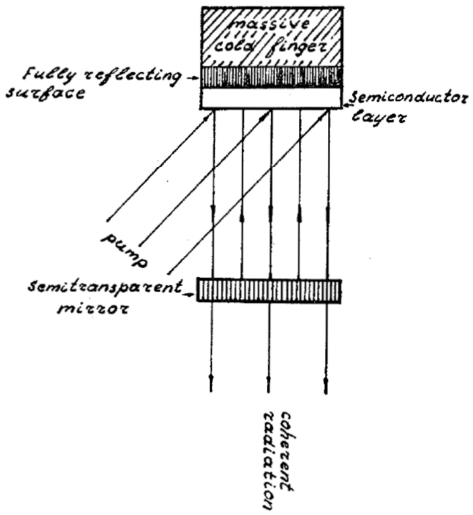

Fig. 1.1. A radiative mirror concept as in [15].

Later there were some reports considering such type of lasers [16]. However, in most cases external optical pumping was considered as a drawback and a cumbersome part of a semiconductor laser. The potential of it was envisioned by Le et al. in 1991 [17]. In their work, a semiconductor mirror was pumped by a Ti:Sapphire laser for a pulsed operation. The practical potential of SDL and its basic design principles were shown and discussed by Kuznetsov et al in 1999 [18]. They reported 0.52 W in CW with fundamental transverse mode output beam. After this, interest in SDLs increased and further improvements and modifications came rapidly.

During their development and recent status, SDLs hold a number of advantages as compared with other semiconductor or other laser types:

- High output power (up to tens of Watts) is achievable with TEM_{00} beam output.
- A number of well-established semiconductor material systems are available for the operation at different wavelengths by direct emission and frequency conversion (UV to >5 μm).
- Diode pump sources are well established and there is no strict restriction for them in terms of wavelength due to a broad absorption band in semiconductors or output beam (can be multi-mode).
- No electrical contacts or p-n junctions are needed in device fabrication which simplifies the fabrication and reduces losses due to free-carrier absorption in doped regions.
- External cavity configurations allows such intracavity techniques as frequency doubling, wavelength tuning, mode-locking, heat removal, multiple gain elements to be exploited.
- High intracavity powers allow efficient intracavity frequency conversion.
- Broad wavelength tuning due to broad gain bandwidth in semiconductors is possible (>100 nm).

For certain applications, the drawbacks of such devices also must be considered:

- An external pump source is required which increases the size, cost and power consumption of the overall device.
- Optical cavity alignment is required and so are robust optomechanical parts for stable device operation.

Due to a thin gain region of typically a few microns, high gain materials are required for SDLs. First SDLs traditionally had gain regions which were exclusively based on QWs. To

achieve QD based gain regions in SDL, a development of high areal density and densely stacked layers of QDs was necessary. One of the first reports of a realized QD based SDL was published in 2005 [19]. The authors demonstrated output powers up to 120 mW with emission near 1300 nm. Later, more powerful QD SDLs based on InAs/GaAs sub monolayer (SML) and InGaAs Stranski-Krastanow (S-K) grown QDs gain material were reported in 2008. Output powers of 1.4 W at 1040 nm and 0.5 W at 950 nm for SML samples and 300 mW at 1040 nm and 1210 nm for S-K samples were reported [20, 21]. As it can be seen, the area of QD SDLs is relatively new and unexplored. A deeper understanding of these devices is required to be able to explore unique properties of QDs in SDL configuration.

1.2. State of the art semiconductor disk lasers

Since the first demonstration of a practical SDL device [18], this type of laser undergone a wide range of development and improvements, both in engineering solutions and in output parameters. As mentioned before, external cavity configuration allows a number of different intracavity techniques to be exploited allowing a wider use of SDLs. Thus, in this part, some of the state of the art QW and QD based SDLs will be reviewed in terms of CW output power, wavelength coverage, tuneability and mode-locking. Also, some products available on the market and based on SDL technology will be overviewed.

1.2.1. High power semiconductor disk lasers and wavelength coverage

Power scalability is one of the major advantages in SDLs. The output power can be scaled by increasing the size of the area where pump spot and laser cavity mode overlaps. Thus,

using a powerful enough pump source, the output power can basically be scaled by adjusting the pump and cavity optics until heat dissipation becomes the limiting factor. Practically, SDLs are operated with a wide range of pump spots diameters, namely 30 – 900 µm. The power can also be scaled by using multiple gain elements in the cavity. To date, QW SDLs with output power of 55 W with M^2~1.3 and with more than 60 W in multimode CW regime were demonstrated from frequency doubled (532 nm) three-gain chip SDLs with 900 µm pump spot diameters [22]. More than 20 W output power from a single gain chip was achieved at 960 nm with M^2~1.1 [23]. Also, 20 W of second harmonic light in TEM_{00} mode and further scaling of output power were reported recently [24, 25]. Performance demonstrated by QW SDLs at wavelengths close to those discussed in this thesis are: 8 W at 1050 nm [26], 35 W at 1060 nm [22], 11 W at 1180 nm [27], and 1.46 W at 1240 nm [28].

SDL technology was also proven to be superior for intracavity frequency doubling and allowed the coverage of shorter wavelengths in the visible spectral region from the UV by using forth harmonic generation [29] to red by frequency doubling a 1234 nm GalnNAs/GaAs SDL [30]. Additionally, there were a number of directly emitting SDLs reported in the red spectral region by using AlInGaP materials composition [31] as well as InP/AlGaInP quantum dots [32].

In the near-infrared spectral region, a number of SDLs were also reported using phosphite, nitride or antimonide based semiconductor compositions [33-35]. Emission wavelengths from SDLs based on PbTe were demonstrated up to 5.6 µm [36].

A graphical overview of SDL wavelength coverage to date and output power scaling is shown in Fig. 1.2. Symbols represent direct emission in single and multi-transverse modes

as well as frequency doubled and quadrupled SDL devices. More information about these results and all references to them which are not yet presented in the text can be found at [37].

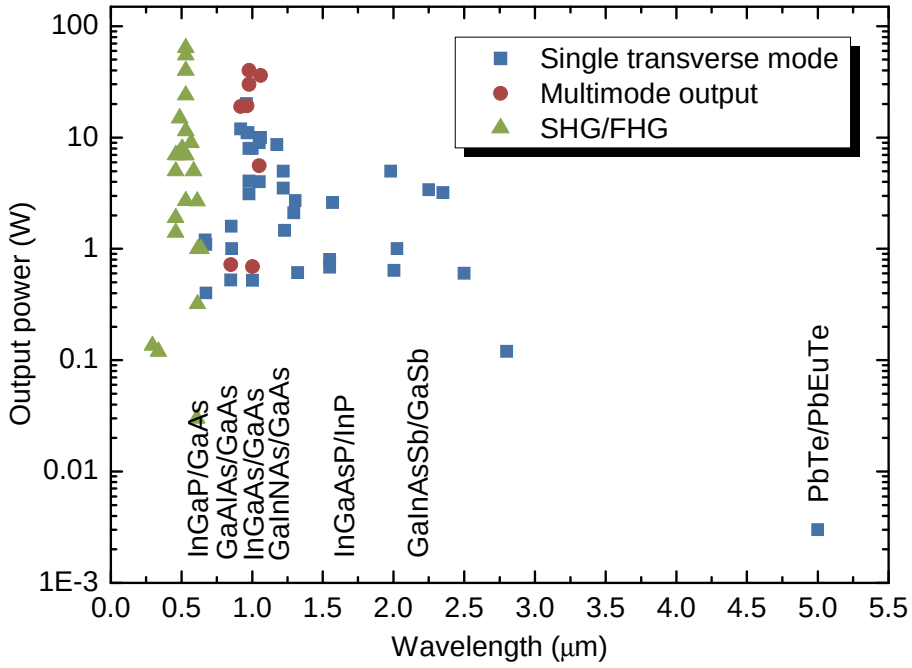

Fig. 1.2. Output powers and wavelength coverage by QW SDLs to date. Semiconductor compositions used for different spectral regions are also shown below

QD based SDLs emerged recently and thus power scaling in such devices was demonstrated only in the last few years. Multi-Watt output powers were reported in a wide spectral region which can be covered by QDs' emission, namely 960-1300 nm [19, 38-42]. These will be extensively discussed in later chapters of this thesis. Fig. 1.3 shows most of the to date reported QD SDLs at different wavelengths covered by direct emission or through second harmonic generation together with their output powers. Circled data will be presented in this work.

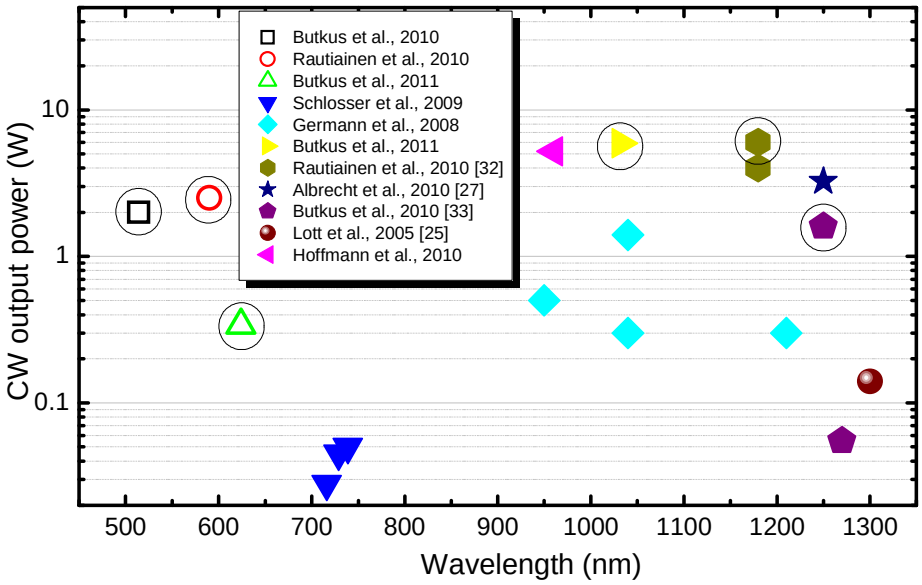

Fig. 1.3. QD SDLs with their output powers at different wavelengths demonstrated to date. Solid symbols show direct emission while open symbols demonstrate SHG. Circled data is presented in this work.

1.2.2. Tuneable semiconductor disk lasers

For some applications, especially in spectroscopy and biology, wavelength tuneability may be required and thus such properties are often desired in a laser source. The wavelength in an SDL can be tuned as the gain material often exhibits a broad gain bandwidth of a few tens of nanometers and tuning elements can be incorporated in external cavity configuration.

The achievable tuning in quantum dot based SDLs is considered one of their main advantages as the inhomogeneously broadened density of states in QDs supports a broad gain bandwidth. Thus combining this feature with tuning targeted design can result in a broadly tuneable semiconductor laser source with potential tuning range of ~100 nm.

Table 1.1 shows some of the to date demonstrated SDLs with the widest tuning ranges [43]. The semiconductor composition of the active SDL region is shown as well as tuning range in nm, wavenumbers and percentile. As in general, the tuning range increases with emission wavelength. QD SDLs presented in this thesis are shown in bold and it can be seen that at 1040 nm and 1180 they exhibit one of the widest tuning ranges as compared to QW based SDLs.

Material	**Tuning range (nm)**	**Tuning (nm)**	**Tuning (cm^{-1})**	**Tuning ($\Delta\lambda/\lambda$, %)**	**Reference**
InGaP	668-678	10	220	1.5	[44]
GaAs	830-863	33	460	3.9	[45]
InGaAs	955-995	40	425	4.1	[46]
InGaAs QDs	**1003-1063**	**60**	**563**	**5.8**	[47]
InGaAs	1147-1197	50	364	4.3	[48]
InGaAs QDs	**1147-1210**	**63**	**454**	**5.3**	[47]
GaInNAs	1163-1193	30	216	2.5	[49]
InGaAs QDs	**1237-1262**	**25**	**160**	**2.0**	[41]
GaInSb	1924-2080	156	390	7.8	[50]
GaInAsSb	2189-2318	129	254	5.7	[51]

Table 1.1. Some of to date SDLs with widest wavelength tuning ranges at different spectral regions. QD SDLs presented in this thesis are shown in bold.

It must be noted that some of the solid state or dye lasers are also capable of wide spectral tuning. For example, a well-developed Ti:Sapphire laser usually can be tuned over a wide

range, 700-1100 nm. However, such lasers are often complicated and expensive as compared to SDL units. Tuneable QD SDLs potentially can be successfully used where wavelength tuning for specifically targeted applications is required.

1.2.3. Mode-locked SDLs

Mode-locking is a powerful technique which enables the pulsed operation of lasers. For an SDL, passive mode-locking using semiconductor saturable absorber mirrors (SESAMs) is a standard technique for pulse generation. The mode-locking of SDLs was extensively studied, as a broad gain bandwidth from QWs and QDs can support ultrashort (< 1 ps) pulse generation. In addition, QDs have proven to be highly advantageous for SESAM structures, enabling a fast recovery time [52] and simultaneous control of both saturation fluence and modulation depth [53] – key parameters for saturable absorbers [54].

Since the first demonstration of a passively mode-locked SDL [55], these devices were extensively theoretically and experimentally studied. This has resulted in the production of mode-locked SDLs with pulse durations as short as 60fs [56], multi-Watt average output powers (2.1 W) [57], high-peak powers up to 315 W [58] and up to 1.8 kW using spontaneous mode-locking [140] and a wide range of repetition rates from several hundreds of MHz to 50 GHz [59] and up to 147 GHz using harmonic mode-locking [60]. In terms of wavelength coverage, most devices were concentrated in the 950-1050 nm range, however, there were also reports on mode-locked SDLs at 489 nm [61] and in the near-IR, namely at 1.3, 1.55 and 2 μm [62-64]. As can be seen, the parameters of mode-locked VECSELs may be quite versatile and enable the use of such lasers in specific applications. In terms of

achievable average output power at GHz repetition rates mode-locked SDLs are also fully comparable to ultrafast solid-state lasers as can be seen in Fig. 1.4 [65].

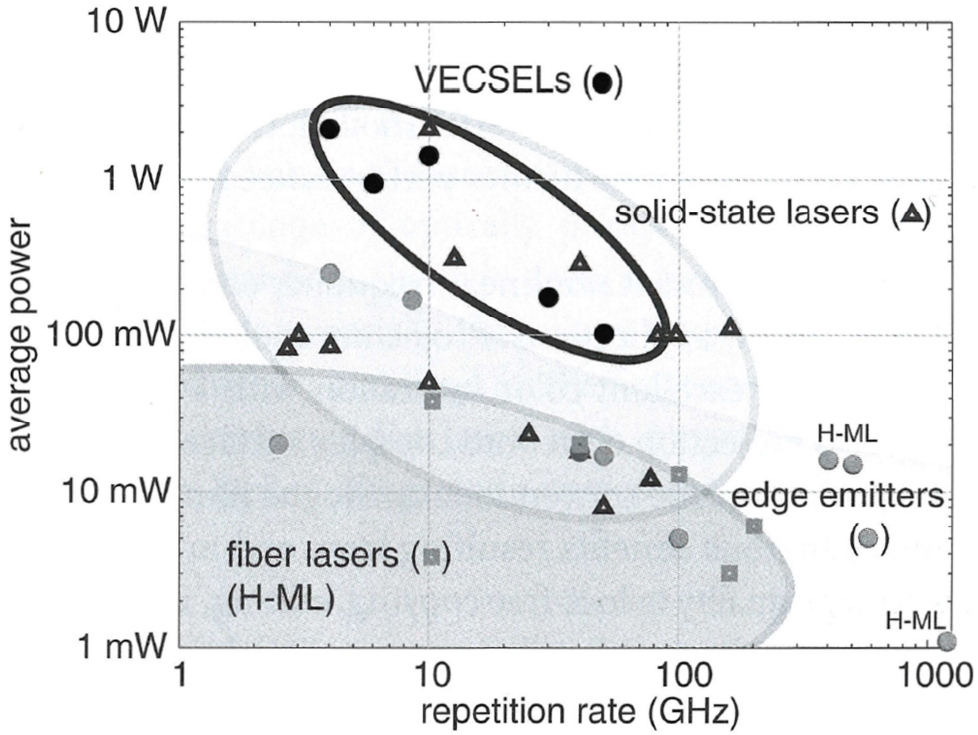

Fig. 1.4. Output power for different types of ultrafast lasers operating at GHz repetition rates [65].

QD based SDLs also attracted much attention in mode-locking experiments due to the novel properties of quantum dots incorporated both as active region in SDLs and in SESAMs. As QD based SESAMs feature low saturation fluence, they were highly advantageous for high repetition rate operation [59] and SDL/SESAM integrated devices called MIXSELs [66]. Table 1.2 shows a summary of a few recently published results including QD structures.

Type	Pulse duration (ps)	Average output power (mW)	Repetition rate (GHz)	Wavelength (nm)	Reference
QW SDL/QD SESAM	3.3	100	50	958.5	[59]
MIXEL	28	6400	2.5	960	[66]
QW SDL/QD SESAM	0.87	45.5	0.896	1028.5	[67]
QD SDL/QD SESAM	10	22	2.54	1054	[68]
QD SDL/QD SESAM	0.784	1050	5.4	971	[69]

Table 1.2. Mode-locked SDLs' performance with incorporated quantum dots in gain, SESAM or both regions.

1.2.4. Commercially available semiconductor disk lasers

Engineering development resulted in a number of robust and stable SDLs now available on the market. There are a number of companies involved in the development and sale of such devices. SDLs are offered by Coherent Inc., Solus Technologies Ltd., M Squared Lasers, Fraunhofer Institute and others. Commercially available continuous wave SDL sources cover the whole visible region with various output powers up to few hundred mW and up to 10 W in green light and also are available in 1.x μm and 2.x μm spectral regions for various applications. The prices of such devices depend on the complexity of the devices and range from a few thousand to a few tens of thousands of pounds.

Fig. 1.5. Semiconductor disk laser family for visible spectral region offered by Coherent Inc. Picture from www.coherent.com.

1.3. Applications of semiconductor disk lasers

The versatility of SDL technology allowed it to be adapted for a number of different commercial and scientific applications. First of all, SDLs are often used to pump other solid-state lasers, like Ti:Sapphire lasers [70]. Green emitting SDLs don't suffer from "green noise" which is problematic in other DPSS lasers used as Ti:Sapphire pumps. Tm(3+) and Ho(3+) doped tellurite glass and KYW lasers as well as silica fibre lasers doped by the same ions and emitting at ~2 μm were also pumped by SDLs in near-IR region [71]. SDLs were also used to pump Raman lasers [72] and optical parametric oscillators (OPO) [73, 74]. 980 nm emitting SDLs served as pump sources for Er-doped fiber lasers [75] and amplifiers [76] as well as glass-waveguide amplifiers for optical fiber telecommunication systems [77].

For more direct applications, visible spectrum region frequency-doubled SDL sources are used in many applications. For example, blue and green emitting SDLs replaced Ar-ion lasers in some of the applications. They are widely used in biophotonics, for example in confocal fluorescence microscopy [78], flow cytometry [79], optical trapping and cell

manipulation [80] and other laser-imaging or spectroscopy based techniques. SDLs were also used for medical applications in ophthalmology for photocoagulation treatment of eye diseases [81]. Other applications include forensics, RGB laser projectors, laser television, laser shows and so on.

By utilizing the advantages of external cavity configurations, applications such as high-sensitivity intracavity absorption spectroscopy [82] or mW output power level THz generation by the means of intracavity difference frequency generation within a dual wavelength SDL [83] were demonstrated. THz generation was also demonstrated using photoconductive antennas and SDL as a pump source [84].

A set of important applications can be found at the spectral region ~2.x μm. SDLs emitting at this wavelength usually also exhibit a broad tuning range and thus can be successfully applied in spectroscopic techniques like molecular spectroscopy or remote gas sensing, as a number of atmospheric gases like CO, CH_4 or NH_3 have strong absorption lines in this spectral region [85]. Also, laser surgery or non-invasive optical blood glucose monitoring are potential applications as human tissue exhibit distinctive absorption spectrum in this spectral region [86, 87].

Regarding the implementation of QD based SDLs, most of the above mentioned applications could be addressed, where wavelength coverage by QD emission is available. However, as QW SDLs are further developed at present, applications exploiting the specific competitive advantages of QDs should beaddressed. One of those advantages is wavelength coverage in the 1100-1300 nm spectral region where coverage by QW structures face specific material issues [88]. Fig. 1.6 shows extinction of a few important components of human tissue – water, melanin and hemoglobin, indicating their low light absorption in the

spectral region of 1-1.3 μm. Such a feature can be successfully addressed in biophotonic applications. Thus QD SDLs, especially in the mode-locked ultrafast (τ < 1 ps) regime potentially can be successfully applied in such bio-imaging areas as nonlinear fluorescent microscopy.

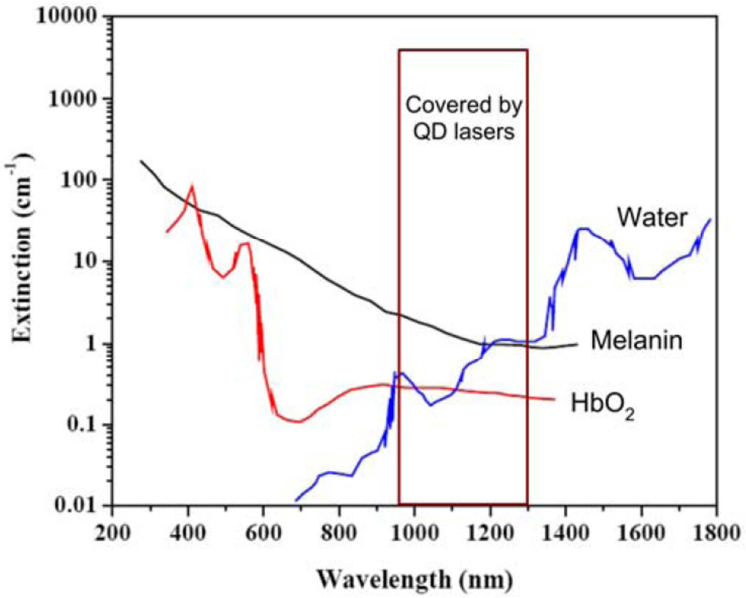

Fig. 1.6. Extinction coefficient for water, melanin and HbO_2 at different wavelengths.

To date, the use of lasers emitting pulses in the femtoseconds range as excitation sources has improved not only in the resolution and 3D imaging capabilities of microscopy by multi-photon excitation – e.g. Two- or Three Photon Excitation Fluorescence (TPEF) - but has also demonstrated the possibilities for new detection techniques by exploiting non-linear excitation effects, e.g. Second-Harmonic Generation (SHG) and Third Harmonic Generation (THG). The basic principle underlying these techniques is that for focused fs laser pulses, the photon density is high enough to induce multi-photon absorption or other nonlinear (coherent) processes within the focal volume. Fluorophores whose excitation maximum is in the UV or in the visible spectral range can be excited by two or three

infrared photons through multi-photon absorption. Since nonlinear absorption and thus induced fluorescence occurs solely at the focal volume of the laser beam, a high axial resolution and consequently the 3-D imaging capability of confocal microscopy can be attained without the use of a confocal aperture. Furthermore, there is no interfering fluorescence from the surrounding structures and “out of focal plane” photobleaching and phototoxicity can be significantly reduced. More precisely, for nonlinear techniques, the efficiency of the generated signal scales nonlinearly with the intensity of the excitation beam. Thus, the use of fs lasers enables high peak powers for efficient nonlinear excitation, but at low enough energies so that biological specimens are not damaged. Additionally, the use of infrared light implicates a high penetration depth into tissues and it could exceed 200 μm due to the low absorption of the primary cellular components (Fig. 1.6). For SHG and THG, an additional advantage derives from the fact that no energy of the incident light is deposited (absorbed) by specimens, thus sample disturbance (e.g., thermal, mechanical side-effects) is minimal. 3-D fluorescence imaging based on nonlinear fluorophore excitation enables a number of potential applications in life science, such as high-resolution imaging of biological activities in living cells and tissues, studying cell motility and the distribution of a neurotransmitter in living cells.

However, all of the above techniques usually use ultrafast solid state lasers, such as a Ti:Sapphire laser. These sources are usually well developed, but on the other hand they are bulky and expensive, thus a successful development of compact, price efficient and easy to use QD SDL could be attractive pump source for many biophotonic imaging and detection techniques. In the frames of the FAST-DOT project, multi-photon fluoresce imaging was already demonstrated using a 965 nm SDL mode-locked with QD SESAM and emitting 1.5 ps pulses at 500 MHz repetition rate and 287 mW average output power [89].

Another potential application for QD based SDLs could be optical coherence tomography (OCT) where as broad as possible optical bandwidth is required for highest resolution. Ultrafast or swept laser sources [90] are usually used. Lasers with wavelengths accessed by QD emission could be advantageously exploited in this application by allowing a deeper penetration into the monitored tissue [91].

To sum up, SDLs have already been applied in many different areas. QD based SDLs, being a new area of research, will find its niche applications as the development of these lasers will progress. The novel features offered by QDs will be exploited:

- 1-1.3 µm spectral coverage can be applied in biophotonic applications
- Broad wavelength tuneability also can be exploited where compact and cheap tuneable laser sources arerequired
- Other features like low thermal sensitivity and low operation threshold will improve the performance efficiency of some devices by making them cheaper, battery powered, more integrated and handheld, etc.
- QDs are successfully exploited as saturable absorbers for mode-locked SDLs and other types of lasers.

1.4. Operational principles of Semiconductor Disk Lasers

Having briefly reviewed the path of the SDL development, their properties and applications, it is now necessary to discuss the operational principles of the SDL more thoroughly. In this chapter all basic components of the SDL device will be reviewed.

As already mentioned before, the SDL consists of a gain medium grown on a fully reflecting distributed Bragg reflector (DBR) and is optically pumped by a diode laser. An external cavity is formed by a dielectric mirror or a few of them and they control the fundamental mode operation. For more specific applications like mode-locking, second harmonic generation, etc., other intracavity optical elements are also used. Fig. 1.7 shows a schematic picture of the SDL in simplest straight cavity configuration. Here, the semiconductor part of the SDL is bonded to the heatsink to dissipate heat. Then it is pumped by a fiber coupled laser diode emitting at 808 nm, as it was in our experiments.

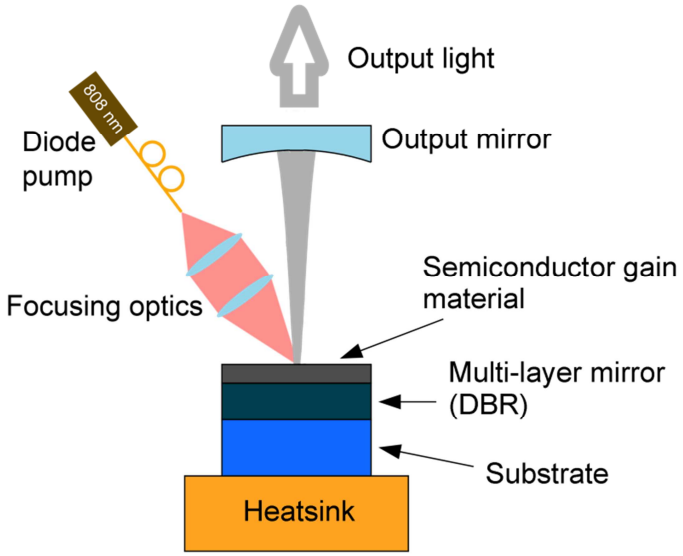

Fig. 1.7. Schematic drawing of the semiconductor disk laser with its main components in a straight cavity configuration.

1.4.1. Semiconductor gain region

Semiconductor gain structure grown on the top of distributed Bragg reflector (DBR) is by far the most important part of the SDL. Pump light photons are absorbed in the absorbing regions which also serve as separators between QD or QW layers (in this chapter, only QD layers will be mentioned, however, most of the concepts are the same for QW based SDLs).

Several semiconductor materials systems are available for different pump wavelengths, usually with a broad absorption bandwidth and thus with relaxed requirements for the pump source. Pump light is absorbed exponentially in non-transparent material, which is described by (1.1).

$$I = I_0 e^{-\alpha z} \tag{1.1}$$

Here I and I_0 are light intensity in the material and incident light intensity, α is the absorption coefficient of the material for specific photon energy and z is the length of the material. With a high enough absorbing layer thickness, most of the pump light can be absorbed in one pass.

Absorbed photons then excite electrons and holes in spacer material, i.e., the GaAs layers grown between the QD layers. The non-equilibrium carriers diffuse and are trapped into QD layers which have a lower potential energy and then recombine, emitting lower energy photons. As the condition of population inversion is reached, stimulated emission starts amplifying coherent light and lasing is initiated. A thin, lower refractive index layer is usually grown near the top of the surface and is called the barrier layer. It creates a barrier to the excited carriers so they cannot diffuse to the surface of the device where nonradiative recombination would occur due to surface defects and would decrease the performance of the device. A typical potential energy structure of semiconductor gain mirror with lasing processes is shown in Fig. 1.8 [18]. Here, black lines represent energy profiles of conduction and valence bands across the SDL semiconductor part.

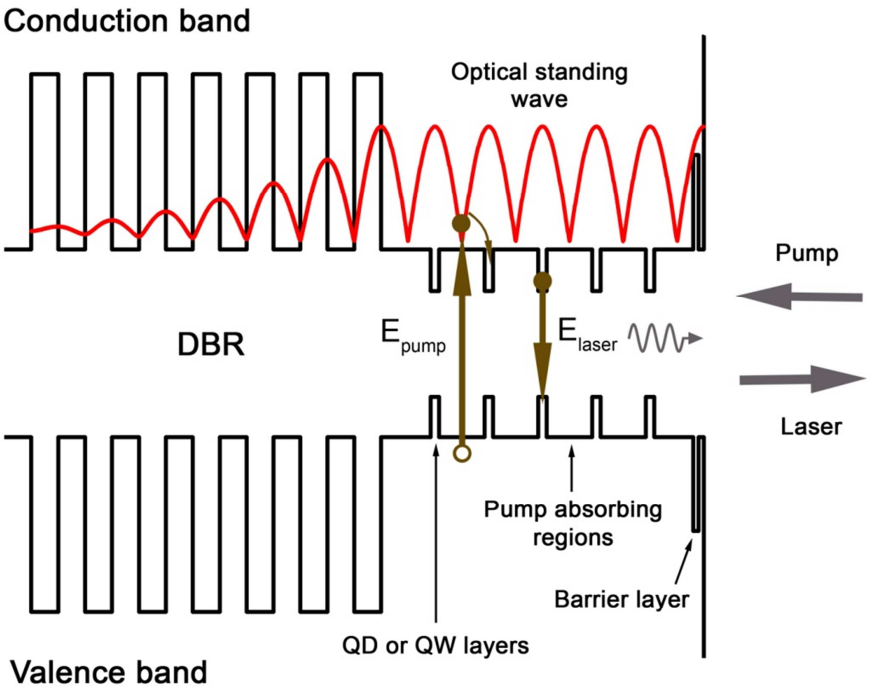

Fig. 1.8. Schematic drawing of potential energy bands in typical SDL semiconductor gain mirror. Prepared using [18].

Optical waves in the semiconductor subcavity are constantly reflected, and by interfering with each other they create an optical standing wave pattern. Such a standing wave of electric field modulus is shown in red in Fig. 1.8. The gain from each QD layer is strongly determined by the local intensity of this standing wave pattern in the QD layer. This effect is often described by the enhancement factor [82]. For maximum gain, QD layers are usually positioned in the antinodes of the optical standing wave by choosing specific thicknesses of pump absorbing regions. This is called resonant periodic gain (PRG) structure [92, 93]. Such configuration allows maximum gain from each active layer as well as it reduces the operational threshold of the device.

Optical waves are reflected from the DBR as well as from semiconductor – air interface thus creating a Fabry Perot etalon. Such an etalon affects the initial gain bandwidth

determined by the gain media, i.e. it acts as a spectral filter and thus it must be considered in the design of the semiconductor active region. The transmission of such an etalon can be calculated by (1.2):

$$T(\lambda) = \frac{T_1 T_2}{1 + R_1 R_2 - 2\sqrt{R_1 R_2}\cos(4\pi n L_c/\lambda)} \quad (1.2)$$

Here T_1, T_2, R_1 and R_2 are the transmission and reflection of both facets of the etalon, L_c is the thickness of the etalon, n is refractive index of the medium and λ is the wavelength of light.

When designing the active region of the SDL, two cases usually are used – the overall thickness of the active region is chosen so as it would be the multiple of λ/4 or of λ/2, i.e., the formed Fabry Perot etalon is either in antiresonance or in resonance with laser design wavelength. Fig. 1.9 shows both cases in the design of a real 1040 nm SDL sample with 63 layers of QDs. In it, the electric field pattern (a,b) is shown together with the calculated reflectivity spectrum, transmission spectrum of formed Fabry-Perot etalon and photoluminescence spectrum of QDs for 1040 nm SDL (c, d).

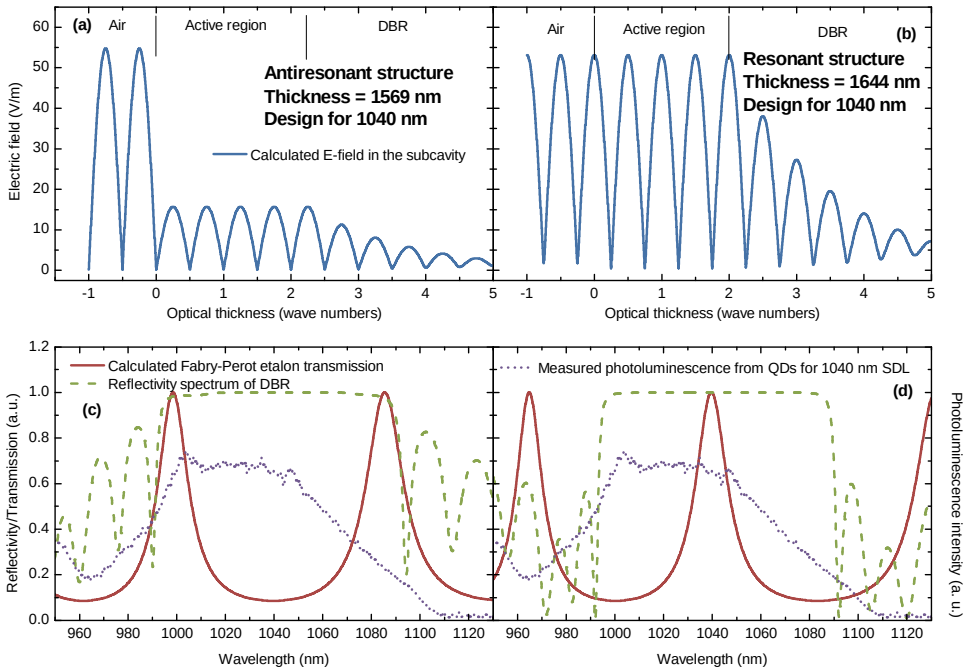

Fig. 1.9. Standing electric field pattern for a) antiresonant and b) resonant cases of subcavity formed Fabry-Perot etalon. c and d show calculated Fabry-Perot etalon transmission, reflectivity of the structure and QD photoluminescence spectra of the same structures shown in a and b.

First it can be seen (from parts a and b) that the resonant case supports a higher amplitude of the standing wave in the subcavity than the antiresonant design. When etalon filtering effect is considered, it can be seen that in the antiresonant case, the transmission of the Fabry–Perot etalon is at a minimum at the design wavelength (c part). Thus in practical operation it reduces the intrinsic gain at the centre wavelength, although increasing it at the wings. It was shown by [82] that the resulting effective gain bandwidth can even be broader than intrinsic bandwidth from the active region.Such a broad gain bandwidth configuration is favourable for the tuneability of the device as well as for the ultrafast mode-locked sources where broad gain bandwidth is desired. This configuration is also favorable for

high power operation as it is less temperature-sensitive as the gain maximum shift will not be so significant for the overall effective bandwidth. It also has a higher damage threshold at high intracavity powers as the optical standing wave has a node at the semiconductor – air interface, where many surface defects occur.

In the resonant case of the Fabry – Perot etalon, the transmission peak is at the center of the design wavelength (Fig. 1.9 d). It then enhances the gain intensity in the middle of the bandwidth and reduces it at the wings. In such a configuration, the electric field is higher in the subcavity region and thus is favorable for low threshold or low gain devices. For high power operation, the active region must be designed very carefully as the gain maximum shifts quickly from the peak wavelength with increased temperature, thus decreasing the performance of the device. It is especially important for thick subcavities containing many QD layers as the etalon transmission peak gets narrower with increased etalon thickness.

As the gain bandwidth of QDs was not measured in our experiments for this wavelength, QD photoluminescence is shown in the graphs in Fig. 1.9 c and d. This photoluminescence is then filtered by the subcavity forming the Fabry – Perot etalon. This effect will be discussed in more detail in chapter 3.3.

1.4.2. Distributed Bragg reflector

A distributed Bragg reflector (DBR) usually is grown together with the active region and acts as one of the cavity mirrors. It is well established technique used in many semiconductor lasers and allows an easy monolithic integration with active region of the laser.

The DBR consists of a number of periodically repeated high-low refractive index semiconductor layers pairs. Each layer is a quarter wavelength thick. Light waves reflected from each interface in the DBR interferes constructively thus creating a high reflectivity stop band. As QDs have quite a low gain, high reflectivity DBRs are usually needed to have a low operation threshold and to maximize the performance of the device. $GaAs/Al_xGa_{1-x}As$ DBRs are typically used for QD SDLs and this material combination can cover the whole 1 – 1.3 µm spectral region and is suitable for lattice matched growth together with the active QD region. A reflectivity of > 99.9 % is usually reached with 28-35 material pairs. To simulate the reflectivity spectra of various DBRs, ABCD matrix transfer calculations are usually used. A reflectivity value for certain wavelength can also be calculated using (1.3):

$$R = \left(\frac{n_i n_{high}^{2N} - n_e n_{low}^{2N}}{n_i n_{high}^{2N} + n_e n_{low}^{2N}}\right)^2 \quad (1.3)$$

Here n_i and n_e are the refractive indexes of incident and exit materials, n_{low} and n_{high} are the refractive indexes of the DBR layers and N is the number of material pairs used in the DBR. A simulated typical DBR reflectivity spectrum for different Al concentration in $GaAs/Al_xGa_{1-x}As$ is shown in Fig. 1.10 a. Fig. 1.10 b shows reflectivity of GaAs/AlAs DBR at different N values at different wavelengths. It can be seen that the reflectivity value is mainly determined by the number of pairs while the width of the spectrum mainly depends on the refractive index contrast between two composition materials.

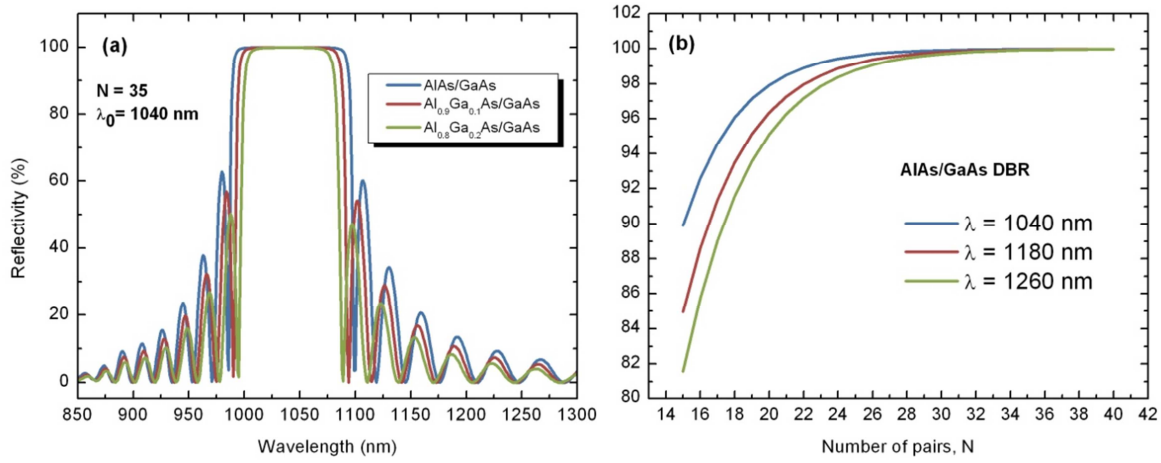

Fig. 1.10. a. Simulated spectra of DBR for different materials compsitions; b. DBR reflectivities at different N values.

As the DBR is placed between the active region and substrate or heatsink, it must not be forgotten that the thermal impedance must be considered as pump induced heat in the active region dissipates through the DBR layers. Thus the thickness of the mirror should be kept to minimum while maintaining a high reflectivity value. Heat dissipation in the SDL will be discussed in more detail in chapter 1.5.

If the entire pump light is not absorbed in the active region due to a low absorption factor or thin absorbing region, the DBR is also sometimes used to back reflect the pump wavelengths. Such a multiple stop-band DBR can be specially designed [94] or several DBRs for different wavelengths can be grown on each other [69]. As previously mentioned, QD based SDLs already have GaAs/$Al_xGa_{1-x}As$ based DBRs which can cover wavelengths of interest. However, for certain materials, especially for QW based SDLs emitting in the 1.3 - 1.6 µm region, no high refractive index contrast materials with lattice matching exist and many layers need to be deposited to achieve the desired reflectivity. For such cases, a wafer fusion technique has been successfully demonstrated where a separately grown DBR is optically bonded to the active region [33, 95,96].

1.4.3. External cavity

As discussed in the introduction, the external cavity of the SDL is formed by adding additional dielectric mirrors to form various shape cavities. In the simplest case, this is a straight cavity comprising a gain mirror and one additional external mirror as was shown in Fig. 1.7. Such a configuration is easy to align and usually is used for operation in the CW regime. For more sophisticated uses, more complex cavity configurations are used which involves multiple external mirrors or other components such as saturable absorbers, second harmonic generation crystals, birefringent filters or multiple gain elements. A few possible cavity configurations for different applications are shown in Fig. 1.11[37].

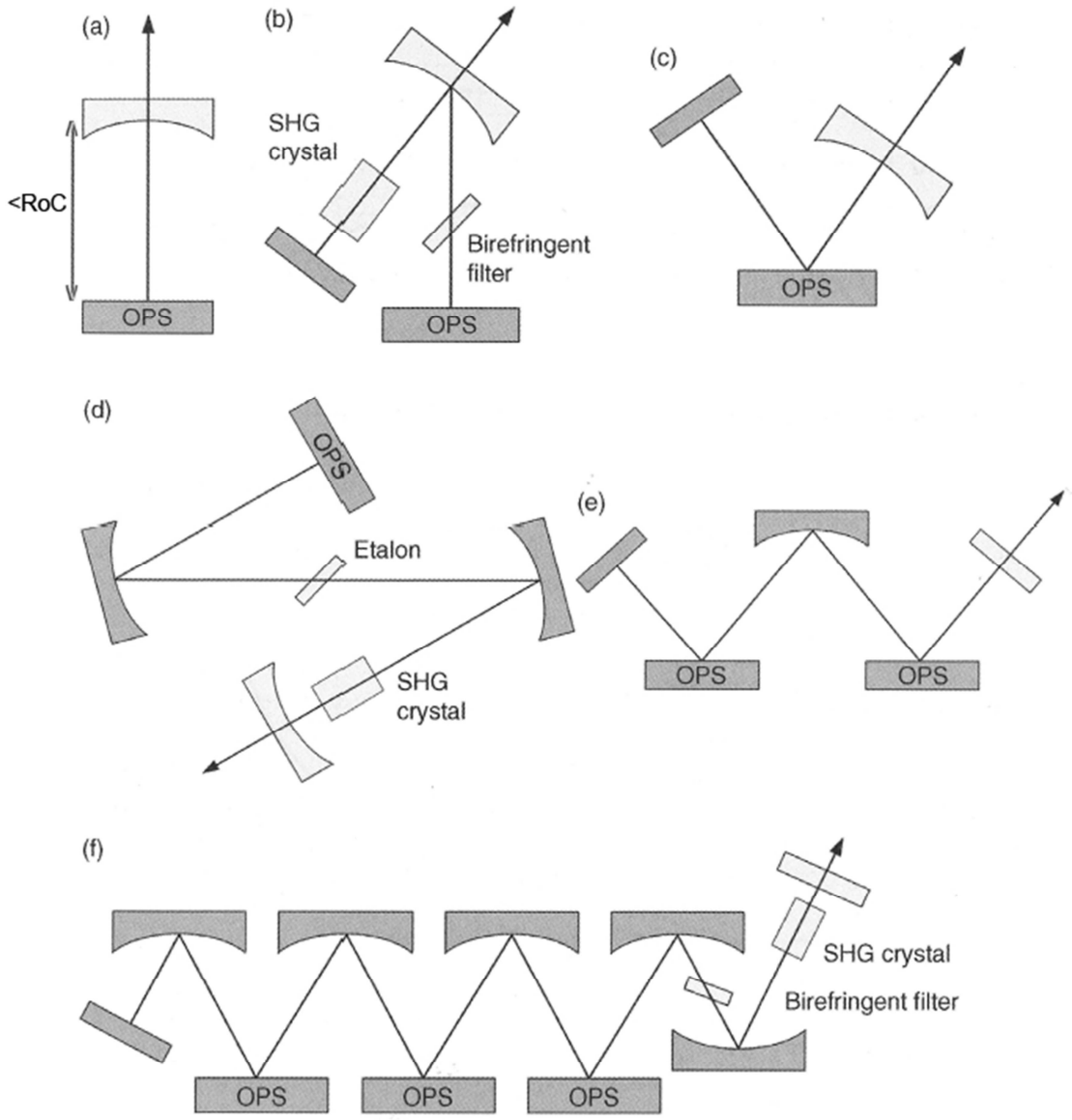

Fig. 1.11.Various SDL cavity configurations. a - straight cavity configuration, b, c - V-shape cavity, d - Z-shape cavity, e - W-shape cavity with two gain chips, f - SDL with three gain chips. Here OPS - optically pumped semiconductor [37].

One of the roles of the external cavity is to control the fundamental transverse mode operation in the SDL. For the optimum operation, the cavity mode and pump spot must be well overlapped to have maximum gain out-coupling from the active region. The sizes of

these spots are chosen according to the available pump source and cavity stability limits so as to maintain the operation below the thermal rollover. Respectively, the cavity stability is determined by optical cavity elements and distances between them. For example, straight cavity shown in Fig. 1.11.(a) can be formed by placing the curved mirror at the distance to SDL chip not longer than the mirror's radius of curvature. QD SDLs are usually operated under pump spot diameter sizes of 100 – 200 µm. Such a size allows efficient heat extraction, lowers the light intensity at the surface of the semiconductor and eases the alignment tolerances. The TEM_{00} laser mode radii w_1 and w_2 on both gain mirror and spherical mirror in straight cavity configuration can be calculated by:

$$w_1 = \left(\frac{L\lambda}{\pi}\right)^{1/2} \left[\frac{g_2}{g_1(1-g_1g_2)}\right]^{1/4} \tag{1.4}$$

$$w_2 = \left(\frac{L\lambda}{\pi}\right)^{1/2} \left[\frac{g_1}{g_2(1-g_1g_2)}\right]^{1/4} \tag{1.5}$$

Here L is the length of the cavity, λ is laser light wavelength, $g_1 = 1 - L/R_1$ and $g_2 = 1 - L/R_2$, where R_1 and R_2 are radii of curvature of the first and second cavity mirrors. Fig. 1.12 shows calculated w_1 and w_2 values at different cavity lengths for a 1040 nm SDL in a straight cavity configuration. In a given case, $R_1 = \infty$ and R_2 = -75 mm. Such a configuration was often used in our experiments for the CW regime and 74 mm cavity length was used to achieve a 120 µm diameter spot on the gain mirror. As single pass gain is relatively small due to a thin active region and lower QD gain as compared to QWs, only a small portion of intracavity power can exit through the output coupler. In QD based SDLs, output couplers with reflectivity > 99% are typically used.

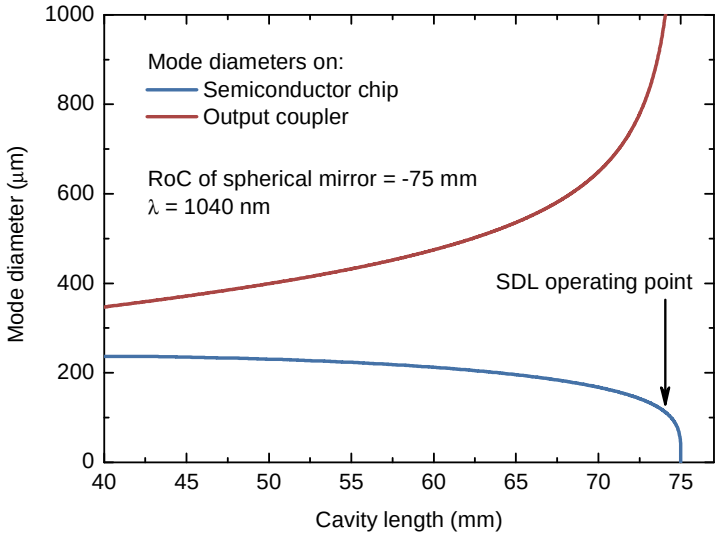

Fig. 1.12. Mode diameters in straight cavity laser configuration. An arrow indicates the operating point of SDL in our experiment.

Another important part of the SDL is the pump source. Market available CW diode lasers are usually used for this purpose. They are often fiber coupled for easier light delivery to the SDL. Depending on the SDL application, various power sources are used, namely from a few Watts to > 100 W. As already mentioned, the pump wavelength is not strictly limited due to the broad absorption bandwidth of the absorbing semiconductor. 808 nm and 830 nm pump sources are often used for SDLs operating ~1 μm, as well established laser diodes at these wavelengths are available. However, to reduce the quantum defect-induced heat, direct in-well pumping schemes were also realized in QW SDLs using pump wavelengths close to the ones emitted [85, 97, 98]. With such designs, slope efficiencies > 60 % were demonstrated. However, light absorption is poorer in such pump schemes as the total thickness of the absorbing QW sheets is much smaller than the thickness of barrier layers.

Pump light is focused on the surface of the semiconductor chip to the calculated spot size. The angle of incidence varies from 20 to 45 deg. Such pump angles are available as the pump light is absorbed in a thin region of approximately 1 µm thickness.

1.5. Power scaling and thermal management in semiconductor disk lasers

Power scaling is one of the attractive features of SDL. It is mainly enabled by optical pumping as the pump spot size can be increased and external optics adjusted while still maintaining single transverse mode operation. Optical pumping allows a uniform pump of the area, contrary to electrical pumping, where large aperture operation is only available at the expense of beam quality. To date, SDLs with pump spot sizes between 30 and 900 µm were demonstrated. However, the size of the pump spot cannot be extended infinitely. On the other hand, for limited pump power and for efficient operation, one would need the smallest pump spot size while still maintaining operation of the laser. Here the main, but not the only, limit in power scaling is heat dissipation from the active region, as it is in most types of lasers. Additional effects limiting the output power are diffraction losses due to the surface roughness and amplified spontaneous emission in the lateral direction [99], however those are considered to be minor compared to the heating of the active region.

As the pump irradiance is increased, the absolute temperature in active region rises as the energy difference between pump and lasing photons is transferred to the heat. This temperature increase decreases the performance of SDL mainly in two ways [100]:

- The peak gain from individual QDs decreases,
- The peak gain and wavelength of optical standing waves in the subcavity are spectrally shifted to red wavelengths at different rates (usually differs 2-4 times)

with increasing temperature and walks away from the resonant periodic gain condition. These two effects are observed as both bandgap energy and refractive index of semiconductor depends on temperature.

Ultimately, the SDL approaches thermal rollover and with further pump power (temperature) increase, its operation is terminated.

In the unprocessed sample, heat from the active region flows down through the DBR and substrate towards the heat spreader, as shown schematically in Fig. 1.13 a. Thus, good thermal conductivity and small physical thickness are desired properties of these elements. However, the typical thermal conductivity of GaAs/AlAs based DBR is quite low, 60W/mK and even smaller for GaAs based substrates [100]. Meanwhile, if the thickness of the semiconductor active region where most of the heat is generated is ~ 1 µm, the thickness of the DBR is usually 5 – 6 µm and the thickness of substrate reaches 500 µm. Thus, in an unprocessed sample heat is not efficiently dissipated and this limits power scaling. In QD SDLs, using an unprocessed sample, the output power typically does not exceed a hundred mW [39].

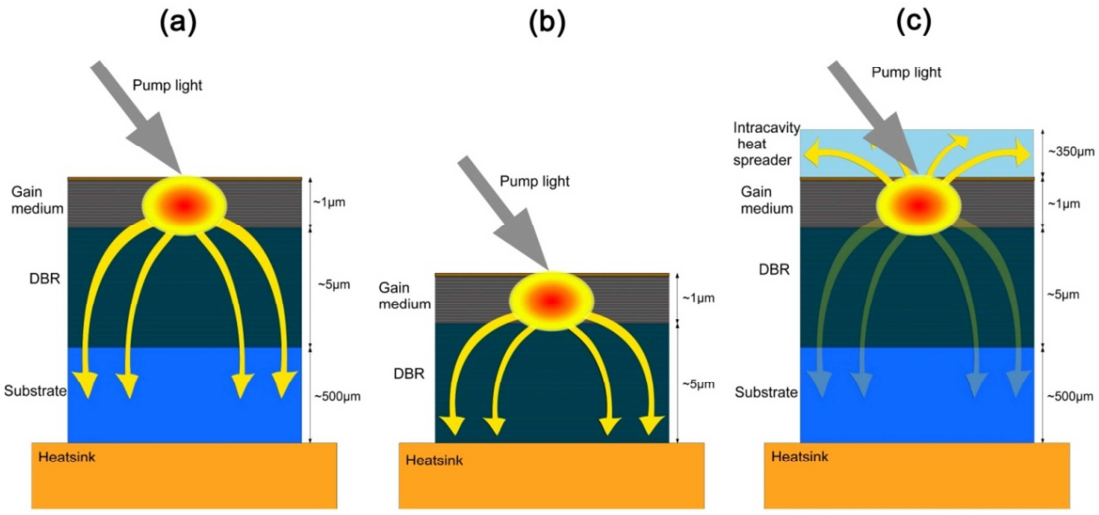

Fig. 1.13. Schematic drawing of heat flow in SDL and different thermal management techniques: (a) unprocessed sample, (b) substrate removal, (c) intracavity heat spreader. The thicknesses of layers are not to scale.

The efficient removal of heat from the active region was widely studied by several groups [22, 23, 43,100-102]. There are two main approaches for heat removal in the SDL:

- Substrate thinning or removal
- Use of an intracavity heat spreader

In the first approach, the thick substrate of semiconductor is removed and the active region with the DBR is directly soldered onto a copper heatsink (Fig. 1.13 b). In such a case, heat can be dissipated more easily by one dimensional heat flow towards the heatsink. Such a device is usually grown in reverse order, i.e. the active region is grown directly onto the substrate and DBR is grown as top element. After that, a piece of the wafer is soldered onto the heatsink and the substrate is etched using wet chemical etching. Thus such structure is also known as a “flip-chip” SDL [103]. Often, a high thermal conductivity material (e.g.

diamond) is also inserted between the DBR and the heatsink to improve heat flow and to ease the handling of the sample [18]. To date this thermal management technique has allowed the demonstration of high powers of several tens of watts operation in QW SDLs [22, 23] and has already been applied in QD based SDLs, allowing 0.5 W output power at1180 nm [103].

The second thermal management technique employs a few hundred microns thick intracavity heat spreader which exhibits a high thermal conductivity. Such a heat spreader is bonded to the top of the semiconductor part and then the whole chip is mounted onto the copper mount. As the top heat spreader exhibits much higher thermal conductivity than the DBR and substrate, most of the heat is extracted directly from the top of the active region as shown in Fig. 1.13 c [100]. Such a heat spreader is transparent to pump and lasing wavelengths. A several materials were used for intracavity heat spreaders, such as silicon carbide, sapphire or diamond. Literature available thermal conductivity values of various SDL parts and potential heat spreaders used are shown in Table 1.3 for comparison.

Element of the SDL	Thermal conductivity (W/mK)
InGaAs/GaAs based gain	24
AlGaAs/GaAs DBR	61
GaAs Substrate	44
Copper	400
Indium	84
Potential heat spreaders	
Sapphire heat spreader	50
Silicon carbide heat spreader	490
Diamond heat spreader	2000

Table 1.3. Thermal conductivity values for different elements of an SDL chip and potential heat spreaders.

Thermal management using different techniques was extensively theoretically and experimentally studied in [100, 104]. In these works, the temperature increase in the active region of the SDL was calculated using the equation below:

$$\Delta T_{max} = \eta \frac{\Lambda+(\Lambda_0/2)}{\pi r^2}\left(\frac{2}{\Lambda_0}P_{out}\frac{\lambda_L}{\lambda_P}+\frac{hc}{\lambda_P}\frac{\pi r^2}{\sigma_e \tau}\right)\left(\frac{t}{2k}+\frac{1}{H}\right) \quad (1.6)$$

Here, η is the fraction of pump power converted to heat, Λ is the single-pass passive loss, Λ_0 is the output coupler transmission, r is the radius of the pump and laser mode, P_{out} is the output power, λ_L and λ_P are laser and pump wavelengths, σ_e is the stimulated emission cross section, τ is the upper level lifetime, k is the thermal conductivity, t is the thickness of the disk and H is the heat transfer coefficient between the disk and the heatsink. The maximum temperature rise was calculated for several different thermal management techniques and is shown in Fig. 1.14. For this simulation, InGaAs based SDLs for 980 nm were assumed with a 2.25 µm thick active region, 4.6 µm thick DBR, 500 µm thick substrate and 250 µm thick

diamond heat spreader. Here, three different thermal management techniques are considered: a thin-device attached directly to copper (solid diamonds), a thin-device soldered to the diamond and then to the copper (open circles) and a device with an intracavity diamond heat spreader (closed triangles). It can be seen that the SDL with a diamond heat spreader has the lowest temperature rise with increased pump power as compared with other techniques. However, it is worth noting that such behaviour is expected at a pump power up to ~20 W as a thin-device bonded to diamond and copper shows a close performance. A thin-device directly bonded to the thermoelectric cooler also shows good performance, however, for practical handling, a copper sub-mount will be necessary.

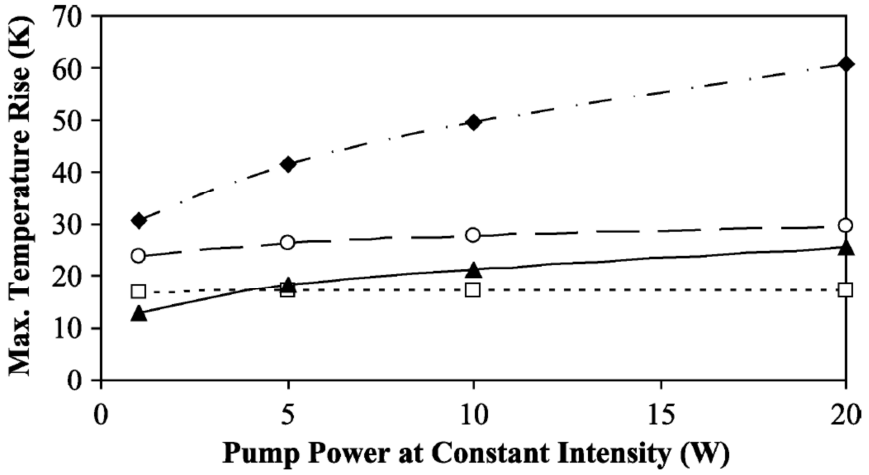

Fig. 1.14. Maximum temperature rise in the active region of SDL using different thermal management techniques for different pump powers. Solid diamonds: thin-device soldered to a copper mount. Open circles: thin-device soldered to diamond and copper. Closed triangles: diamond heat spreader in a copper mount. Open squares: thin-device directly cooled at the bottom of the DBR [101].

A thermal management technique using a transparent intracavity heat spreader was also successfully applied for a number of QD SDLs and allowed the demonstration of the highest output powers to date [39, 40].

Another issue regarding heat induction, especially in solid state lasers, is thermal lensing. This effect is noticeable in microchip VECSELs, where a multilayer dielectric mirror is formed on the top of the heatspreader. However, for conventional high power SDLs, thermal lensing was shown to have a minor effect due to a scalable pump area [22].

1.6. Semiconductor quantum dots as the active medium

For a long time since the development of SDLs, the semiconductor active parts of these lasers were mainly based on quantum wells (QWs).Such structures supported enough gain for efficient SDL operation and allowed the demonstrations of output power reaching tens of Watts. Several semiconductor material combinations were used for different wavelength operation (Fig. 1.2). More recently, SDLs based on quantum dot (QD) structures in the active medium were demonstrated [20, 39]. In this chapter QDs as the active medium in the SDL will be overviewed. Also, the fabrication principles and optical properties of QDs will be discussed.

1.6.1. Quantum dots as an alternative to quantum well active region

QDs are nano-size islands of semiconductor structures embedded in another semiconductor material having a larger bandgap. The first lasing using QD materials in diode lasers was demonstrated in 1994 [105, 106] and has been extensively explored since then. The use of

QDs allowed some new features in semiconductor lasers to be exploited that were not achievable using QWs. These included reduced lasing threshold, lower thermal sensitivity and higher differential gain [107]. Important improvements using QDs were also achieved using them in saturable absorber mirrors [52-54]. QD based SDLs were also demonstrated recently [20, 39] and potentially can be developed as ultrafast or CW widely tuneable laser sources in near-IR spectral region.

The above mentioned features of QD lasers mainly come from the property of size quantization in QDs. As electrons are confined in tiny QD structures in all three directions, the energy spectrum becomes different from other semiconductor structures. To understand this concept better, let's consider the density of states in semiconductors. The density of states (DOS) shows how many energy states are available within unit energy interval in a crystal of unit volume, i.e. it shows how many states excited electrons of certain energies can occupy. In general it is written as (1.7):

$$DOS = \rho(E) = \frac{1}{V}\frac{dN}{dE} \tag{1.7}$$

The shape of the DOS function depends on the chemical nature of the crystal host, the crystalline structure and some other parameters. Usually, only the states near the band edge are of primary importance as charge carriers rapidly relax to the bottom (top) of corresponding band after being excited to higher energy states. These states near the band edges are mostly determined by the dimensionality of the system [108]. A bulk semiconductor is called a three dimensional structure as the carriers are free to move in all three directions. QWs confine carriers in one dimension and are considered to be two dimensional, while quantum wires are one dimensional system. QDs confine carriers in all three dimensions in a space of size comparable with the de Broglie wavelength, which in

III-V compound semiconductors is in the range of tens of nanometers. As electrons are confined in such a tiny space, they only have certain allowed energy levels which bring new features for such structures. The function of the DOS at different energies for carriers confinement configurations in semiconductor structures are shown in Fig. 1.15 [109]. It can be seen that in 3D bulk semiconductors, the DOS has a continuous function shape due to many overlapped energy sub-bands. However, as the carriers are confined in one, two or all three directions, the function becomes quasi-continuous and is narrowed to approach a Delta function, as is the case for QDs. In this case, carriers occupy only a certain restricted sets of energy levels like electrons do in the atoms and thus QDs are sometimes referred as "artificial atoms".

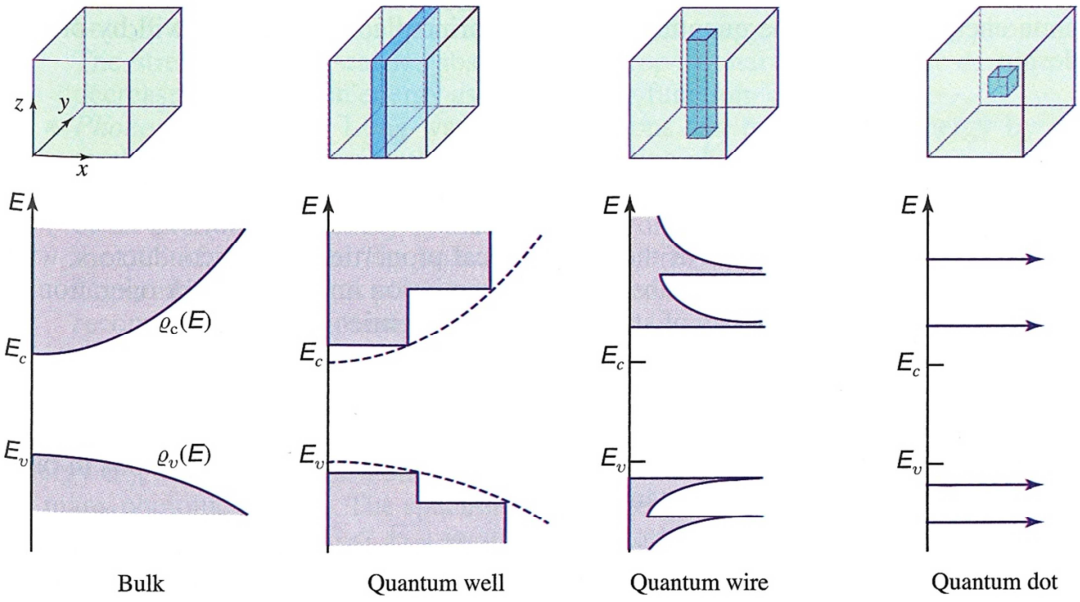

Fig. 1.15. Density of states functions for semiconductor structures with different carriers' confinement configurations. Bulk - 3D, quantum well - 2D, quantum wire - 1D, quantum dot - 0D[109].

When compared with higher dimension structures, it can be seen that the DOS function in QDs has more advantages for applications in photonics. In such structures, only allowed

energy states correspond to discrete quantum levels in QDs. Thus, the density of charge carriers accumulated at the energy of operational transitions is significantly enhanced at the expense of the higher energies in the continuous DOS function. I.e., for a given energy range, the number of carriers necessary to fill in these states is reduced significantly thus reducing the threshold value for QD based lasers and increasing the gain at a given carrier density [108, 110, 111]. Indeed, the threshold current in laser diodes was reduced via decreasing the dimensionality in carriers' confinement, as it is shown in Fig. 1.16 [112].

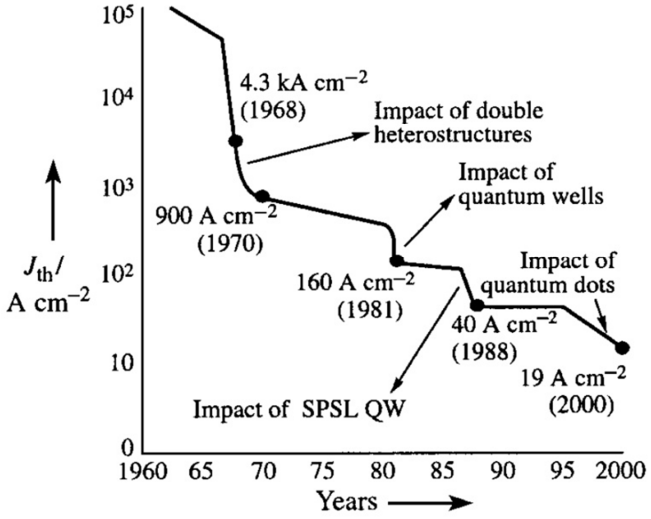

Fig. 1.16. The reduction of threshold current density in laser diodes during the years using different semiconductor structures [112].

Discrete energy levels also allow reduced threshold sensitivity to surrounding temperatures which is of great advantage for all semiconductor lasers. A theoretical simulation of threshold current dependence on temperature for different carrier confinement configurations is shown in Fig. 1.17 [112].

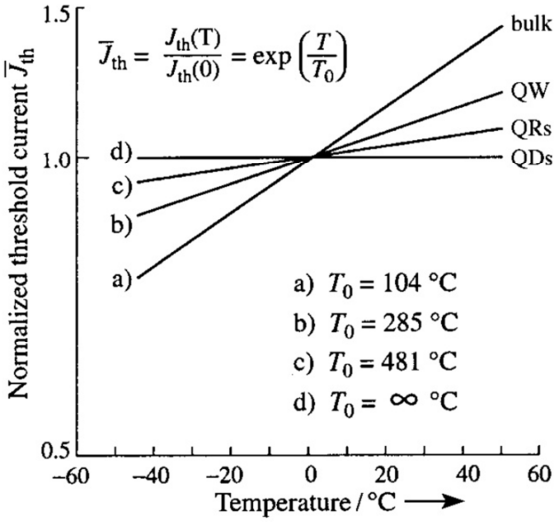

Fig. 1.17. A theoretical simulation of threshold current dependence on the temperature for different carrier confinement configurations [112].

As mentioned before, lasing in QDs was first demonstrated in laser diodes. However, as multilayer QD stacks were well developed, they were also successfully implemented in SDLs. Many of these results will be extensively discussed in this thesis. The advantages of QDs were also demonstrated in QD SDL with temperature stable threshold, slope efficiency and emission wavelength operation [21]. However, to date there are very little publications reporting temperature performance in QD SDLs. Thus, deeper research in this field would be of great interest and would help to increase the efficiency of QD SDLs.

1.6.2. The fabrication of Quantum Dots

After the successful development of QW heterojunctions and their applications in optoelectronics [5], the potential of lower dimension of structures was realized. First attempts to reduce dimensionality in semiconductors were realized by placing a QW laser

in a high magnetic field perpendicular to the QW plane in 1982. In this configuration, charge carriers were confined in two or all three dimensions and a strong reduction of threshold current dependence on temperature was reported [113]. After this successful demonstration, the first semiconductor QDs were grown embedded in a glass matrix [114]. However, the breakthrough for real optoelectronic applications came after QDs were successfully fabricated in a semiconductor matrix [115].

Epitaxial growth using molecular beam epitaxy (MBE) technique became a standard for fabrication of III-V semiconductor QDs. In MBE growth, semiconductor components in the form of chemical vapour are deposited over the heated substrate to form thin epitaxial layers. MBE technology has many degrees of parameter control and thus epitaxial deposition of high structural quality and high purity of semiconductor layers with few angstrom precision is possible.

As quantum wells were grown layer after layer with constant thickness across the growth region, the fabrication of QDs involve more complex processes as under certain conditions the atoms of deposited materials tend to reorganize themselves and form QDs. For QD SDLs there are a few growth regimes that are usually used, namely the Stranski-Krastanow and sub-monolayer regimes.

Self-formation of QDs mainly employs artificially created strain between deposited layers. A defect free epitaxial growth can be performed when the lattice constants between the grown materials are the same. If a small variation in lattice constant exists, an approximate match is still possible. In such cases, if there is an elastic strain in the interface, the atoms are slightly displaced from their positions in the interfaces between the different materials and the strain energy is stored in the crystal [108]. For example, this is the case in the

growth of GaAs/AlAs heterostructures where the lattice mismatch is about 0.1%. However, many III-V material compositions have much higher lattice mismatch. For example, the lattice mismatch between GaAs and InAs is 7% and after exceeding the critical thickness, defects start forming to reduce the strain. When growing QWs, this should be well managed to produce high quality structures. At the same time, it limits the materials' usage for certain spectral ranges [49].

Contrary to the growth of QWs, the relaxation of elastic strain energy in deposited lattice mismatched layers is the driving force in the formation of QDs. In the Stranski-Krastanow (S-K) growth regime, a semiconductor material is deposited on top of another material with a lattice constant a few percent smaller thus creating a tension force between the layers [116]. In the first few atomic layers, atoms arrange themselves and form a plane layer called a wetting layer. With further growth after the critical thickness is reached, spontaneous formation of QDs starts in order to reduce the strain energy in the layer. Thus, such QDs are often called self-assembled. For InGaAs QDs in GaAs, the critical thickness of InGaAs is from 1.7 to 4 mono-layers depending on the mole fraction value of indium [117, 118]. QDs are formed with a typical areal density of $10^9 – 10^{11}$ cm^{-2}. QDs are then overgrown with the host material and another layer of them is then formed in case of multilayer growth. The S-K growth regime is usually used to form InAs/GaAs, InP/GaInP or Ge/Si QDs [108]. Fig. 1.18 shows transmission electron microscopy (TEM) images of the areal view of InAs S-K grown QDs and the cross-section of a multilayer InGaAs QD sample [119].

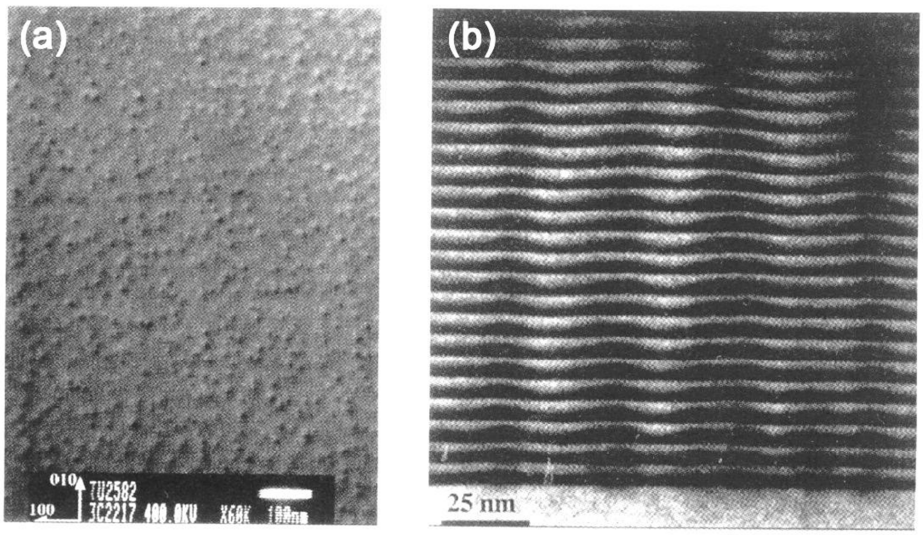

Fig. 1.18. (a) A TEM image of a single sheet of InAs quantum dots grown on GaAs. (b) A TEM image of a cross-section of a 25 layer thick stack of InGaAs quantum dots (thicker dark regions) grown on GaAs substrate (lighter area in the bottom of the picture and surrounding the InGaAs layers). The QDs are connected within the layers by the wetting layers (thin dark regions).

It was shown that the existence of the wetting layer sets a limit in the performance of QDs in terms of relaxation dynamics and confinement energy as charge carriers are captured and reemittted into QDs through the wetting layer as well, as the wetting layer also creates energy states in addition to the localized QD states [120-122]. To avoid this obstacle, the sub-monolayer (SML) QD growth regime was developed [123, 124]. In this regime, the main difference from the S-K grown QDs is that no wetting layer is formed during the growth process. In SML growth, the material is deposited in cycles by thin layers of sub-monolayer thickness and causes an initial formation of strain in the latice. This layer is then covered by a host material of a few monolayers thickness. The deposited thickness of one layer is below the critical thickness for S-K QDs formation, but when a few of these layers are deposited, QDs are formed due to non-uniform lateral strain distribution caused by the underlying strained islands [125]. Also, SML growth is thought to provide a more uniform

sizes of QDs and typically shows narrower emision spectrum [20, 126]. Fig. 1.19 shows a schematic drawing of both S-K and SML grown QDs.

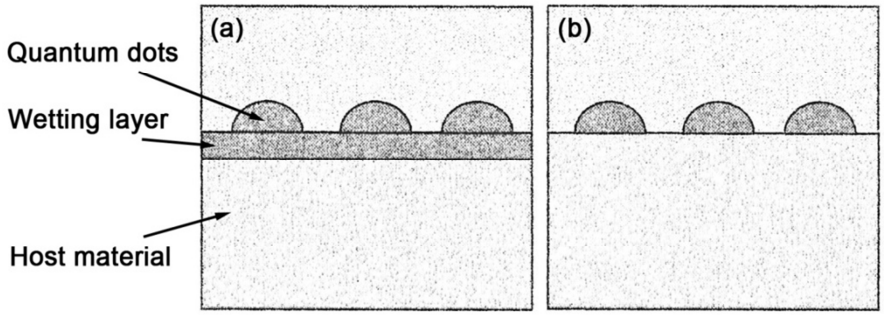

Fig. 1.19. Schematic drawing of (a) Stranski-Krastanow and (b) Sub-monolayer grown quantum dots.

Both S-K and SML QDs were used for different laser sources, edge and surface emitters as well as for other applications. To sum up, S-K QDs are preferred where broad gain bandwidth is necessary, while SML QDs were shown to be more advantageous for thermal stability and have faster carrier dynamics in directly modulated laser sources [127-129]. Both types of QDs were also used in SDLs [20, 39, 130]. In the work presented in this thesis, only S-K grown QDs were used for the SDL active region and SESAMs.

1.6.3. Optical properties of quantum dots

As the QD based SDL is a relatively new field of research, it is neccessary to understand the fundamental properties of QDs that reflect on the performance of the complete devices. Thus, in this chapter QD properties such as the energy levels, gain, emission wavelength and others will be discussed. InGaAs QDs in GaAs will be discussed as these dots were studied most widely and they were used for the research presented in this thesis.

The available energetic levels in QDs and consequently the allowed optical transitions are determined by the arrangment of the atoms and lattice strain in QDs and the surrounding material [108, 131]. Thus, QD parameters such as size, shape and composition mainly determine their optical properties.

As was shown in the densities of states graph (Fig. 1.15), QDs feature distinct strongly localized energy states due to three-dimensional carrier confinement. Theoretically, a QD has a multiple localized energy level system including ground and multiple excited states. In practice, two states – the ground and first excited states are observed and they contribute to the lasing parameters strongly. The ground state (GS) usually can be occupied by two electrons with different spins and first excited state can be occupied by a twofold higher number of carriers due to a higher degeneracy. As a result, theoretically ES transitions support twice higher gain per QD layer as compared to the GS as the saturated gain is linearly proportional to the degeneracy [108, 132, 133]. Fig. 1.20schematically shows the optical gain‘s dependence on the pump current density in a QD based laser diode [108]. In it, contributions from both GS and ES transitions are shown as well as the behaviour of an ideal QD. It can be seen that as the pump current is applied, charge carriers are generated and are localized firstly at the ground state. However, with the increase of pump current, gain from the GS transitions gets saturated and as enough carriers are generated it is then mainly driven by the transitions from the ES. Thus for devices where low operational threshold is required, the operation of the device at the GS transition is advantageous while for high power operation ES may be preferred. The operating transition also depends on the losses in the laser cavity.

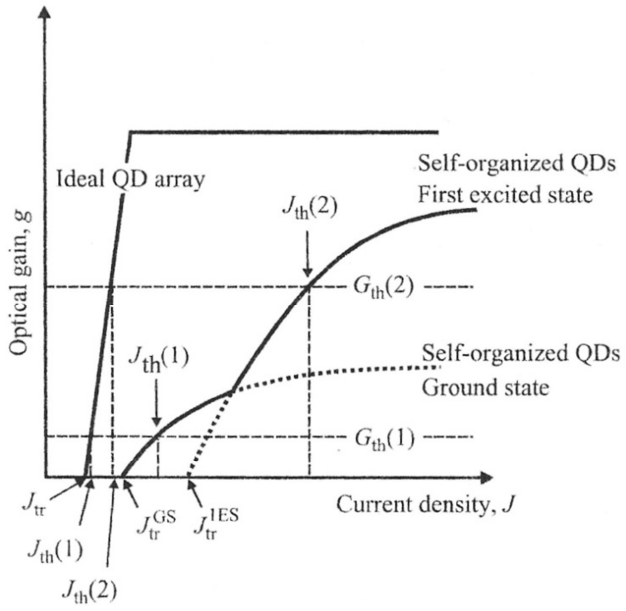

Fig. 1.20. Optical gain dependence on the pump current density in a QD based laser diode. Contributions from both ground and excited states are shown [108].

GS and ES transitions contribute to the different emission wavelengths in the operation of the laser. The spectral gap between these states is about 70 nm and varies depending on the size of the QDs. Practical devices are usually designed for only one of the optical transitions. However, simultaneous two wavelength operation has also been demonstrated and potentially it can be applied for coherent anti-stokes Raman spectroscopy (CARS), THz generation, wavelength division multiplexing and other applications [134, 135]. ES transitions were also shown to be more preferable for QD based SESAM operation [136].

Another important property of QD structures is inhomogeneous spectral broadening. The self-assembly process during the growth of QDs leads to a Gaussian distribution of QD sizes. Thus, although QDs are supposed to have a delta-function-like localized energy states, as is shown by theoretical density of states calculations, the nonuniform sizes of QDs add additional overlaping states and consequently broadens the spectrum of the QD assembly. This process is schematically shown in Fig. 1.21.

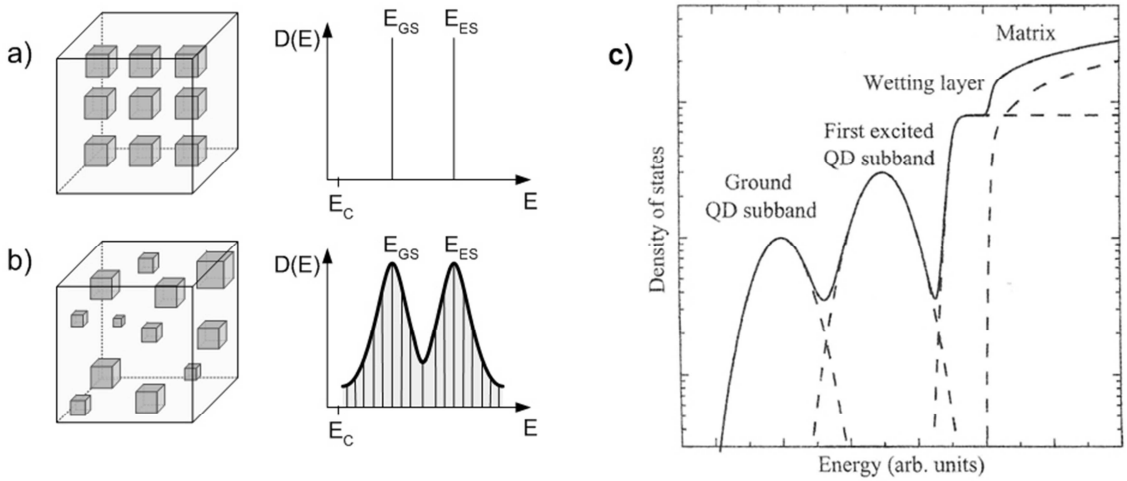

Fig. 1.21. Density of states function in an (a) ideal and (b) real QDs. Density of states for self-assembled QD system is shown in (c) [108].

In Fig. 1.21(a), the ideal case is shown where all QDs are identical in size and two main clearly resolved localized energy states exist, corresponding to the GS and ES. However, in real devices, as is shown case (b), the sizes of dots vary and additional energy states are added to the density of states function. Fig. 1.21 (c) also shows the density of states function in a real QD system, but with the energy of states in the wetting layer and semiconductor matrix added to the overall picture. The last two also often contribute to carrier recombination, especially if the carriers are not confined in QDs effectively [108, 110].

As can be seen, inhomogeneous broadening has a big impact on the shape of the density of states function for QDs. Consequently, this broadens the gain bandwidth and the emission spectrum of the structure. The effect of inhomogeneous broadening is a disadvantage from the reduced dimensionality point of view as the energy states are not delta-function-like anymore. This increases the threshold of lasing and reduces modal and differential gain and reduces the gain saturation value [137, 138]. On the other hand, a broad gain bandwidth is

highly advantageous for ultrashort pulse generation in mode-locked devices as well as for wavelength tuning [139]. Another advantage, especially for SDLs, is that as the gain is constant across a wide spectral range, the temperature sensitivity is partly reduced.

Another important feature of QDs is ultrafast carrier dynamics. It is of particular importance for QDs embedded in saturable absorbers for ultrafast pulse generation. This will be discussed in more detail in the mode-locking chapter of this thesis.

1.7. Chapter conclusions

The development of semiconductor disk lasers was overviewed in the introduction chapter. Also, the to date achievements in output power, wavelength coverage, tunability and SDL mode-locking technology were reviewed. The operation principles of SDL and its key elements were introduced. Also, the existing and potential applications of SDLs were overviewed. The use of quantum dots as SDL gain medium ant their optical properties were introduced. Further chapters will concentrate on the particular QD SDL samples and their design followed by experimental results achieved during the time of studies.

References

[1] T. H. Maiman, "Stimulated Optical Radiation in Ruby," *Nature*, vol. 187, pp. 493-494, 1960.

[2] D. A. Mayer, "Photonics in Europe Economic Impact," European Technology Platform Photonics21, Duseldorf, Germany, 2007.

[3] G. Hall, J. D. Kingsley, T. J. Soltys, R. O. Carlson, "Coherent Light Emission From GaAs Junctions," *Physical Review Letters,* vol. 9, pp. 366–368, 1962.

[4] W. P. D. Marshall, I. Nathan, G.Burns, F.H. Dill, G.Lasher "Stimulated emission of radiation from GaAs p-n junctions," *Applied Physics Letters,* vol. 1, pp. 62-65, 1962.

[5] V. M. A. Zh.I. Alferov, D. Z. Garbuzov, Yu.V. Zhilyaev, E. P. Morozov, E. L. Portnoi, V. G. Trofim, "Investigation of the influence of the AlAs/GaAs heterostructure parameters on the laser threshold current and the realization of continuous emission at room temperature," *Sov. Phys.-Semicond.,* vol. 9, pp. 1573–1575, 1971.

[6] D. F. Welch, "A brief history of high-power semiconductor lasers," *IEEE Journal of Selected Topics in Quantum Electronics,* vol. 6, pp. 1470-1477, 2000.

[7] M. Sagawa, T. Toyonaka, K. Hiramoto, K. Shinoda, K. Uomi, "High-power highly-reliable operation of 0.98 µm InGaAs-InGaPstrain-compensated single-quantum-well lasers with tensile-strained InGaAsP barriers," *IEEE Journal of Selected Topics in Quantum Electronics,* vol. 1, pp. 189-195,1995.

[8] L. J. Mawst, A. Bhattacharya, J. Lopez, D. Botez, D. Z. Garbuzov, L. DeMarco, J. C. Connolly, M. Jansen, F. Fang, and R. F. Nabiev, "8 W continuous wave front-facet power from broad-waveguide Al-free 980 nm diode lasers," *Applied Physics Letters,* vol. 69, pp. 1532-1534, 1996.

[9] A. Al-Muhanna, L. J. Mawst, D. Botez, D. Z. Garbuzov, R. U. Martinelli, and J. C. Connolly, "High-power (> 10 W) continuous-wave operation from 100µm aperture 0.97µm emitting Al-free diode lasers," *Applied Physics Letters,* vol. 73, pp. 1182-1184, 1998.

[10] A. Haglund, J. S. Gustavsson, J. Vukusic, P. Modh, and A. Larsson, "Single fundamental-mode output power exceeding 6 mW from VCSELs with a shallow surface relief," *IEEE Photonics Technology Letters,* vol. 16, pp. 368-370, 2004.

[11] L. A. D'Asaro, J. F. Seurin, and J. D. Wynn, "High-power, high-efficiency VCSELs pursue the goal," *Photonics Spectra,* vol. 39, pp. 62, 2005.

[12] J. F. Seurin, L. A. D'Asaro, and C. Ghosh, "A new application for VCSELs: High-power pump lasers - Recent advances in vertical-cavity surf ace-emitting lasers yield novel high-power, high-reliability lasers for industry, medicine and defense," *Photonics Spectra,* vol. 41, pp. 66, 2007.

[13] C. Stewen, K. Contag, M. Larionov, A. Giesen, and H. Hugel, "A 1-kW CW thin disc laser," *IEEE Journal of Selected Topics in Quantum Electronics,* vol. 6, pp. 650-657, 2000.

[14] A. Giesen and J. Speiser, "Fifteen years of work on thin-disk lasers: Results and scaling laws," *IEEE Journal of Selected Topics in Quantum Electronics,* vol. 13, pp. 598-609, 2007.

[15] N. G. Basov, O. V. Bogdankevich, and A. Z. Grasyuk, "Semiconductor lasers with radiating mirrors," *IEEE Journal of Quantum Electronics,* vol. 2, pp. 594-597, 1966.

[16] Bogdanke.Ov, S. A. Darznek, A. N. Pechenov, B. I. Vasiliev, and M. M. Zverev, "Semiconductor electron-beam-pumped lasers of radiating mirror type",*IEEE Journal of Quantum Electronics,* vol. QE 9, pp. 342-347, 1973.

[17] H. Q. Le, S. Dicecca, and A. Mooradian, "Scalable high-power optically pumped GaAs-laser," *Applied Physics Letters,* vol. 58, pp. 1967-1969, 1991.

[18] M. Kuznetsov, F. Hakimi, R. Sprague, and A. Mooradian, "Design and characteristics of high-power (> 0.5-W CW) diode-pumped vertical-external-cavity surface-emitting semiconductor lasers with circular TEM_{00} beams," *IEEE Journal of Selected Topics in Quantum Electronics*, vol. 5, pp. 561-573, 1999.

[19] J. A. Lott, A. R. Kovsh, N. N. Ledentsov, D. Bimberg, "*GaAs-Based InAs/InGaAs quantum dot vertical cavity and vertical external cavity surface emitting lasers emitting near 1300 nm*," Pacific Rim Conference onLasers and Electro-Optics, pp. 160 – 161, Tokyo, Japan, 2005.

[20] T. D. Germann, A. Strittmatter, U. W. Pohl, D. Bimberg, J. Rautiainen, M. Guina, and O. G. Okhotnikov, "Quantum-dot semiconductor disk lasers," *Journal of Crystal Growth*, vol. 310, pp. 5182-5186, 2008.

[21] T. D. Germann, A. Strittmatter, J. Pohl, U. W. Pohl, D. Bimberg, J. Rautiainen, M. Guina, and O. G. Okhotnikov, "Temperature-stable operation of a quantum dot semiconductor disk laser," *Applied Physics Letters*, vol. 93, 051104, 2008.

[22] J. Chilla, Q. Z. Shu, H. L. Zhou, E. Weiss, M. Reed, and L. Spinelli, "Recent advances in optically pumped semiconductor lasers," *Solid State Lasers XVI: Technology and Devices*, vol. 6451, H. J. Hoffman, R. K. Shori, and N. Hodgson, Eds., Bellingham, SPIE-Int. Soc. Optical Engineering, pp. 45109-45109, 2007.

[23] B. Rudin, A. Rutz, M. Hoffmann, D. Maas, A. R. Bellancourt, E. Gini, T. Suedmeyer, and U. Keller, "Highly efficient optically pumped vertical-emitting semiconductor laser with more than 20 W average output power in a fundamental transverse mode," *Optics Letters*, vol. 33, pp. 2719-2721, 2008.

[24] J. D. Berger, D. W. Anthon, A. Caprara, J. L. Chilla, S. V. Govorkov, A. Y. Lepert, W. Mefferd, Q. Shu, and L. Spinelli, "20-watt CW TEM00 intracavity doubled

optically pumped semiconductor laser at 532 nm," SPIE Photonics West, San Francisco, US, 2012.

[25] T. Wang, J. Hader, Y. Kaneda, J. V. Moloney, B. Kunert, and W. Stolz, "Strategies for power scaling VECSELs," SPIE Photonics West, San Francisco, US, 2012.

[26] E. J. Saarinen, A. Harkonen, S. Suomalainen, and O. G. Okhotnikov, "Power scalable semiconductor disk laser using multiple gain cavity," *Optics Express,* vol. 14, pp. 12868-12871,2006.

[27] V. M. Korpijärvi, T. Leinonen, J. Puustinen, A. Härkönen, and M. D. Guina, "11 W single gain-chip dilute nitride disk laser emitting around 1180 nm," *Optics Express,* vol. 18, pp. 25633-25641, 2010.

[28] J. Konttinen, A. Harkonen, P. Tuomisto, M. Guina, J. Rautiainen, M. Pessa, and O. Okhotnikov, "High-power (> 1 W) dilute nitride semiconductor disk laser emitting at 1240 nm," *New Journal of Physics*, vol. 9, 140, 2007.

[29] Y. Kaneda, M. Fallahi, J. Hader, J. V. Moloney, S. W. Koch, B. Kunert, and W. Stoltz, "Continuous-wave single-frequency 295 nm laser source by a frequency-quadrupled optically pumped semiconductor laser," *Optics Letters,* vol. 34, pp. 3511-3513, 2009.

[30] J. Rautiainen, A. Harkonen, P. Tuornisto, J. Konttinen, L. Orsila, M. Guina, and O. G. Okhotnikov, "1 W at 617 nm generation by intracavity frequency conversion in semiconductor disk laser," *Electronics Letters*, vol. 43, pp. 980-981, 2007.

[31] J. E. Hastie, L. G. Morton, A. J. Kemp, M. D. Dawson, A. B. Krysa, and J. S. Roberts, "Tunable ultraviolet output from an intracavity frequency-doubled red vertical-external-cavity surface-emitting laser," *Applied Physics Letters,* vol. 89, 061114, 2006.

[32] P. J. Schlosser, J. E. Hastie, S. Calvez, A. B. Krysa, and M. D. Dawson, "InP/AlGaInP quantum dot semiconductor disk lasers for CW TEM_{00} emission at 716-755 nm," *Optics Express,* vol. 17, pp. 21782-21787, 2009.

[33] J. Lyytikainen, J. Rautiainen, L. Toikkanen, A. Sirbu, A. Mereuta, A. Caliman, E. Kapon, and O. G. Okhotnikov, "1.3 µm optically-pumped semiconductor disk laser by wafer fusion," *Optics Express,* vol. 17, pp. 9047-9052, 2009.

[34] H. Lindberg, A. Strassner, E. Gerster, and A. Larsson, "0.8W optically pumped vertical external cavity surface emitting laser operating CW at 1550 nm," *Electronics Letters,* vol. 40, pp. 601-602, 2004.

[35] A. Harkonen, M. Guina, O. Okhotnikov, K. Rossner, M. Hummer, T. Lehnhardt, M. Muller, A. Forchel, and M. Fischer, "1-W antimonide-based vertical external cavity surface emitting laser operating at 2 µm," *Optics Express,* vol. 14, pp. 6479-6484, 2006.

[36] A. Khiar, M. Rahim, M. Fill, F. Felder, F. Hobrecker, and H. Zogg, "Continuously tunable monomode mid-infrared vertical external cavity surface emitting laser on Si," *Applied Physics Letters,* vol. 97, 151104, 2010.

[37] M. Kuznetsov, "VECSEL Semiconductor Lasers: A path to High-Power, Quality Beam and UV to IR Wavelength by Design," in *Semiconductor Disk Lasers: Physics and Technology*, O. G. Okhotnikov, Ed., Weinheim: Wiley-VCH Verlag GmbH & Co. KGaA, pp. 1-71, 2010.

[38] M. Hoffmann, W.P. Pallmann, O.D. Sieber, V.J. Wittwer, I.L. Krestnikov, S.S. Mikhrin, D.A. Livshits, G. Malcolm, C. Hamilton, Y. Barbarin, T. Sudmeyer, and U. Keller, "All Quantum-Dot Based SESAM modelocked VECSEL with sub-

picosecond Pulses," The 4th EPS-QEOD Europhoton Conference, Hamburg, Germany, 2010.

[39] M. Butkus, K. G. Wilcox, J. Rautiainen, O. G. Okhotnikov, S. S. Mikhrin, I. L. Krestnikov, A. R. Kovsh, M. Hoffmann, T. Sudmeyer, U. Keller, and E. U. Rafailov, "High-power quantum-dot-based semiconductor disk laser," *Optics Letters*, vol. 34, pp. 1672-1674, 2009.

[40] J. Rautiainen, I. Krestnikov, M. Butkus, E. U. Rafailov, and O. G. Okhotnikov, "Optically pumped semiconductor quantum dot disk laser operating at 1180 nm," *Optics Letters*, vol. 35, pp. 694-696, 2010.

[41] M. Butkus, J. Rautiainen, O. G. Okhotnikov, S. S. Mikhrin, I. L. Krestnikov, E. U. Rafailov, "*1270 nm Quantum Dot Based Semiconductor Disk Lasers*," 22nd IEEE International Semiconductor Laser Conference, Kyoto, Japan, 2010.

[42] A. R. Albrecht, T. J. Rotter, C. P. Hains, A. Stintz, J. V. Moloney, K. J. Malloy, and G. Balakrishnan, "Multi-watt 1.25 μm quantum dot VECSEL," *Electronics Letters*, vol. 46, pp. 856, 2010.

[43] S. Calvez, J. E. Hastie, A. J. Kemp, N. Laurand, and M. D. Dawson, "Thermal Management, Structure Design, and Integration Considerations for VECSELs," in *Semiconductor Disk Lasers: Physics and Technology*, O. G. Okhotnikov, Ed., Darmstadt: Wiley-VCH Verlag GmbH & Co., pp. 73-117, 2010.

[44] J. E. Hastie, S. Calvez, M. D. Dawson, T. Leinonen, A. Laakso, J. Lyytikainen, and M. Pessa, "High power CW red VECSEL with linearly polarized TEM_{00} output beam," *Optics Express*, vol. 13, pp. 77-81, 2005.

[45] J. E. Hastie, J. M. Hopkins, S. Calvez, C. W. Jeon, D. Burns, R. Abram, E. Riis, A. I. Ferguson, and M. D. Dawson, "0.5-W single transverse-mode operation of an

850-nm diode-pumped surface-emitting semiconductor laser," *IEEE Photonics Technology Letters*, vol. 15, pp. 894-896, 2003.

[46] R. Abram, M. Schmid, E. Riis, and A. I. Ferguson, “Optically pumped VECSELs for high resolution spectroscopy: The new Ti:Sapphire,” in *Laser Spectroscopy XVI*, pp. 369-373, 2004.

[47] M. Butkus, J. Rautiainen, O. G. Okhotnikov, C. J. Hamilton, G. P. A. Malcolm, S. S. Mikhrin, I. L. Krestnikov, D. A. Livshits, and E. U. Rafailov, "Quantum Dot Based Semiconductor Disk Lasers for 1-1.3 µm," *IEEE Journal of Quantum Electronics*, vol. 17, pp. 1763-1771, 2011.

[48] L. Fan, C. Hessenius, M. Fallahi, J. Hader, H. Li, J. V. Moloney, W. Stolz, S. W. Koch, J. T. Murray, and R. Bedford, "Highly strained InGaAs/GaAs multiwatt vertical-external-cavity surface-emitting laser emitting around 1170 nm," *Applied Physics Letters*, vol. 91, 131114, 2007.

[49] S. L. Vetter, J. E. Hastie, V. M. Korpijarvi, J. Puustinen, M. Guina, O. Okhotnikov, S. Calvez, and M. D. Dawson, "Short-wavelength GaInNAs/GaAs semiconductor disk lasers," *Electronics Letters*, vol. 44, pp. 1069-1070, 2008.

[50] J. Paajaste, S. Suomalainen, R. Koskinen, A. Harkonen, M. Guina, and M. Pessa, "High-power and broadly tunable GaSb-based optically pumped VECSELs emitting near 2 µm," *Journal of Crystal Growth*, vol. 311, pp. 1917-1919, 2009.

[51] D. Burns, J. M. Hopkins, A. J. Kemp, B. Rosener, N. Schulz, C. Manz, K. Kohler, M. Rattunde, and J. Wagner, "Recent developments in high-power, short-wave mid-infrared semiconductor disk lasers," in *Solid State Lasers Xviii: Technology and Devices*. vol. 7193, W. A. Clarkson, N. Hodgson, and R. K. Shori, Eds., Bellingham: SPIE-Int. Soc. Optical Engineering, 2009.

[52] E. U. Rafailov, S. J. White, A. A. Lagatsky, A. Miller, W. Sibbett, D. A. Livshits, A. E. Zhukov, and V. M. Ustinov, "Fast quantum-dot saturable absorber for passive mode-locking of solid-state lasers," *IEEE Photonics Technology Letters*, vol. 16, pp. 2439-2441, 2004.

[53] D. Maas, A. R. Bellancourt, M. Hoffmann, B. Rudin, Y. Barbarin, M. Golling, T. Sudmeyer, and U. Keller, "Growth parameter optimization for fast quantum dot SESAMs," *Optics Express,* vol. 16, pp. 18646-18656, 2008.

[54] A. A. Lagatsky, C. G. Leburn, C. T. A. Brown, W. Sibbett, S. A. Zolotovskaya, and E. U. Rafailov, "Ultrashort-pulse lasers passively mode locked by quantum-dot-based saturable absorbers," *Progress in Quantum Electronics*, vol. 34, pp. 1-45, 2010.

[55] S. Hoogland, S. Dhanjal, A. C. Tropper, J. S. Roberts, R. Haring, R. Paschotta, F. Morier-Genoud, and U. Keller, "Passively mode-locked diode-pumped surface-emitting semiconductor laser," *IEEE Photonics Technology Letters,* vol. 12, pp. 1135-1137, 2000.

[56] A. H. Quarterman, K. G. Wilcox, V. Apostolopoulos, Z. Mihoubi, S. P. Elsmere, I. Farrer, D. A. Ritchie, and A. Tropper, "A passively mode-locked external-cavity semiconductor laser emitting 60-fs pulses," *Nature Photonics,* vol. 3, pp. 729-731, 2009.

[57] A. Aschwanden, D. Lorenser, H. J. Unold, R. Paschotta, E. Gini, and U. Keller, "2.1-W picosecond passively mode-locked external-cavity semiconductor laser," *Optics Letters,* vol. 30, pp. 272-274, 2005.

[58] K. G. Wilcox, A. H. Quarterman, H. Beere, D. A. Ritchie, and A. C. Tropper, "High Peak Power Femtosecond Pulse Passively Mode-Locked Vertical-External-Cavity

Surface-Emitting Laser," *IEEE Photonics Technology Letters,* vol. 22, pp. 1021-1023, 2010.

[59] D. Lorenser, D. Maas, H. J. Unold, A. R. Bellancourt, B. Rudin, E. Gini, D. Ebling, and U. Keller, "50-GHz passively mode-locked surface-emitting semiconductor laser with 100-mW average output power," *IEEE Journal of Quantum Electronics,* vol. 42, pp. 838-847, 2006.

[60] A. H. Quarterman, A. Perevedentsev, K. G. Wilcox, V. Apostolopoulos, H. E. Beere, I. Farrer, D. A. Ritchie, and A. C. Tropper, "Passively harmonically mode-locked vertical-external-cavity surface-emitting laser emitting 1.1 ps pulses at 147 GHz repetition rate," *Applied Physics Letters*, vol. 97, 251101, 2010.

[61] O. Casel, D. Woll, M. A. Tremont, H. Fuchs, R. Wallenstein, E. Gerster, P. Unger, M. Zorn, and M. Weyers, "Blue 489-nm picosecond pulses generated by intracavity frequency doubling in a passively mode-locked optically pumped semiconductor disk laser," *Applied Physics B-Lasers and Optics,* vol. 81, pp. 443-446, 2005.

[62] A. Rutz, V. Liverini, D. Maas, B. Rudin, A. R. Bellancourt, S. Schon, and U. Keller, "Passively modelocked GaInNAs VECSEL at centre wavelength around 1.3 µm," *Electronics Letters,* vol. 42, pp. 926-928, 2006.

[63] H. Lindberg, M. Sadeghi, M. Westlund, S. M. Wang, A. Larsson, M. Strassner, and S. Marcinkevicius, "Mode locking a 1550 nm semiconductor disk laser by using a GaInNAs saturable absorber," *Optics Letters,* vol. 30, pp. 2793-2795, 2005.

[64] A. Harkonen, J. Rautiainen, L. Orsila, M. Guina, K. Rossner, M. Hummer, T. Lehnhardt, M. Muller, A. Forchel, M. Fischer, J. Koeth, and O. G. Okhotnikov, "2-µm mode-locked semiconductor disk laser synchronously pumped using an

amplified diode laser," *IEEE Photonics Technology Letters*, vol. 20, pp. 1332-1334, 2008.

[65] T. Sudmeyer, D. Maas, and U. Keller, "Mode-Locked Semiconductor Disk Lasers," in *Semiconductor Disk Lasers: Physics and Technology*, O. G. Okhotnikov, Ed., Darmstadt: Wiley-VCH Verlag GmbH & Co., pp. 213-261, 2010.

[66] B. Rudin, V. J. Wittwer, D. Maas, M. Hoffmann, O. D. Sieber, Y. Barbarin, M. Golling, T. Sudmeyer, and U. Keller, "High-power MIXSEL: an integrated ultrafast semiconductor laser with 6.4 W average power," *Optics Express*, vol. 18, pp. 27582-27588,2010.

[67] K. G. Wilcox, M. Butkus, I. Farrer, D. A. Ritchie, A. Tropper, and E. U. Rafailov, "Subpicosecond quantum dot saturable absorber mode-locked semiconductor disk laser," *Applied Physics Letters*, vol. 94, 251105, 2009.

[68] M. Hoffmann, Y. Barbarin, D. Maas, A. R. Bellancourt, M. Shafiei, M. Golling, T. Sudmeyer, U. Keller, I. L. Krestnikov, S. S. Mikhrin, A. R. Kovsh, “All Quantum Dot Modelocked Vertical External Cavity Surface Emitting Laser,” *CLEO/QELS*, Munich, Germany, 2009.

[69] M. Hoffmann, O. D. Sieber, V. J. Wittwer, I. L. Krestnikov, D. A. Livshits, Y. Barbarin, T. Sudmeyer, and U. Keller, "Femtosecond high-power quantum dot vertical external cavity surface emitting laser," *Optics Express*, vol. 19, pp. 8108-8116, 2011.

[70] B. Resan, E. Coadou, S. Petersen, A. Thomas, P. Walther, R. Viselga, J. M. Heritier, J. Chilla, W. Tulloch, and A. Fry, "Ultrashort pulse Ti : Sapphire oscillators pumped by optically pumped semiconductor (OPS) pump lasers - art. no. 687116," in *Solid State Lasers Xvii: Technology and Devices*. vol. 6871, W. A.

Clarkson, N. H. Hodgson, and R. K. Shori, Eds., Bellingham: SPIE-Int. Soc. Optical Engineering, pp. 87116-87116, 2008.

[71] S. L. Vetter, L. J. McKnight, S. Calvez, M. D. Dawson, F. Fusari, A. A. Lagatsky, W. Sibbett, C. T. A. Brown, V. M. Korpijarvi, M. Guina, B. Richards, G. Jose, and A. Jha, "GaInNAs semiconductor disk lasers as pump sources for Tm(3+)(,Ho(3+))-doped glass, crystal and fibre lasers," in *Solid State Lasers Xviii: Technology and Devices*. vol. 7193, W. A. Clarkson, N. Hodgson, and R. K. Shori, Eds., Bellingham: SPIE-Int. Soc. Optical Engineering, 2009.

[72] D. C. Parrotta, W. Lubeigt, A. J. Kemp, D. Burns, M. D. Dawson, and J. E. Hastie, "Continuous-wave Raman laser pumped within a semiconductor disk laser cavity," *Optics Letters*, vol. 36, pp. 1083-1085, 2011.

[73] D. J. M. Stothard, J. M. Hopkins, D. Burns, and M. H. Dunn, "Stable, continuous-wave, intracavity, optical parametric oscillator pumped by a semiconductor disk laser (VECSEL)," *Optics Express*, vol. 17, pp. 10648-10658, 2009.

[74] G. K. Samanta and M. Ebrahim-Zadeh, "High-power, continuous-wave, optical parametric oscillator pumped by an optically pumped semiconductor laser at 532 nm," *Optics Letters*, vol. 35, pp. 1986-1988, 2010.

[75] L. Fan, M. Fallahi, J. Hader, A. R. Zakharian, M. Kolesik, J. V. Moloney, T. Qiu, A. Schulzgen, N. Peyghambarian, W. Stolz, S. W. Koch, and J. T. Murray, "Over 3 W high-efficiency vertical-external-cavity surface-emitting lasers and application as efficient fiber laser pump sources," *Applied Physics Letters*, vol. 86, 211116, 2005.

[76] G. E. Giudice, S. C. Guy, S. G. Crigler, L. A. Zenteno, and B. S. Hallock, "Effect of pump, laser noise on an erbium-doped fiber-amplified signal," *IEEE Photonics Technology Letters*, vol. 14, pp. 1403-1405, 2002.

[77] J. B. Schlager, B. E. Callicoatt, R. P. Mirin, N. A. Sanford, D. J. Jones, and J. Ye, "Passively mode-locked glass waveguide laser with 14-fs timing jitter," *Optics Letters,* vol. 28, pp. 2411-2413, 2003.

[78] E. Esposito, S. Keatings, K. Gardner, J. Harris, E. Riis, and G. McConnell, "Confocal laser scanning microscopy using a frequency doubled vertical external cavity surface emitting laser," *Review of Scientific Instruments,* vol. 79, 083702, 2008.

[79] M. Schulze, "OPSLs for quick flow cytometry," *Optik & Photonik,* vol. 4, pp. 41-43, 2010.

[80] T. K. Lake, A. E. Carruthers, L. Paterson, M. Taylor, F. Gunn-Moore, J. W. Allen, W. Sibbett, and K. Dholakia, "Optical trapping and fluorescence excitation with violet diode lasers and extended cavity surface emitting lasers," *Optics Express,* vol. 12, pp. 670-678, 2004.

[81] A. Masters, "Yellow Lasers Target Macular Degeneration," *Biophotonics International,* vol. 14, 2007.

[82] A. Garnache, A. A. Kachanov, F. Stoeckel, and R. Houdre, "Diode-pumped broadband vertical-external-cavity surface-emitting semiconductor laser applied to high-sensitivity intracavity absorption spectroscopy," *Journal of the Optical Society of America B-Optical Physics,* vol. 17, pp. 1589-1598, 2000.

[83] M. Scheller, J. M. Yarborough, J. V. Moloney, M. Fallahi, M. Koch, and S. W. Koch, "Room temperature continuous wave milliwatt terahertz source," *Optics Express,* vol. 18, pp. 27112-27117, 2010.

[84] Z. Mihoubi, K. G. Wilcox, S. Elsmere, A. Quarterman, R. Rungsawang, I. Farrer, H. E. Beere, D. A. Ritchie, A. Tropper, and V. Apostolopoulos, "All-semiconductor

room-temperature terahertz time domain spectrometer," *Optics Letters*, vol. 33, pp. 2125-2127, 2008.

[85] N. Schulz, J. M. Hopkins, M. Rattunde, D. Burns, and J. Wagner, "High-brightness long-wavelength semiconductor disk lasers," *Laser & Photonics Reviews*, vol. 2, pp. 160-181, 2008.

[86] B. Jean and T. Bende, "Mid-IR laser applications in medicine," *Solid-State Mid-Infrared Laser Sources*, vol. 89, pp. 511-544, 2003.

[87] J. T. Olesberg, "Noninvasive blood glucose monitoring in the 2.0-2.5 µm wavelength range," in *LEOS 2001: 14th Annual Meeting of the IEEE Lasers &Electro-Optics Society, Vols 1 and 2, Proceedings*, pp. 529-529, 2001.

[88] V. M. Korpijarvi, M. Guina, J. Puustinen, P. Tuomisto, J. Rautiainen, A. Harkonen, A. Tukiainen, O. Okhotnikov, and M. Pessa, "MBE grown GaInNAs-based multi-Watt disk lasers," *Journal of Crystal Growth*, vol. 311, pp. 1868-1871, 2009.

[89] R. Aviles-Espinosa, G. Filippidis, C. Hamilton, G. Malcolm, K. J. Weingarten, T. Sudmeyer, Y. Barbarin, U. Keller, S. I. C. O. Santos, D. Artigas, and P. Loza-Alvarez, "Compact ultrafast semiconductor disk laser: targeting GFP based nonlinear applications in living organisms," *Biomedical optics express*, vol. 2, pp. 739-47, 2011.

[90] B. J. Stevens, D. T. D. Childs, K. M. Groom, M. Hopkinson, and R. A. Hogg, "All semiconductor swept laser source utilizing quantum dots," *Applied Physics Letters*, vol. 91, 121119, 2007.

[91] X. D. Li, S. Martin, C. Pitris, R. Ghanta, D. L. Stamper, M. Harman, J. G. Fujimoto, and M. E. Brezinski, "High-resolution optical coherence tomographic imaging of

osteoarthritic cartilage during open knee surgery," *Arthritis Research & Therapy,* vol. 7, pp. R318-R323, 2005.

[92] S. W. Corzine, R. S. Geels, J. W. Scott, R. H. Yan, and L. A. Coldren, "Design of Fabry-Perot surface-emitting lasers with a periodic gain structure," *IEEE Journal of Quantum Electronics,* vol. 25, pp. 1513-1524, 1989.

[93] M. Y. A. Raja, S. R. J. Brueck, M. Osinski, C. F. Schaus, J. G. McInerney, T. M. Brennan, and B. E. Hammons, "Resonant periodic gain surface-emitting semiconductor-lasers," *IEEE Journal of Quantum Electronics,* vol. 25, pp. 1500-1512, 1989.

[94] C. P. Lee, C. M. Tsai, and J. S. Tsang, "Dual-wavelength Bragg reflectors using GaAs/AlAs multilayers," *Electronics Letters,* vol. 29, pp. 1980-1981, 1993.

[95] A. Rantamaki, A. Sirbu, A. Mereuta, E. Kapon, and O. G. Okhotnikov, "3 W of 650 nm red emission by frequency doubling of wafer-fused semiconductor disk laser," *Optics Express,* vol. 18, pp. 21645-21650, 2010.

[96] J. Lyytikainen, J. Rautiainen, A. Sirbu, V. Iakovlev, A. Laakso, S. Ranta, M. Tavast, E. Kapon, and O. G. Okhotnikov, "High-Power 1.48 µm Wafer-Fused Optically Pumped Semiconductor Disk Laser," *IEEE Photonics Technology Letters,* vol. 23, pp. 917-919, 2011.

[97] M. Schmid, S. Benchabane, F. Torabi-Goudarzi, R. Abram, A. I. Ferguson, and E. Riis, "Optical in-well pumping of a vertical-external-cavity surface-emitting laser," *Applied Physics Letters,* vol. 84, pp. 4860-4862, 2004.

[98] S. S. Beyertt, U. Brauch, F. Demaria, N. Dhidah, A. Giesen, T. Kubler, S. Lorch, F. Rinaldi, and P. Unger, "Efficient gallium-arsenide disk laser," *IEEE Journal of Quantum Electronics,* vol. 43, pp. 869-875, 2007.

[99] R. G. Bedford, M. Kolesik, J. L. A. Chilla, M. K. Reed, T. R. Nelson, and J. V. Moloney, "Power-limiting mechanisms in VECSELs," in *Enabling Photonics Technologies for Defense, Security, and Aerospace Applications*. vol. 5814, A. R. Pirich, Ed., Bellingham: SPIE-Int. Soc. Optical Engineering, pp. 199-208, 2005.

[100] A. J. Kemp, G. J. Valentine, J. M. Hopkins, J. E. Hastie, S. A. Smith, S. Calvez, M. D. Dawson, and D. Burns, "Thermal management in vertical-external-cavity surface-emitting lasers: Finite-element analysis of a heatspreader approach," *IEEE Journal of Quantum Electronics,* vol. 41, pp. 148-155, 2005.

[101] S. Giet, A. J. Kemp, D. Burns, S. Calvez, M. D. Dawson, S. Suomalainen, A. Harkonen, M. Guina, O. Okhotnikov, and M. Pessa, "Comparison of thermal management techniques for semiconductor disk lasers - art. no. 687115," in *Solid State Lasers Xvii: Technology and Devices*. vol. 6871, W. A. Clarkson, N. H. Hodgson, and R. K. Shori, Eds., Bellingham: SPIE-Int. Soc. Optical Engineering, pp. 87115-87115, 2008.

[102] P. Millar, R. B. Birch, A. J. Kemp, and D. Burns, "Synthetic diamond for intracavity thermal management in compact solid-state lasers," *IEEE Journal of Quantum Electronics,* vol. 44, pp. 709-717, 2008.

[103] J. Rautiainen, A. Rantamäki, M. Butkus, S. S. Mikhrin, I. L. Krestnikov, E. U. Rafailov, and O. G. Okhotnikov, "1.2 µm Quantum Dot Semiconductor Disk Laser with 0.5 W of Output Power," *1st EOS Topical Meeting on Lasers*, Capri, Italy, 2009.

[104] A. J. Kemp, A. J. Maclean, J. M. Hopkins, J. E. Hastie, S. Calvez, M. D. Dawson, and D. Burns, "Thermal management in disc lasers: doped-dielectric and

semiconductor laser gain media in thin-disc and microchip formats," *Journal of Modern Optics,* vol. 54, pp. 1669-1676, 2007.

[105] N. N. Ledentsov, V. M. Ustinov, A. Y. Egorov, A. E. Zhukov, M. V. Maksimov, I. G. Tabatadze, and P. S. Kopev, "Optical-properties of heterostructures with InGaAs-GaAs quantum clusters," *Semiconductors,* vol. 28, pp. 832-834, 1994.

[106] N. Kirstaedter, N. N. Ledentsov, M. Grundmann, D. Bimberg, V. M. Ustinov, S. S. Ruvimov, M. V. Maximov, P. S. Kopev, Z. I. Alferov, U. Richter, P. Werner, U. Gosele, and J. Heydenreich, "Low-threshold, large T-O injection-laser emission from (InGa)As quantum dots," *Electronics Letters,* vol. 30, pp. 1416-1417, 1994.

[107] D. Bimberg, M. Grundmann, F. Heinrichsdorff, N. N. Ledentsov, V. M. Ustinov, A. E. Zhukov, A. R. Kovsh, M. V. Maximov, Y. M. Shernyakov, B. V. Volovik, A. F. Tsatsulnikov, P. S. Kopev, and Z. I. Alferov, "Quantum dot lasers: breakthrough in optoelectronics," *Thin Solid Films,* vol. 367, pp. 235-249, 2000.

[108] V. M. Ustinov, A. E. Zhukov, A. Y. Egorov, and N. A. Maleev, *"Quantum Dot Lasers"*. Oxford: Oxford University Press, 2003.

[109] B. E. A. Saleh and M. C. Teich, *"Fundamentals of Photonics"*, Second Edition New Jersey: John Wiley & Sons, Inc., 2007.

[110] M. A. Cataluna, "Ultrashort-pulse generation from quantum-dot semiconductor diode lasers," PhD thesis, University of St Andrews, St Andrews, 2007.

[111] E. U. Rafailov, M. A. Cataluna, and E. A. Avrutin, *"Ultrafast Lasers based on Quantum Dot Structures: Physics and Devices,"* Weinheim: Wiley-VCH Verlag GmbH & Co, 2011.

[112] Z. I. Alferov, "Nobel Lecture: The double heterostructure concept and its applications in physics, electronics, and technology," *Reviews of Modern Physics*, vol. 73, pp. 767-782, 2001.

[113] Y. Arakawa and H. Sakaki, "Multidimensional quantum well laser and temperature-dependence of its threshold current," *Applied Physics Letters*, vol. 40, pp. 939-941, 1982.

[114] A. I. Ekimov and A. A. Onushchenko, "Quantum size effect in 3-dimensional microscopic semiconductor crystals," *JETP Letters*, vol. 34, pp. 345-349, 1981.

[115] L. Goldstein, F. Glas, J. Y. Marzin, M. N. Charasse, and G. Leroux, "Growth by molecular-beam epitaxy and characterization of InAs/GaAs strained-layer superlattices," *Applied Physics Letters*, vol. 47, pp. 1099-1101, 1985.

[116] N. N. Ledentsov, V. A. Shchukin, M. Grundmann, N. Kirstaedter, J. Bohrer, O. Schmidt, D. Bimberg, V. M. Ustinov, A. Y. Egorov, A. E. Zhukov, P. S. Kopev, S. V. Zaitsev, N. Y. Gordeev, Z. I. Alferov, A. I. Borovkov, A. O. Kosogov, S. S. Ruvimov, P. Werner, U. Gosele, and J. Heydenreich, "Direct formation of vertically coupled quantum dots in Stranski-Krastanow growth," *Physical Review B*, vol. 54, pp. 8743-8750, 1996.

[117] D. Leonard, G. Medeirosribeiro, H. Drexler, K. Pond, W. Hansen, J. P. Kotthaus, and P. M. Petroff, "Progress in self-assembled quantum dots of $In_xGa_{1-x}As$on GaAs," in *Compound Semiconductors 1994*, H. Goronkin and U. Mishra, Eds., Bristol: IOP Publishing Ltd, pp. 819-824, 1995.

[118] A. Y. Egorov, A. E. Zhukov, P. S. Kopev, N. N. Ledentsov, M. V. Maksimov, and V. M. Ustinov, "Effect of deposition conditions on the formation of (InGa)As quantum clusters in a GaAs matrix," *Semiconductors*, vol. 28, pp. 809-811, 1994.

[119] P. Yu and M. Cardona, *"Fundamentals of Semiconductors: physics and materials properties,"* 3 ed. Heidelberg: Springer-Verlag, 2001.

[120] T. Vallaitis, C. Koos, R. Bonk, W. Freude, M. Laemmlin, C. Meuer, D. Bimberg, and J. Leuthold, "Slow and fast dynamics of gain and phase in a quantum dot semiconductor optical amplifier," *Optics Express,* vol. 16, pp. 170-178, 2008.

[121] S. Fathpour, Z. Mi, and P. Bhattacharya, "High-speed quantum dot lasers," *Journal of Physics D-Applied Physics,* vol. 38, pp. 2103-2111, 2005.

[122] D. R. Matthews, H. D. Summers, P. M. Smowton, and M. Hopkinson, "Experimental investigation of the effect of wetting-layer states on the gain-current characteristic of quantum-dot lasers," *Applied Physics Letters,* vol. 81, pp. 4904-4906, 2002.

[123] M. Strassburg, R. Heitz, V. Turck, S. Rodt, U. W. Pohl, A. Hoffmann, D. Bimberg, I. L. Krestnikov, V. A. Shchukin, N. N. Ledentsov, Z. I. Alferov, D. Litvinov, A. Rosenauer, and D. Gerthsen, "Three-dimensionally confined excitons and biexcitons in submonolayer-CdSe/ZnSe superlattices," *Journal of Electronic Materials,* vol. 28, pp. 506-514, 1999.

[124] I. L. Krestnikov, N. N. Ledentsov, A. Hoffmann, and D. Bimberg, "Arrays of two-dimensional islands formed by submonolayer insertions: Growth, properties, devices," *Physica Status Solidi a-Applied Research,* vol. 183, pp. 207-233, 2001.

[125] U. W. Pohl and D. Bimberg, "Semiconductor Disk Lasers Based on Quantum Dots" *Semiconductor Disk Lasers: Physics and Technology*, O. Okhotnikov, Ed., Weinheim: Wiley-Vch, 2010.

[126] Z. C. Xu, D. Birkedal, M. Juhl, and J. M. Hvam, "Submonolayer InGaAs/GaAs quantum-dot lasers with high modal gain and zero-linewidth enhancement factor," *Applied Physics Letters*, vol. 85, pp. 3259-3261, 2004.

[127] N. N. Ledentsov, D. Bimberg, F. Hopfer, A. Mutig, V. A. Shchukin, A. V. Savelev, G. Fiol, E. Stock, H. Eisele, M. Daehne, D. Gerthsen, U. Fischer, D. Litvinov, A. Rosenauer, S. S. Mikhrin, A. R. Kovsh, N. D. Zakharov, and P. Werner, "Submonolayer quantum dots for high speed surface emitting lasers," *Nanoscale Research Letters*, vol. 2, pp. 417-429, 2007.

[128] F. Hopfer, A. Mutig, G. Fiol, M. Kuntz, V. A. Shchukin, V. A. Haisler, T. Warming, E. Stock, S. S. Mikhrin, I. L. Krestnikov, D. A. Livshits, A. R. Kovsh, C. Bornholdt, A. Lenz, H. Eisele, M. Dahne, N. N. Ledentsov, and D. Bimberg, "20 Gb/s 85 degrees C error-free operation of VCSELs based on submonolayer deposition of quantum dots," *IEEE Journal of Selected Topics in Quantum Electronics*, vol. 13, pp. 1302-1308, 2007.

[129] N. N. Ledentsov, F. Hopfer, A. Mutig, V. A. Shchukin, A. V. Savel'ev, G. Fiol, M. Kuntz, V. A. Haisler, T. Warming, E. Stock, S. S. Mikhrin, A. R. Kovsh, C. Bornholdt, A. Lenz, H. Eisele, M. Dahne, N. D. Zakharov, P. Werner, and D. Bimberg, "Novel concepts for ultrahigh-speed quantum-dot VCSELs and edge-emitters," in *Physics and Simulation of Optoelectronic Devices Xv*. vol. 6468, M. Osinski, F. Henneberger, and Y. Arakawa, Eds., Bellingham: SPIE-Int. Soc. Optical Engineering, 2007.

[130] A. R. Albrecht, C. P. Hains, T. J. Rotter, A. Stintz, K. J. Malloy, G. Balakrishnan, and J. V. Moloney, "High power 1.25 μm InAs quantum dot vertical external-cavity

surface-emitting laser," *Journal of Vacuum Science & Technology B,* vol. 29,03C113,2011.

[131] O. Stier, M. Grundmann, and D. Bimberg, "Electronic and optical properties of strained quantum dots modeled by 8-band k center dot p theory," *Physical Review B,* vol. 59, pp. 5688-5701, 1999.

[132] K. Kim, T. B. Norris, S. Ghosh, J. Singh, and P. Bhattacharya, "Level degeneracy and temperature-dependent carrier distributions in self-organized quantum dots," *Applied Physics Letters,* vol. 82, pp. 1959-1961, 2003.

[133] S. W. Osborne, P. Blood, P. M. Smowton, Y. C. Xin, A. Stintz, D. Huffaker, and L. F. Lester, "Optical absorption cross section of quantum dots," *Journal of Physics-Condensed Matter,* vol. 16, pp. S3749-S3756, 2004.

[134] A. Markus, J. X. Chen, C. Paranthoen, A. Fiore, C. Platz, and O. Gauthier-Lafaye, "Simultaneous two-state lasing in quantum-dot lasers," *Applied Physics Letters,* vol. 82, pp. 1818-1820, 2003.

[135] M. A. Cataluna, D. I. Nikitichev, S. Mikroulis, H. Simos, C. Simos, C. Mesaritakis, D. Syvridis, I. Krestnikov, D. Livshits, and E. U. Rafailov, "Dual-wavelength mode-locked quantum-dot laser, via ground and excited state transitions: experimental and theoretical investigation," *Optics Express,* vol. 18, pp. 12832-12838, 2010.

[136] M. P. Lumb, E. Clarke, E. Harbord, P. Spencer, R. Murray, F. Masia, P. Borri, W. Langbein, C. G. Leburn, C. Jappy, N. K. Metzger, C. T. A. Brown, and W. Sibbett, "Ultrafast absorption recovery dynamics of 1300 nm quantum dot saturable absorber mirrors," *Applied Physics Letters,* vol. 95, 041101, 2009.

[137] O. Qasaimeh, "Effect of inhomogeneous line broadening on gain and differential gain of quantum dot lasers," *IEEE Transactions on Electron Devices*, vol. 50, pp. 1575-1581, 2003.

[138] H. Dery and G. Eisenstein, "The impact of energy band diagram and inhomogeneous broadening on the optical differential gain in nanostructure lasers," *IEEE Journal of Quantum Electronics*, vol. 41, pp. 26-35, 2005.

[139] K. A. Fedorova, M. A. Cataluna, I. Krestnikov, D. Livshits, and E. U. Rafailov, "Broadly tunable high-power InAs/GaAs quantum-dot external cavity diode lasers," *Optics Express*, vol. 18, pp. 19438-19443, 2010.

[140] Y. F. Chen, Y. C. Lee, H. C. Liang, K. Y. Lin, K. W. Su, and K. F. Huang, "Femtosecond high-power spontaneous mode-locked operation in vertical-external cavity surface-emitting laser with gigahertz oscillation," *Optics Letters*, vol. 36, pp. 4581-4583, 2011.

2. Design, fabrication and luminescence characterization of the SDL samples

In this chapter the design, growth and fabrication of the samples used in our experiments is overviewed. Also, initial photoluminescence characterisation of the samples is discussed. Samples preparation for the experimental testing is overviewed at the end of the chapter.

2.1. Design of the semiconductor disk lasers

The design of experimental SDL is mainly focussed on the calculation of semiconductor chip parameters. Such a design is based on concepts discussed in chapter 1.4. When designing the active region of SDL a few parameters need to be considered:

- The reflectivity and spectral bandwidth of the DBR
- The number of QD layers
- The emission wavelength and optical transition (GS or ES)
- Whether the subcavity is resonant or antiresonant with the designed wavelength

The reflectivity of the DBR is required to be as high as possible to reduce the losses in the laser cavity and to maintain good lasing parameters. In our samples, a reflectivity value of >99.9% was reached by using 30-35 pairs of quarter-wave thick GaAs/AlGaAs layers. The spectral position of DBR reflectivity is determined by choosing a layer thickness of $\lambda/4$ where λ is the design wavelength. The width of the reflectivity stop band is determined by the refractive index contrast of the neighbouring layers and can typically be up to 100 nm wide. Although many pairs of DBR layers provide a high reflectivity value, each layer increases the thermal impedance of the structure and so a compromise must be reached.

This is especially important if the heat generated by optical pumping is dissipated through the bottom on the device.

The number of QD layers is related to the effective gain of the device. A higher number of QD layers leads to a higher output power up to a certain level. However, the number of layers is limited by the growth capabilities i.e. after a certain number of QD layers, the overall stress accumulated during the growth can initiate the formation of defects which have a strong detrimental effect on the performance of the device. Using current self-assembled QD growth technology, up to ~80 layers of 1040 nm and up to ~40 layers of 1100-1300 nm emission QDs can be grown. Typically 3-7 layers of QDs are deposited under one antinode of the optical standing wave in the subcavity depending on the sizes of QDs, although it has been shown recently that for QDs emitting near 1300 nm, only one QD layer per antinode may be preferred for optimal operation[1]. More research is needed to characterize precisely the relation between the effective gain and the number of QD layers.

The optimum number of layers may also be determined by the preferable length of the subcavity. When setting the length of the subcavity, it must be considered whether or not the subcavity needs to be resonant or antiresonant with the design wavelength, material dispersion and pump light absorption. Preferably, the subcavity length should not be much longer than the pump light absorption path. For GaAs based pump-absorbing regions, all of the incident 808 nm pump light is absorbed in the first 2.5 µm of material.

InGaAs QDs discussed in this thesis currently can cover 960 – 1300 nm region in the optical spectrum. The exact design wavelength is mainly set by the size of the QDs. Longer wavelengths are generated from larger QDs and vice versa. The optical transition for the

design wavelength also needs to be chosen according to the applications for the device. Optical properties of GS and ES transitions were discussed in chapter 1.6.3.

Finally the thickness of the subcavity needs to be chosen to be either resonant or anti-resonant with the design wavelength. This is a particularly important factor in determining some of the lasing parameters as was shown in 1.4.1.

Near the top of the structure a thin low refractive index material layer is grown to create a barrier for excited carriers. This prevents carriers from diffusing to the surface of the device and recombining non-radiatively through the surface defects. The barrier layer is then covered by a thin layer of GaAs to avoid oxidation processes.

In the work presented in this thesis, a number of SDLs were designed and grown. The designed samples are listed in table 2.4. Samples DO1845, DO2251 and DO2254 are shown in underlined format. These samples operated at three different wavelengths and allowed to achieve the best performance in continuous wave regime.

	Sample no	Design wavelength, nm	DBR structure	Number of DBR pairs	Subcavity length, optical	Subcavity length, physical, μm	Number of QD layers	Type	Reference
1.	**DO1845**	1040 nm	GaAs/ $Al_{0.9}Ga_{0.1}As$	29.5	3.75	1.1222	35	antiresonant	[2]
2.	**DO2100**	1270 nm	GaAs/AlAs	36	3.5	1.294	19	resonant	[3]
3.	**DO2251**	1180 nm	GaAs/AlAs	35	7.25	2.492	39	antiresonant	[4]
4.	**DO2254**	1260 nm	GaAs/AlAs	35	7.25	2.678	39	antiresonant	[5]
5.	**DO2565**	1180 nm	GaAs/AlAs	35.5	8	2.478	45	resonant	
6.	**DO2917**	1180 nm	GaAs/AlAs	35.5	8	2.666	42	resonant	
7.	**DO2919**	1180 nm	GaAs/AlAs	35.5	8.25	2.752	42	antiresonant	
8.	-	1180 nm	GaAs/AlAs	36	6.5	2.236	36	resonant, flip chip	[6]
9.	**DO3170**	1040 nm	GaAs/ $Al_{0.9}Ga_{0.1}As$	35	5.25	1.564	63	antiresonant	
10.	**DO3171**	1040 nm	GaAs/ $Al_{0.9}Ga_{0.1}As$	35	5.5	1.639	63	resonant	

Table 2.4. Details of SDLs subcavities designed for the work presented in this thesis. Underlined numbers represent samples which provided best results in CW experiments.

Additional aspects need to be considered when designing a mode-locked SDL including the design of the saturable absorber and additional dispersion control that can be used in the subcavity.

A schematic design of the SDLs used in this research can be seen in Fig. 2.22. It shows three main QD SDLs at different wavelengths that provided the best results throughout the studies. The diagrams show the potential energy profile (black line) and calculated optical standing wave in the subcavity (red line).The samples shown were designed for emission wavelengths of (a) 1040 nm, (b) 1180 nm, and (c) 1260 nm. It can be seen that the QD layers were positioned at the antinodes of the standing wave for the maximum gain. For the 1040 nm device, 7 QD layers were placed under each antinode. For the 1180 and 1260 nm emitters, larger QDs were used and three layers of QDs were positioned under each antinode. All three samples were designed to be in antiresonance with the design wavelength as the standing optical wave has the node at the semiconductor – air interface. Also, the samples have AlGaAs based carrier confinement layers close to the surface.

Finally, an external cavity completes the SDL, the design of which is based upon a number of parameters. Firstly, the shape of the cavity was chosen to suit the SDL configuration as discussed in section 1.4.3. Secondly, the lengths of the cavity arms were calculated to ensure the overlap between the pump spot and laser mode. For the calculation of these lengths, software based on the ABCD matrix formalism was used. The optimum output coupling was determined experimentally. For the QD based SDLs used in this thesis, an output coupling up to 1% was typically used.

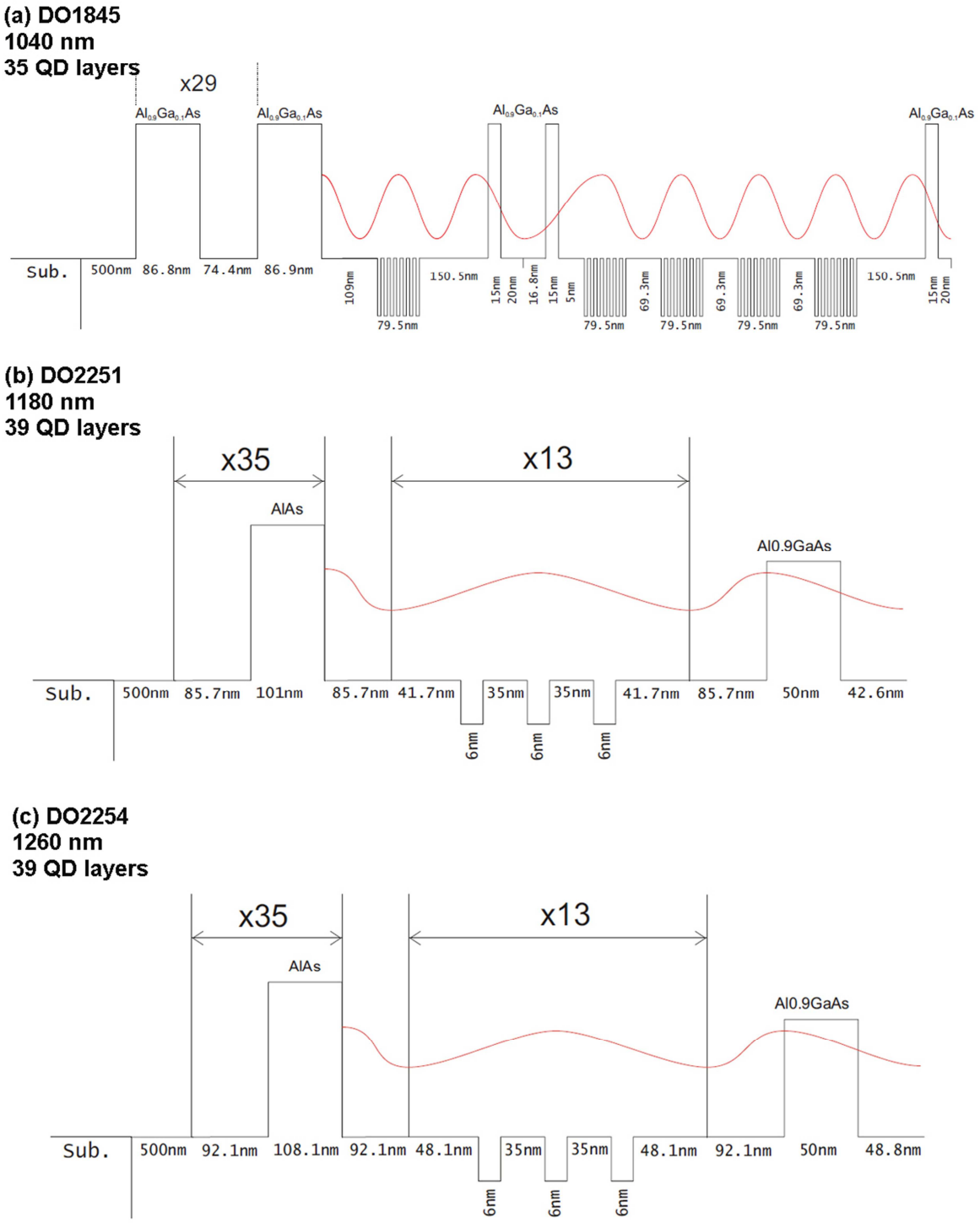

Fig. 2.22. The design for 1040, 1180 and 1260 nm QD SDLs used in the research. Black line shows the profile of the potential energy in semiconductor structure. Red line represents the intensity pattern of the optical standing wave.

2.2. Growth of the SDL semiconductor part

All the QD SDL semiconductor wafers used in this thesis were grown within the facilities of Innolume GmbH, Germany. Wafers were grown using molecular beam epitaxy (MBE) technology in Stranski – Krastanow growth regime. Three wafers, labelled DO1845, DO2251 and DO2254 produced emission wavelengths of 1040, 1180 and 1260 nm respectively. Their growth procedures are described below.

2.2.1. Sample DO1845 growth (1040 nm)

Sample DO1845 was designed for the emission wavelength of 1040 nm. The whole structure was grown on a GaAs substrate by MBE under standard conditions. The structure consisted of a 29.5 pair quarter-wavelength thick GaAs/$Al_{0.9}Ga_{0.1}As$ distributed Bragg reflector (DBR) grown at a design wavelength of 1040 nm. The reflectivity was calculated to be >99.99 % at 1040 nm. The active region, grown on top of the DBR, was 7.5λ/2 long and consisted of five groups of 7 QD layers, positioned at the antinodes of the E-field standing wave. Each QD layer was formed by cyclically (9 times) depositing InAs (0.06nm) and GaAs (0.06nm) at the temperature of 480 ^{o}C. The thickness of QD layers was 2.8 nm and they were separated by 10 nm GaAs spacer layers to minimize material defects [7]. The dot density was ~$3x10^{10}$ cm^{-2}. Between the groups of QD layers GaAs, spacers served the dual purpose of being transparent spacers at the laser design wavelength and pump absorber regions at the 808 nm pump light wavelength. A 15 nm thick $Al_{0.9}Ga_{0.1}As$ cap layer was used to prevent surface recombination of the excited carriers. Finally a 20 nm GaAs cap layer was placed at the semiconductor-air interface to avoid oxidation.A cross section SEM picture of DO1845 sample is shown in Fig. 2.23. In the image, multilayer DBR can clearly be seen with substrate below and active region on top of it.

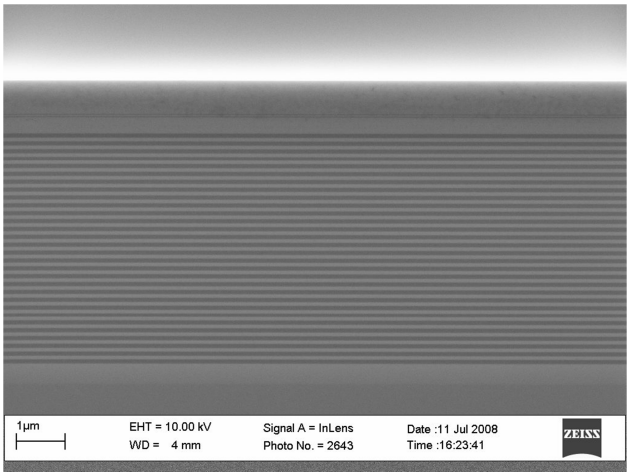

Fig. 2.23. A cross section SEM image of DO1845 sample

2.2.2. Sample DO2251 growth (1180 nm)

Wafer DO2251 was designed for wavelength emission at 1180 nm. The QD-based amplifying mirror structure was fabricated by MBE on a GaAs substrate. The highly reflective DBR consisting of 35 pairs of quarter-wavelength thick AlAs/GaAs layers was grown first on the substrate. Next, the active region with 39 layers of QDs was grown on top of the DBR. The 6-nm thick QD layers were arranged in 13 identical groups with 3 QD layers in each group. QD layers were separated by 35 nm thick GaAs layers. Each QD group was positioned at the antinode of the standing-wave optical field by choosing the appropriate thickness of GaAs spacers between the QD layers groups. A wide-bandgap50 nm thick $Al_{0.9}GaAs$ window was then grown on top of the active region and prevented carrier recombination at the surface of the structure and finally the structure was protected against oxidation with a 42.6 nm thick GaAs layer.

2.2.3 Sample DO2254 growth (1260 nm)

The gain structure of DO2254 was designed for wavelength emission at 1260 nm and was grown by MBE under S-K growth mechanism. The whole structure was grown on a GaAs substrate followed by 35 pairs of GaAs/AlAs layers DBR, providing >99.99% reflectivity at the design wavelength. The active region, grown on top of the DBR consisted of 39 layers of QDs divided into 13 groups and placed at the antinodes of the e-field standing wave. The QD layers were separated by 35 nm GaAs layers. QD layers were grown at 485^{o}C. The emission wavelength was obtained by InGaAs overgrowth of InAs islands – each QD layer was formed by deposition of 0.8 nm of InAs followed by 5 nm of InGaAs. Such a process leads to the increase of effective QD size providing emission at longer wavelengths [8]. A 50 nm thick cap layer of $Al_{0.9}GaAs$ was used to prevent surface recombination and a 48.8 nm thick top layer of GaAs completed the structure. The subcavity length of all three samples was chosen to be in antiresonance with the design wavelengths. Also, for the QD SDLs, the emission wavelength from QDs under very small excitation at ambient temperature was designed to be 10-20 nm shorter than the design wavelength. Such an offset is necessary as the emission red-shifts with the increased temperature under operating conditions.

The growth procedures of the three main samples for different working wavelengths used in our work have been described above. The growth of other devices was also based on the same principles as they were designed for the same operating wavelengths.

2.3. Wafer inspection and characterisation

Multiple evaluation tests were performed after the SDL semiconductor wafers were grown. These included surface defect density estimation, reflectivity measurements, photoluminescence mapping as well as measurement of the photoluminescence spectra.

To evaluate the quality of the surface of the grown wafers, the surface defect density was measured in the facilities of Innolume GmbH. A TencorSurfScan 4500 surface inspection system was used. Such a system uses a helium-neon laser beam with a beam radius of 50µm which is scanned across the wafer surface, scanning in one line whilst the wafer is pulled perpendicularly to the line (Fig. 2.24).The laser light is then scattered by various defects like pits, scratches, material spikes or particles. This scattered light is collected by fiber collectors and is transmitted to the photomultiplier. The registered signal allows estimating the density of the defects of given range of sizes.

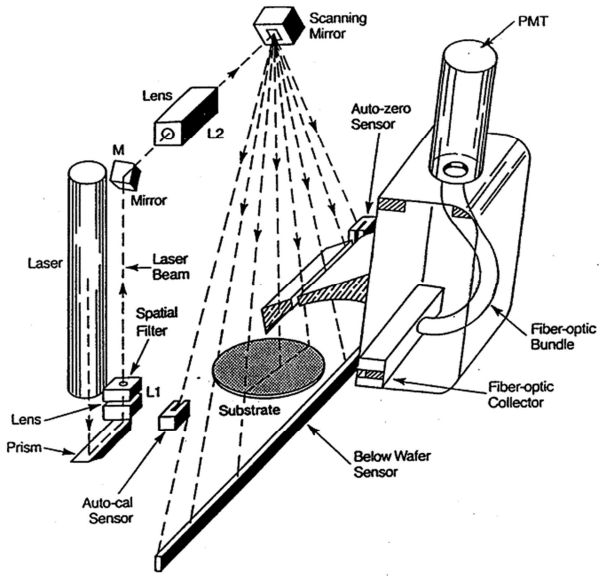

Fig. 2.24. TencorSurfScan 4500 surface inspection system for evaluating the defect density in the surface of grown SDL wafers.

Table 2.2. shows the surface defect density for various samples. It can be seen that the number of defects varies quite significantly from sample to sample due to the complication of the MBE growth. Defect sizes referred in the table below are between 0.7 to 10 µm.

Sample No	Surface defect density (pts/cm^2)
DO2251	63
DO2917c	395
DO2254	400
DO2100	190
DO2956g	505
DO3170	280
DO3171	320

Table 2.5. Surface defect density values for some of the samples

The reflectivity spectra of wafers are also measured after the growth process. This is done to ensure the DBR of the wafer is correctly grown for the design wavelength. A set of measured reflectivity spectra for different samples is shown in Fig. 2.25. It can be seen that all the DBRs have their stop band at the design wavelength as it was intended by the design. Photoluminescence spectra measured from the top of the wafer are also shown together for reference. It can be seen that the top photoluminescence is filtered by the Fabry-Perot etalon effect as it was described in section 1.4.1. Graphs (a), (b) and (c) show antiresonant structures and the etalon peaks are on the sides of operation wavelength of SDL. Graph (d) represents resonant structure where etalon filtered photoluminescence peak

coincides with the operation wavelength. The arrows in the graphs indicate the operation points of different SDL samples. Reflectivity dips at (b) and (c) are due to the photons' absorption at the cavity resonance frequencies. The dips are resolved in greater details for samples DO2251 and DO2254 as they have semiconductor active regions which are almost twice thicker than in the samples DO1845 and DO2100.

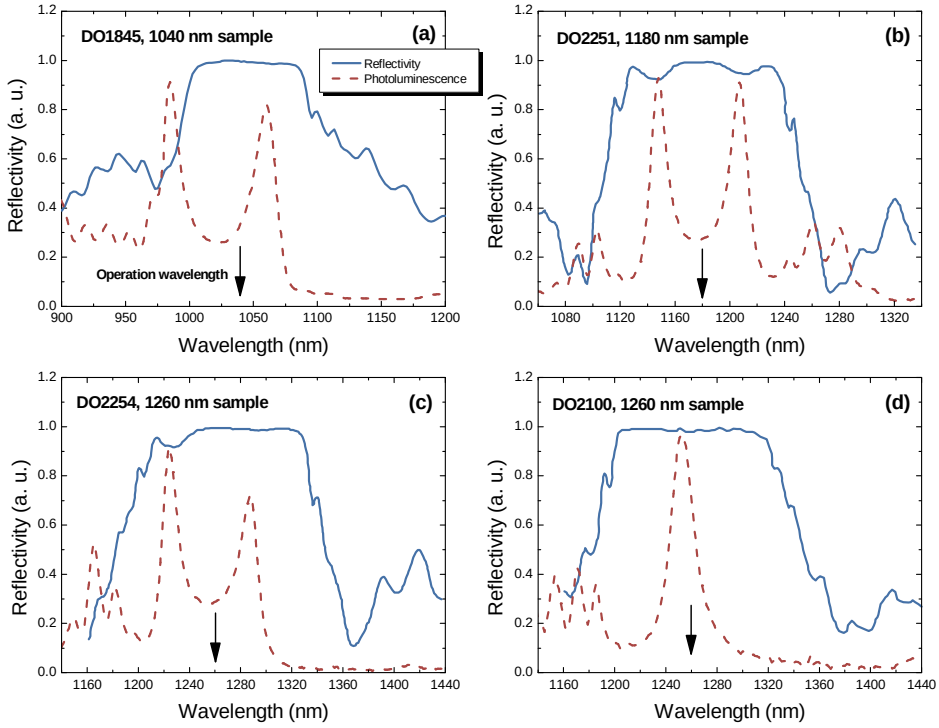

Fig. 2.25. A set of reflectivity spectra for different samples measured after the growth. Top photoluminescence spectra are also shown in red dashed lines. The arrows indicate operation points of different SDL samples.

Photoluminescence mapping of the wafers was conducted within the grower's facilities. This technique involves the measurement of the main photoluminescence peak at different spots on the wafer. It allows for the evaluation of the uniformity of the grown wafer. For

this purpose a NanometricsRPM2000 rapid photoluminescence mapper was used (the same system was used for measuring the photoluminescence and reflectivity spectra). An internally integrated laser source excites the wafer at an angle with the focal low intensity spot of about 100 µm in diameter and the luminescence from the wafer is collected by the monochromator. The wafer is scanned by the translation stages while the excitation beam is positioned. Such a system allows for the spectral mapping of the wafers with 1, 0.5 or 0.2 mm resolutions [9]. The mapping usually takes tens of seconds depending on the required resolution and allows for quick inspection of the growth processes. Examples of the photoluminescence maps for DO2917 and DO29191180 nm samples are shown in Fig. 2.26. It can be seen that the peak photoluminescence changes across the different positions and the emission wavelength can differ up to 20 nm across the 3" wafers. This can be influenced by slightly different thicknesses of the layers across the wafer as well as by the different properties of QDs due to unequal distribution of the gasses or temperature gradients during the growth process.

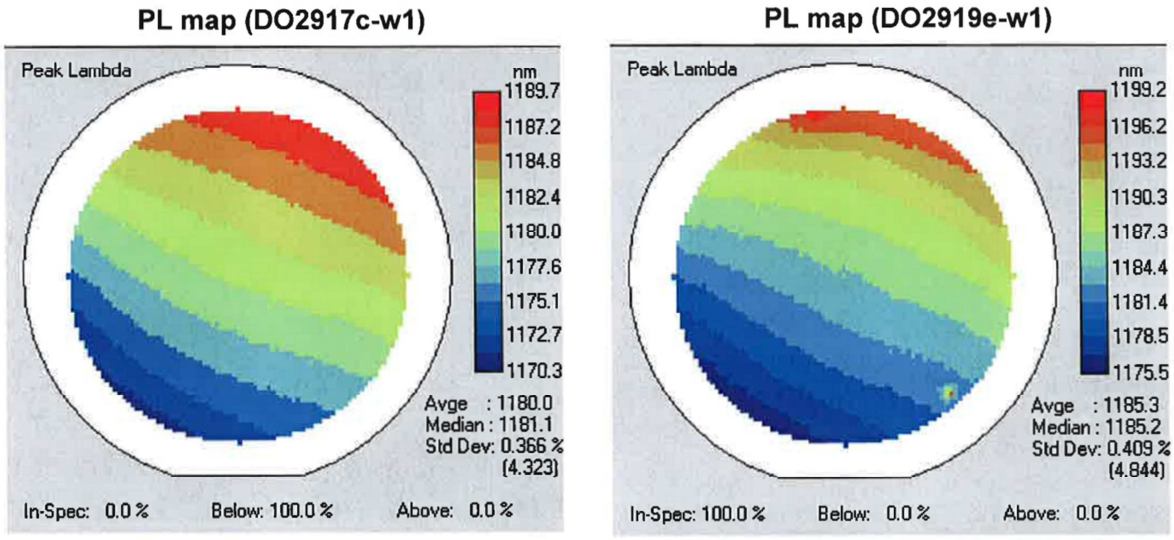

Fig. 2.26. Examples of photoluminescence maps of DO2917 and DO2919 1180 nm samples.

Photoluminescence maps are very advantageous when checking the uniformity of the grown wafer. However it only shows the main peak wavelength of the photoluminescence spectrum. The measurement of the whole spectrum is another powerful tool when analysing samples [10, 11]. It provides information on the emission wavelength from QDs and the intensity of it compared to the other spectrum features. Additional information can be found when the spectra are measured at different excitation regimes reflecting on the behaviour of the excited carriers in the sample. Two types of time-integrated photoluminescence spectra from SDL samples can be measured to acquire different information - the measurement of the luminescence light that is emitted from the surface and from the edge of the semiconductor sample. Luminescence light from the surface of the sample is strongly filtered by the etalon formed between DBR and semiconductor – air interface. Meanwhile luminescence light from the edge of the sample is characteristic to the emission from the QDs and is not modulated by the subcavity filtering effects. Parameters such as quantum efficiency and sample temperature can be calculated by measuring the photoluminescence signal at different temperatures and at different pump intensities.

Fig. 2.27 shows the experimental setup for the photoluminescence measurements. For this experiment a 4 x 4 mm sample was cleaved from the wafer and bonded to a copper heatsink using thermally conductive paint. The sample was then mounted onto a larger copper heatsink which was cooled by circulating water, the temperature of which was controlled by a TEC. The sample was excited by 808 nm light focused to a 120 µm diameter pump spot, close to the edge of the sample. The same laser diode was used for excitation as well as for the SDL operation. After excitation, the photoluminescence light is emitted in a spherical field. Part of it was collected by an aspheric lens both from the surface of the

wafer and from the edge. The aspheric lens used at the edge was positioned at a small angle to the edge plane to avoid any surface guided top photoluminescence. The light was then guided and focussed to the optical spectrum analyser, having first filtered off the residual 808 nm light. The spectrum was measured with 0.1 nm resolution. To measure the light emitted from top or from the edge of the sample, a flipping mirror was used in the optical path.

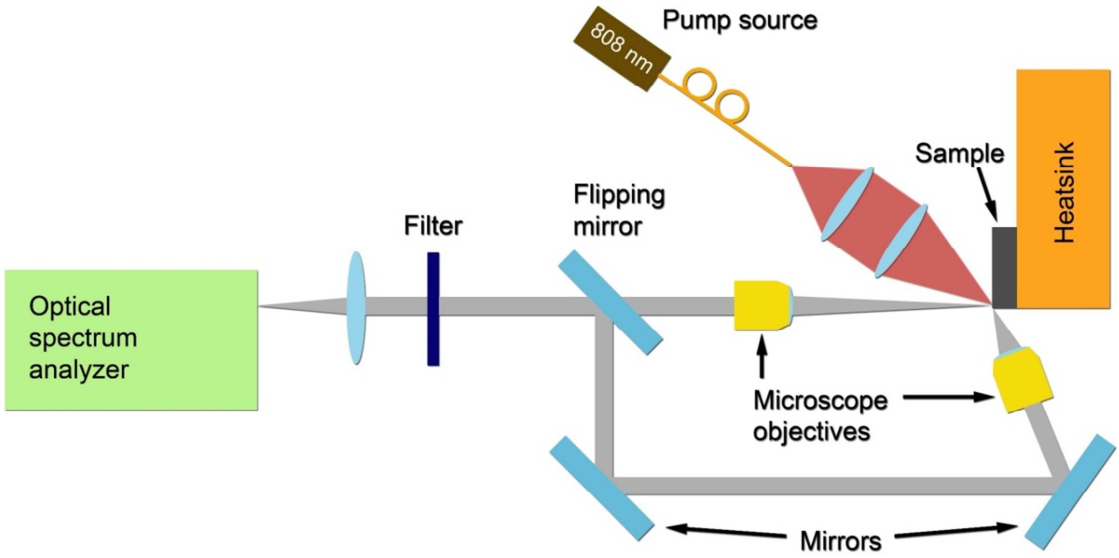

Fig. 2.27. Experimental setup for edge and top photoluminescence measurements

The edge photoluminescence spectra of samples DO1845 (1040 nm), DO2251 (1180 nm) and DO2254 (1260 nm) are plotted in Fig. 2.28. Calculated reflectivity spectra of DBRs for corresponding samples are also shown in dashed lines. It can be seen that 1040 nm sample features a broad luminescence spectrum of about 112 nm at FWHM indicating a broad distribution of QD sizes. The spectra of 1180 nm and1260 nm samples have more resolved peaks. In the spectrum of 1180 nm sample first excited state transition has a peak at1170 nm. Ground state transition is at around 1240 nm and is suppressed when compared to the

spectrum of 1260 nm sample. There is also a peak showing a second excited state transition at 1110 nm. The first excited and ground state peaks are slightly shifted to longer wavelengths in the spectrum of 1260nm sample as the wafers were grown by different growth runs. It must be noted that the spectral lines shown in the graph are of different origin from the ones shown in Fig. 2.25 where photoluminescence is filtered by the Fabry-Perot etalon effect.

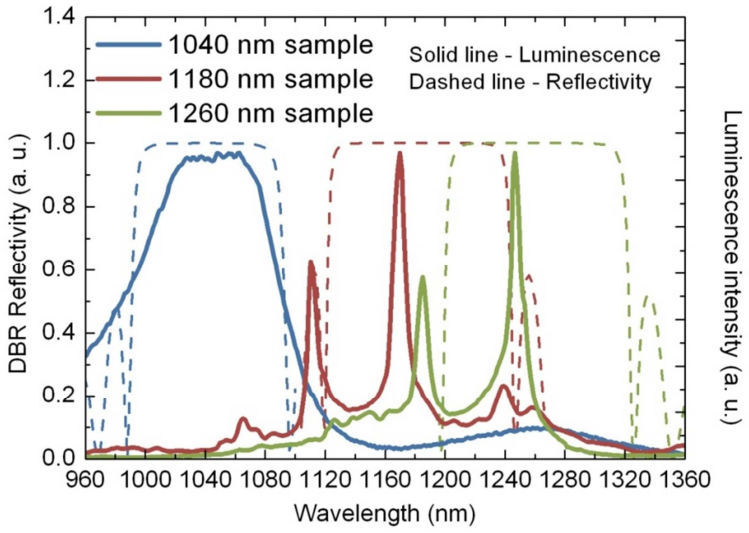

Fig. 2.28. Calculated reflectivity spectra and measured normalized edge photoluminescence spectra of samples emitting at 1040, 1180 and 1260 nm.

Top and edge photoluminescence spectra of the samples used in this work were also measured at different pump intensities and heatsink temperatures. By changing the temperature of the sample, the emission wavelength can be red or blue shifted. Wavelength shift in top measured photoluminescence is mainly influenced by the thermal process leading to the refractive index change and the change of the Fabry - Perot etalon conditions. Meanwhile the wavelength shift in the edge photoluminescence reflects the effect of thermal conditions on the emission from QDs. Pump intensity can also be changed whilst

keeping heatsink temperature constant. In this case wavelength shift and the change of spectrum shape reflect carrier dynamics and pump induced thermal effects.

A set of photoluminescence measurements from a 1040 nm SDL sample is shown in Fig. 2.29. Part (a) in Fig. 2.29 shows top photoluminescence spectra at different pump powers. Two clearly resolved peaks of subcavity resonances can be seen at around 990 nm and 1065 nm. At low pump powers, the spectrum is more intense at longer wavelengths as lower energy states in QDs are filled in first. However, as the pump power is increased above 1 W, the peak at shorter wavelengths, i. e. emission from higher energy states starts dominating. It can be compared with Fig. 2.29(c) where the edge photoluminescence spectra at different pump powers are shown. Here it can be seen that emission at longer wavelengths is more intense at low pump powers and emission at shorter wavelengths gets dominant with increased pump power. The edge photoluminescence is centred at 1040 nm as was intended by the initial design. Also, in part (a) there are some peaks in spectra in 930 – 970 nm range that show the influence of DBR reflectivity peaks at the side of the stop band. The fairly intense peak around 900 nm is due to subcavity resonance enhanced emission in GaAs spacers.

Fig. 2.29(b) and (d) show spectra at constant pump power but at different heatsink temperatures of 5, 25 and 45 ^{o}C. The emission shifts to longer wavelengths with temperature increase and the intensity decreases in both cases. This is because the lattice expands and the interaction that is responsible for the bandgap in semiconductor gets weaker at higher temperatures allowing lower energy photons to be emitted [10].

It is also informative to evaluate the spectral shifts in a quantitative way. For this the exact wavelength value of some specific spectral peak or shoulder can be plotted against

temperature or pump power and the slope calculated. For example in 1040 nm sample, top photoluminescence spectrum shifts with 6.1 nm/W rate when the pump power is increased and with 0.1 nm/K rate when the temperature is changed. For edge photoluminescence the corresponding values are 0.3 nm/W and 0.2 nm/K. A large difference between wavelength shift with pump power in top and edge emitted light spectra indicates that increased pump power has a big influence on the resonance condition in the subcavity resulting in a rapid wavelength shift. The ratio of measured wavelength shifts in top photoluminescence results in the thermal sensitivity of 61 K/W. It is a high value, indicating poor thermal conductivity of the sample. However, the reader must be reminded that no special thermal management techniques were applied in this experiment.

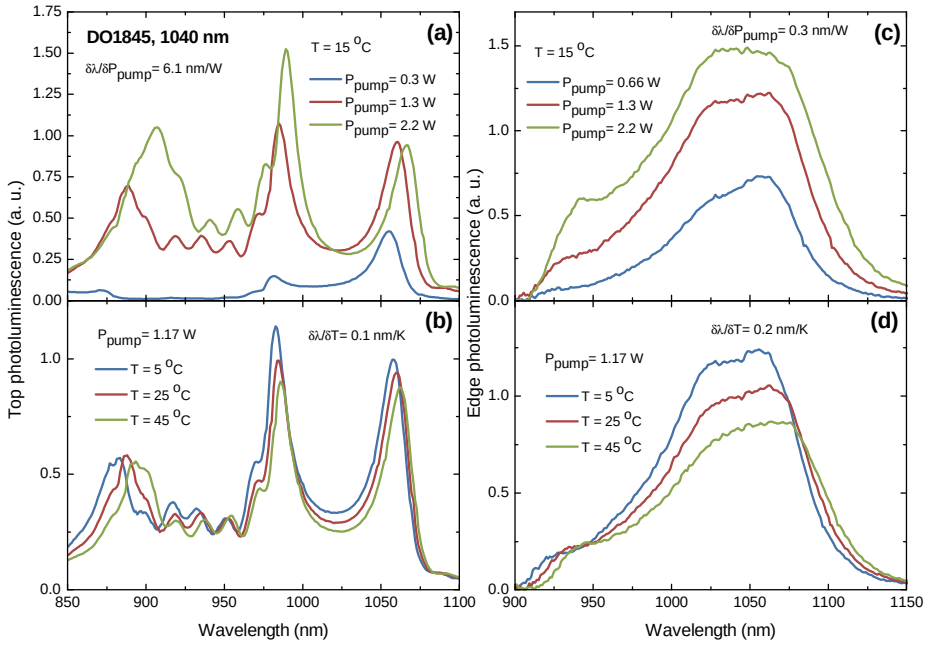

Fig. 2.29. (a), (b) top and (c), (d) edge photoluminescence measurements from 1040 nm SDL sample. (a) and (c) show measurements at constant temperature while (d) and (d) show measurements at constant pump power.

The photoluminescence spectra of other samples used in this work can be interpreted in a similar manner as was discussed before. The spectra measurements for samples DO2251, DO2254 and DO2100 are shown in Fig. 2.30 - Fig. 2.32. Most of the spectra follow the trends discussed before. However, a few exceptions can be noticed. For example, the intensity of the peak around 1200 nm increases with temperature whilst it decreases around 1150 nm in the top luminescence spectra from DO2251 sample (Fig. 2.30, b). This happens because the emission from QDs is also shifted from 1170 nm towards longer wavelengths with increased temperature (Fig. 2.30, d). This also happens with increased pump power in both DO2251 and DO2254 samples. Also, it must be noted that thermal sensitivity of edge emission spectra is much lower in 1040 nm sample than in the rest of the samples.

All of the above discussed photoluminescence spectra were measured from antiresonant type samples. Fig. 2.32 shows luminescence spectra from sample DO2100 which was designed to be resonant at 1260 nm. In this case it can be seen that the main peak in top photoluminescence almost coincides with the spectrum measured from the edge of the sample resulting in sharp and clearly resolved spectral peak. The origin of the ripples in edge luminescence spectrum of this sample is not clear. It might be the influence of surface guided top luminescence light.

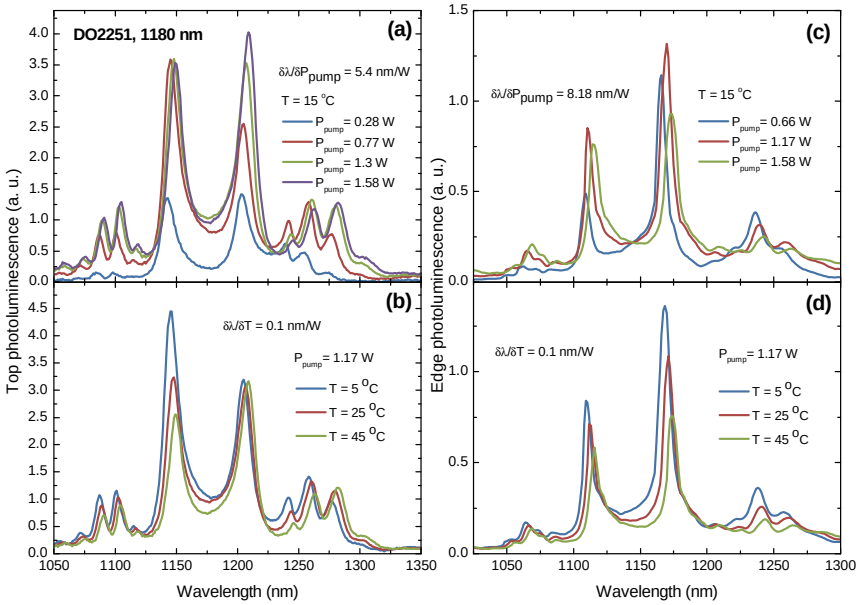

Fig. 2.30. Top and edge photolominescence measurements from DO2251, a 1040 nm SDL sample.

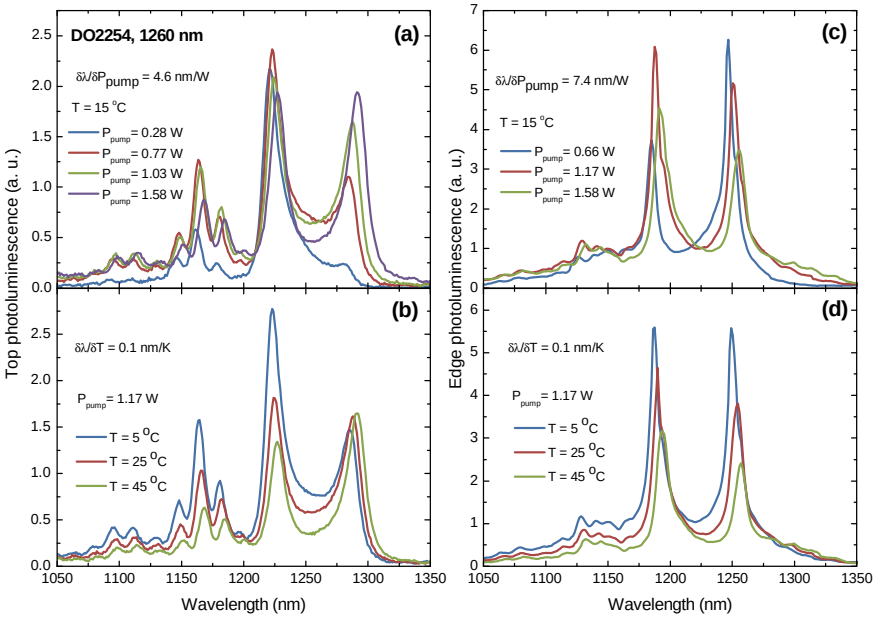

Fig. 2.31. Top and edge photolominescence measurements from DO2254, a 1260 nm SDL sample.

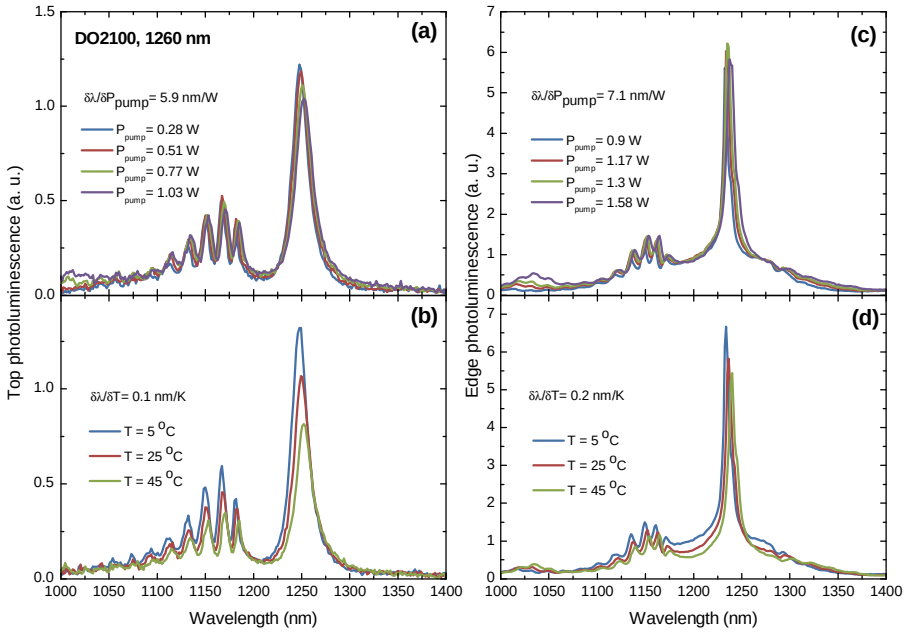

Fig. 2.32. Top and edge photolominescence measurements from DO2100, a 1260 nm SDL sample.

All of the above mentioned techniques allow for an evaluation of the samples' quality. It can provide useful information and help to predict the performance of the SDL.

2.4. Chapter conclusions

Design principles of semiconductor disk lasers were discussed in the second chapter of thesis. The growth processes of three different samples for 1040 nm, 1180 nm and 1260 nm emission wavelengths were described. Different inspection techniques, such as surface defect density, reflectivity and photoluminescence spectra measurements were used to evaluate the quality of the grown samples, Most of the measured sample parameters were in accordance with the initial design.

References

[1] A. R. Albrecht, C. P. Hains, T. J. Rotter, A. Stintz, K. J. Malloy, G. Balakrishnan, and J. V. Moloney, "High power 1.25 µm InAs quantum dot vertical external-cavity surface-emitting laser," *Journal of Vacuum Science & Technology B*, vol. 29, 03C113, 2011.

[2] M. Butkus, K. G. Wilcox, J. Rautiainen, O. G. Okhotnikov, S. S. Mikhrin, I. L. Krestnikov, A. R. Kovsh, M. Hoffmann, T. Sudmeyer, U. Keller, and E. U. Rafailov, "High-power quantum-dot-based semiconductor disk laser," *Optics Letters*, vol. 34, pp. 1672-1674, 2009.

[3] M. Butkus, J. Rautiainen, O. G. Okhotnikov, S. S. Mikhrin, I. L. Krestnikov, and E. U. Rafailov, "Quantum dot semiconductor disk laser operating at 1270 nm," *1st EOS Topical Meeting on Lasers*, Capri, Italy, 2009.

[4] J. Rautiainen, I. Krestnikov, M. Butkus, E. U. Rafailov, and O. G. Okhotnikov, "Optically pumped semiconductor quantum dot disk laser operating at 1180 nm," *Optics Letters*, vol. 35, pp. 694-696, 2010.

[5] M. Butkus, C. J. Hamilton, J. Rautiainen, O. G. Okhotnikov, S. S. Mikhrin, I. L. Krestnikov, and E. U. Rafailov, "Broadly tunable 1250 nm quantum dot-based semiconductor disk laser," *IETOptoelectronics*, vol. 5, pp. 165-167, 2011.

[6] A. Rantamäki, J. Rautiainen, L. Toikkanen, I. Krestnikov, M. Butkus, E. Rafailov, and O. Okhotnikov, "Flip chip quantum dot semiconductor disk laser at 1200 nm," *submitted to Photonics Technology Letters*, 2012.

[7] N. N. Ledentsov, V. A. Shchukin, M. Grundmann, N. Kirstaedter, J. Bohrer, O. Schmidt, D. Bimberg, V. M. Ustinov, A. Y. Egorov, A. E. Zhukov, P. S. Kopev, S. V. Zaitsev, N. Y. Gordeev, Z. I. Alferov, A. I. Borovkov, A. O. Kosogov, S. S. Ruvimov, P. Werner, U. Gosele, and J. Heydenreich, "Direct formation of vertically coupled quantum dots in Stranski-Krastanow growth," *Physical Review B*, vol. 54, pp. 8743-8750, 1996.

[8] B. V. Volovik, A. F. Tsatsulnikov, D. A. Bedarev, A. Y. Egorov, A. E. Zhukov, A. R. Kovsh, N. N. Ledentsov, M. V. Maksimov, N. A. Maleev, Y. G. Musikhin, A. A. Suvorova,

V. M. Ustinov, P. S. Kopev, Z. I. Alferov, D. Bimberg, and P. Werner, "Long-wavelength emission in structures with quantum dots formed in the stimulated decomposition of a solid solution at strained islands," *Semiconductors*, vol. 33, pp. 901-905, 1999.

[9] AZoNanotechnology (2009), RPM2000 Rapid Photoluminescence Mapper - Room Temperature PL Mapping System, URL: *http://www.azonano.com/article.aspx?ArticleID=2308* [13 June 2012].

[10] A. C. Tropper and S. Hoogland, "Extended cavity surface-emitting semiconductor lasers," *Progress in Quantum Electronics*, vol. 30, pp. 1-43, 2006.

[11] M. Kuznetsov, F. Hakimi, R. Sprague, and A. Mooradian, "Design and characteristics of high-power (> 0.5-W CW) diode-pumped vertical-external-cavity surface-emitting semiconductor lasers with circular TEM_{00} beams," *IEEE Journal of Selected Topics in Quantum Electronics*, vol. 5, pp. 561-573, 1999.

3. Results in continuous wave regime

This chapter discusses results achieved in QD SDLs in continuous wave (CW) lasing. First, the sample preparation and experimental setup will be presented. Afterwards, the CW output powers achieved in 1 – 1.3 µm QD SDLs will be presented. It will be followed by the results achieved with intracavity second harmonic generation. Finally, wavelength tuning results will be presented.

3.1. Sample preparation

After the photoluminescence evaluation of the samples, the samples were prepared for the SDL experiments. The main work at this stage was to prepare the samples for thermal management. An intracavity heat spreader approach was used in our experiments.

Optical quality single crystal diamonds were used as intracavity heat spreaders in our experiments as they have demonstrated the best performance in intracavity thermal management for SDLs and solid state thin disk lasers to date.The diamonds were grown using a chemical vapour deposition technique (CVD). Transparency for a wide spectral range and low birefringence of $<10^{-5}$ make the diamond plates fully applicable for optical use. Low thermal expansion reduces the effect of temperature induced stress. 4 mm diameter and 0.5 mm thickness diamond heat spreaders were used. A photo of synthetic diamond window is shown in Fig. 3.33.

Fig. 3.33. A synthetic diamond window for intracavity heat spreader use.

To extract the pump induced heat in the SDL, the optical contact between the diamond plate and semiconductor part of the SDL is created using liquid capillary bonding technique. For effective bonding two surfaces must be clean and flat. The diamond heat spreader had a surface flatness of λ/4 at 632.8 nm and RMS roughness of <5nm/mm^2. First, a piece from semiconductor wafer slightly smaller than the diamond plate was cleaved. The surfaces of both elements were thoroughly cleaned. A small drop of deionized water was placed on the surface of semiconductor and the diamond laid on top of it. The two parts were then slightly squeezed to push out the water between them. A thin layer of water is still left between the elements. The SDL-diamond assembly was left for some time to evaporate water. As the water evaporated from the edges, the two elements were brought together to a very close contact due to the surface tension of the liquid. After there is no water left a strong bond is formed between two elements.

After bonding the SDL-diamond sample was mounted to a copper holder for further heat dissipation and easier handling. To mount the SDL, a small pit in the copper plate was drilled. The depth of the pit must be equal or slightly less than the total thickness of the diamond and semiconductor. The assembly was then placed in the pit with diamond on the top. Another copper plate was attached on the top. The top copper plate had an aperture for

the pump and laser operation and held only the edges of the diamond. A layer of thin indium foil was inserted between copper and the semiconductor – diamond part for a better contact between the elements. A schematic cross section view of the whole assembly is shown in Fig. 3.34. A photo of real device is shown in Fig. 3.35.

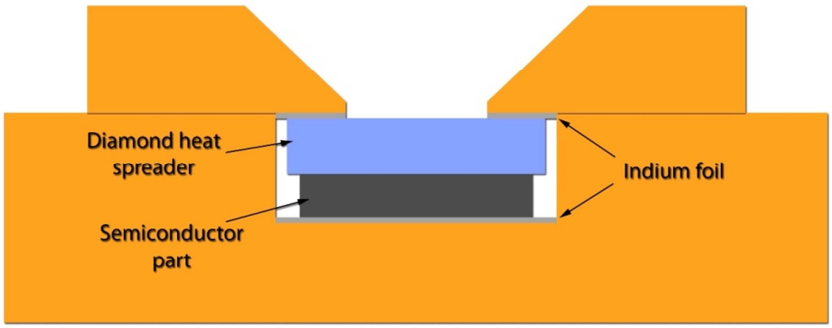

Fig. 3.34. A cross section view of the diamond bonded to the SDL sample and mounted in a copper holder.

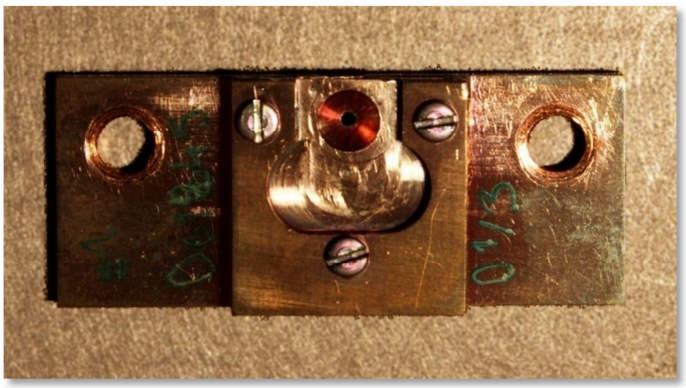

Fig. 3.35. A photo of a SDL sample bonded to the diamond heat spreader and mounted to a copper heatsink.

The assembly was then attached to a larger copper heatsink for the experiment. The temperature of the heatsink was controlled using a thermoelectric Peltier element. Excessive heat from the heatsink was dissipated using a circulating water system and a chiller.

3.2. Experimental setup

The experimental setup was built around the SDL sample mounted in a copper heatsink as described in a previous section. For measurements of CW output power, straight or V-shape cavities were used (Fig.3.36). First the desired lengths of cavity arms were calculated using ABCD matrix formalism based software. After that the external mirrors were positioned at the approximate distances and angles to the sample. The pump light was focussed on the surface of the sample and the mirrors were finely adjusted to start the lasing. Low power visible light laser and a silicon based CCD camera were used for the alignment of the SDL cavity.

A BrightLase Ultra-50 laser diode from QPC lasers, Inc was used as a pump source in our experiments. The pump laser output was coupled to a 100 µm core diameter multimode fiber. The maximum achievable output power from the source was 20.2 W at 808 nm wavelength.

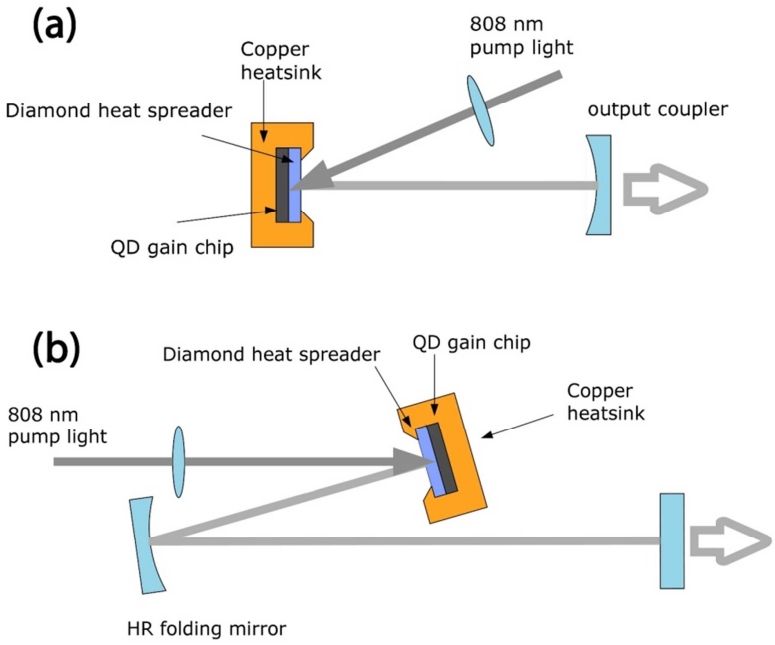

Fig.3.36. (a) straight and (b) V-shape cavity configurations for CW SDL operation.

A number of broadband power meters were used for power measurements. Optical spectra were measured using an Advantest Q8384 optical spectrum analyser providing 0.1 nm resolution. Beam profiles of the output beams were measured using a scanning CCD camera from DataRay Inc.

3.2. SDLs emitting at 1040 nm

Wafer sample DO1845 containing 35 QD layers was used for the QD SDL operation at 1040 nm. Firstly, an unprocessed (without heat spreader) sample was tested. A small sample was cleaved from the wafer and attached to the copper heatsink. The sample was tested in a straight cavity configuration using a RoC = -75 mm output coupler with 0.15 % transmission. The sample produced a maximum output power of 90 mW centred at a wavelength of 1050 nm with the heat sink temperature set to 5 ^{o}C. Pump output power

characteristics of the sample are shown in Fig. 3.37. Thermal rollover occurred at an incident pump power of 1 W. The reason of such laser termination lies in the pump induced heating. Increased temperature reduces the efficiency of lasing as it was discussed earlier. Thus, higher pump intensity is needed to achieve the same gain which leads to further heating and consequently terminates the lasing. The threshold pump power was 2.5 kW/cm^2 and the slope efficiency with respect to incident power was 12 %. As the heat sink temperature was increased the slope efficiency and maximum output power fell rapidly; at 20 ^{o}C, the slope efficiency was 6 % and the maximum output power was only 22 mW at incident pump power of 0.9W.

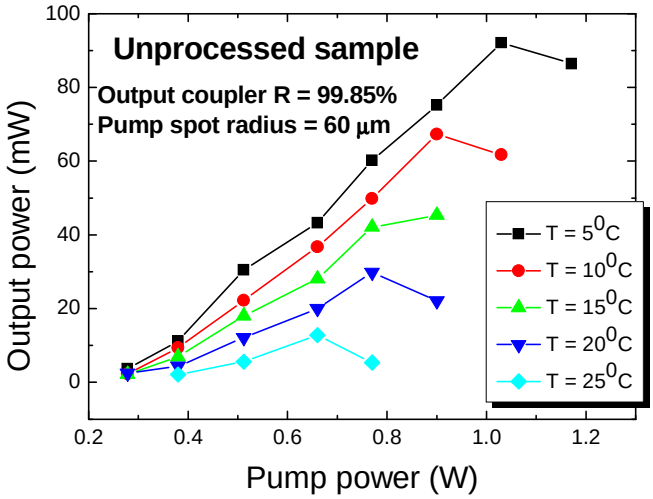

Fig. 3.37. Pump - output power characteristics of the unprocessed DO1845 SDL sample.

The experiment with the unprocessed sample clearly showed the necessity for improvement in thermal management [1]. Thus, sample DO1845 was then bonded to an intracavity diamond heat spreader by the technique described in section 2.4. This sample was tested in V- shape cavity configuration (Fig.3.36, b). The gain chip formed one end of the cavity, a

RoC = -100 mm curved mirror served as a folding mirror and a plane output coupler completed the cavity. The reflectivity of the folding mirror was R = 99.85 % and the output coupler had a reflectivity of R = 99.4 %, resulting in the total output coupling of 0.75 %. Two output beams were used in order to achieve optimal output coupling with available mirrors.

The resulting output power was measured at both mirrors. With the maximum 20 W pump, an output power of up to 6 W (3.6 W at the output coupler and 2.4 W at the folding mirror) was achieved at a heatsink temperature of 5 ^{o}C. The slope efficiency was 32 %. The output power at room temperature reached 5.4 W and the slope efficiency slightly decreased to 29 %. The pump – output power characteristics of the 1040 nm device at different heat sink temperatures are shown in Fig. 3.38. To the best of our knowledge, the achieved results represent the highest output power from a single gain chip QD SDL to date. The output power was limited by the available pump source and a thermal rollover was not reached as can be seen in the graph. Thus higher output power should be achievable with a more powerful pump laser. A significant improvement in the performance of the laser was achieved using an intracavity heat spreader as compared to an unprocessed sample.

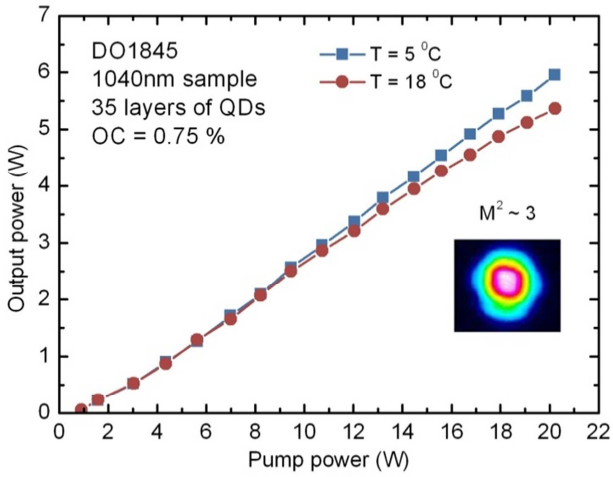

Fig. 3.38. Pump - output power results for 1040 nm QD SDL sample at different heatsink temperatures. Inset shows measured beam profile at the focal spot.

The optical spectrum of the laser was centred at 1038 nm at room temperature at the highest output power and had an associated spectral full-width-half-maximum (FWHM) of 12 nm as can be seen in Fig. 3.39. The distinct periodically spaced peaks in the output spectra were caused by the spectral filtering induced by the etalon formed by the intracavity diamond heat spreader.

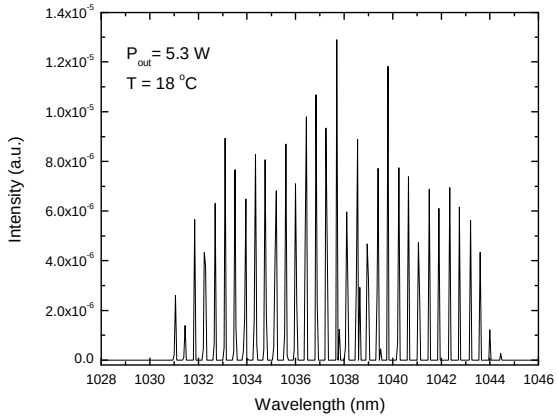

Fig. 3.39. Optical spectrum of the 1040 nm QD SDL sample.

The spatial beam profile of the above discussed laser was measured and it is shown in the inset of Fig. 3.38. A beam quality factor M^2 of ~3 was achieved at the highest output power. The higher order transverse modes were supported due to non-equal distribution of thermal load in the pump region as was shown by [1]. It was also noted that the presence of the intracavity diamond heat spreader also has influence on the output beam quality. Imperfections in diamond structure or reflections from its surface also support the origin of some additional transverse modes. This was noted as the samples which were AR coated on the top typically had lower M^2 values. The beam profile of the unprocessed sample was measured to assess the influence of diamond heat spreader. The sample was tested in a V-shape cavity configuration which allowed for increased control over the cavity mode and produced a low-divergent output beam. The comparison of both cases is shown in Fig. 3.40. The sample without diamond produces a circularly symmetric TEM_{00} mode beam whilst the intracavity diamond heat spreader introduces some distortions resulting in slightly lower beam quality. Although different beam quality parameters were obtained while operating these two setups, it is not possible to define quantitatively the influence of diamond heat spreader from this comparison as the samples were operated under different pump conditions. Also, as it was already mentioned, AR coated or wedged heat spreaders typically allows improved beam quality.

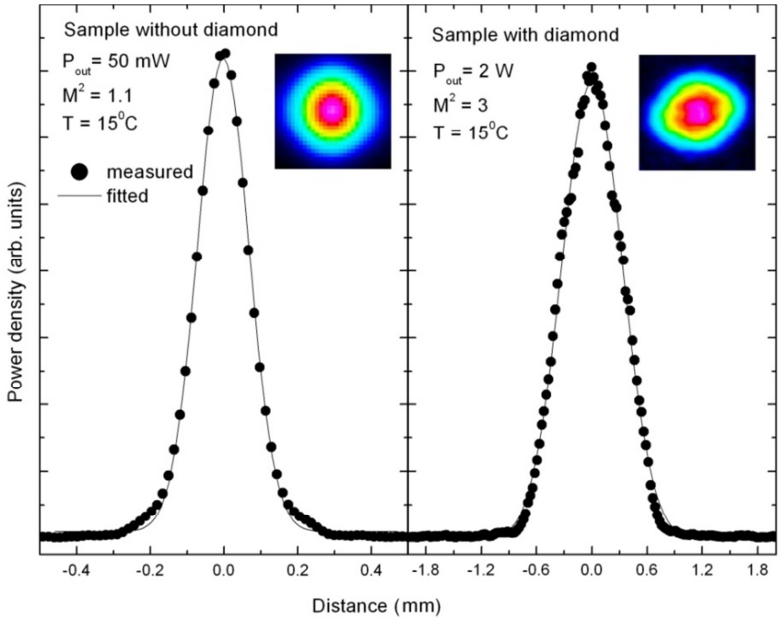

Fig. 3.40. Spatial beam profiles from SDLs without and with intracavity diamond heat spreader.

3.3. SDLs at 1180 nm

A number of QD SDL samples designed for the operation at 1180 nm were tested. These were samples DO2251 and DO2917. Sample DO2251 was tested in a straight cavity configuration using a RoC = -75 mm output coupler with an output transmittance of 0.4 % which was found to be optimal for output power extraction. The pumping conditions were similar to the 1040 nm SDL experiment. The output powers were measured at different heatsink temperatures. Pump – output power characteristics are shown in Fig. 3.41. Output powers up to 2.25 W and 1.85 W were achieved for heat sink temperatures of 5 °C and 18 °C respectively [2]. Slope efficiency was calculated to be 12 % at5 °C and slightly decreased at higher temperatures. The output spectrum of the sample was centred at 1179 nm and is shown in Fig. 3.42. The spectrum is again highly modulated due to the etalon effect in the intracavity diamond heat spreader.

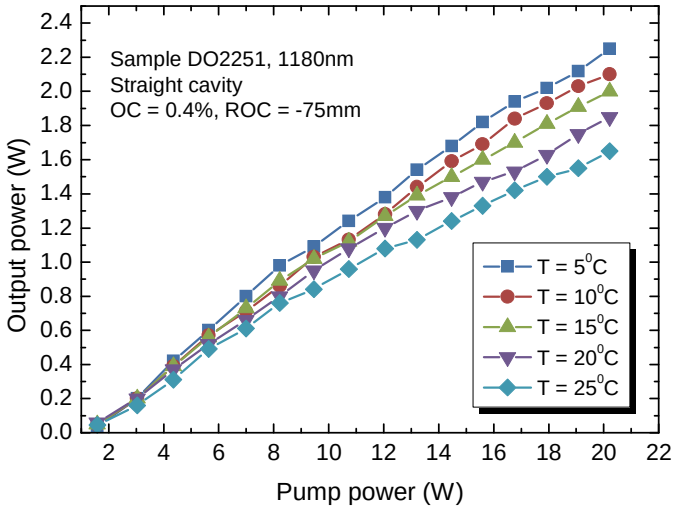

Fig. 3.41. Pump - output power characteristics for DO2251 1180 nm SDL sample at different heatsink temperatures.

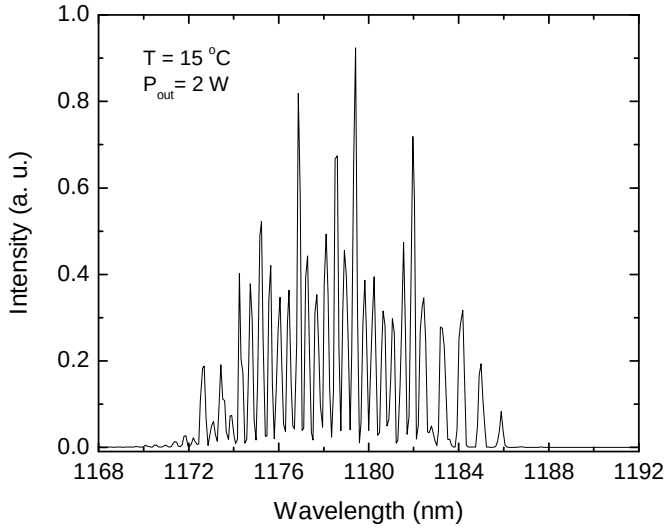

Fig. 3.42. Optical spectrum from DO2251 1180 nm sample.

In collaboration with the Optoelectronics Research Centre in Tampere University of Technology, this structure also was tested in dual gain chip configuration. For this experiment two different samples were bonded to diamond heat spreaders. The top surfaces

of the diamond heat spreaders were coated with an antireflecting coating for the pump and operating wavelengths. The performance of the device increased as more of the pump light could be absorbed and the intracavity losses were reduced. Two individual samples demonstrated output powers of 3 W and 4 W at room temperature when pumped with 30 W of pump power. When combined, the samples were tested in a W – shape cavity configuration where one sample served as an end mirror and other sample acted as a folding mirror in the cavity. The samples were pumped by two separate laser diodes. At 60W of incident power, CW output powers up to 6 W were achieved in such configuration. More details about the experiment can be found at [3, 4].

Another 1180nm sample, labelled DO2917 was tested. This sample had 42 layers of QDs and a resonant subcavity design. The same straight cavity configuration as with previous sample was used for the experiment and a 0.4 % output coupler was used. The sample produced up to 1.2 W of output power. Theoretically, the higher number of QD layers and the resonant design should raise the effective gain of the sample. However, the result was significantly lower than with DO2251 sample. The reason of reduced efficiency could be the interruption in the growth process. The DBR part and active region for sample DO2917, unlike for other samples, were grown in different facilities. The interruption between these growths may have led to the formation of defects in the interface due to temperature changes and surface contamination.

3.4. SDLs at 1260 nm

Similarly to the previous section, two QD SDL samples with intracavity heat spreaders were tested for 1260 nm operation. Sample DO2100 consisted of 19 QD layers and had a resonant subcavity. Meanwhile DO2254 sample was grown with 39 layers of QDs and was antiresonant. Both samples were tested in a straight cavity configuration using RoC = -75 mm output couplers (Fig.3.36, a).

Sample DO2100 produced output powers up to 55 mW with 0.3 % slope efficiency at a heat sink temperature of 5 ^{o}C at a maximum pump power of 20 W. A highly reflective mirror was used as an output coupler. The slope efficiency and threshold did not show any significant dependence on heat sink temperature when tuning it in the 5-25 ^{o}C range. The maximum output power varied by a few mW and decreased down to 50 mW at 25 ^{o}C. It must be noted that the high reflector was not the optimum output coupler and so the output parameters could be improved with optimised output coupler. However, 0.2 % transmission was too high for output coupling and the lasing could not be achieved. The output spectrum was centred at 1270 nm at 15 ^{o}C at maximum pump power. Pump – output power characteristics of DO2100 sample are shown in Fig. 3.43.

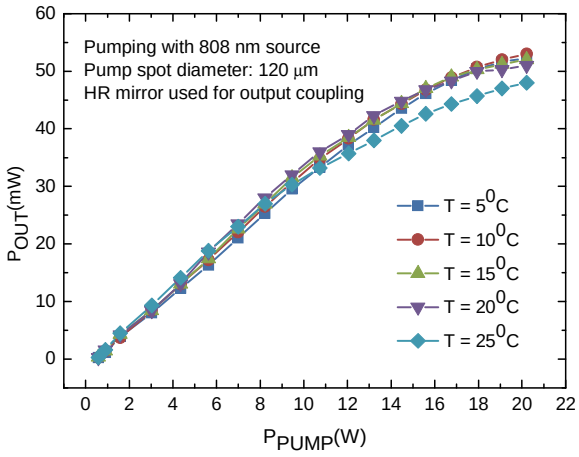

Fig. 3.43. Pump - output power characteristics of DO2100 1260 nm sample.

The second 1260 nm sample, DO2254, produced output powers up to 1.63 W using 0.4 % output coupler at a heat sink temperature of 5 ^{o}C [5]. The slope efficiency was measured to be 9 %. At room temperature, the output power was more than 1 W with 7% slope efficiency. Pump – output power characteristics are shown in Fig. 3.44. The beam quality factor M^2 was found to be ~1.5 at the optimal output power of 0.8 W and slightly increased with higher output powers. The optical output spectrum was centred at 1250 nm at the highest output power and is shown in Fig. 3.45.

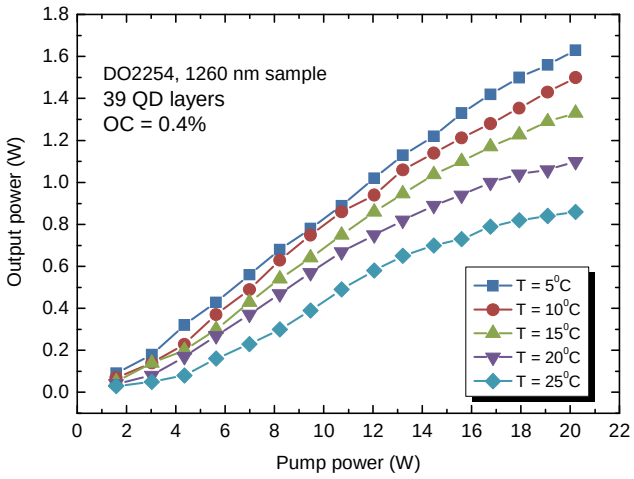

Fig. 3.44. Pump - output power characteristics for DO2254 sample.

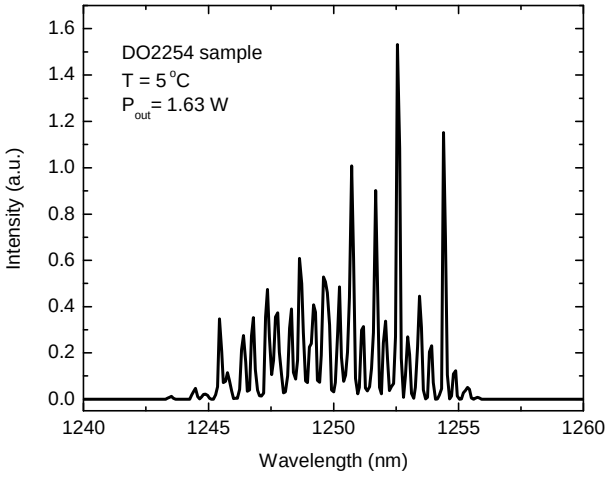

Fig. 3.45. Optical output spectrum of DO2254 sample at the highest output power.

A higher number of QD layers and antiresonant design has proven to be more suitable for the 1260 nm QD SDL in the above described cases. The poor performance of DO2100 sample could be a result of insufficient gain and possible detuning from the cavity

resonance. However, the results represented InGaAs QD based SDLs emitting at one of the longest wavelengths at the time of their publication [6, 7].

3.5. Comparison between ground and excited states lasing

As discussed in the introduction chapter, QDs feature discrete available energy states. The lowest energy state that can be occupied by excited carriers is called the ground state (GS) whilst higher energy states are known as excited states (ES). In InGaAs QDs such as the ones imbedded in our SDL samples, two states are typically considered, i.e., ground state and the first excited state. When designing an SDL sample, the length of the subcavity is chosen to be in resonance or antiresonance with one of the wavelengths coinciding with the transition in corresponding energy state. The sizes of QDs are then adjusted in the growth process for the desired emission. The lasing operation through one or another transmission can lead to different laser properties. In our experiments we compared the difference between achievable output powers [4].

In order to compare the efficiency of the devices by means of ground and excited state transitions in QDs, samples DO2251 and DO2254 were grown with a similar number of QD layers and an antiresonant design was used for both active regions. The samples also had similar sized QDs. However, the subcavity of DO2254 sample was designed for a wavelength of 1260 nm, i.e., it was optimized for the operation through the ground state transition. Meanwhile sample DO2251 was designed to operate at 1180 nm, i.e., the first excited state. The DBRs of the samples were also designed for corresponding wavelengths. The devices were mounted and tested in SDL cavities as has been shown in previous sections. Under similar experimental conditions, output powers up to 2 W were achieved

from the 1180 nm device and 1.3 W from the 1260 nm device at a heatsink temperature of 15 ^{o}C (Fig. 3.46). The better performance of 1180 nm device suggests excited state transitions should be considered as a choice for high power QD SDL designs. This is in line with the predicted two-fold higher amount of states at the excited state resulting in higher gain in such devices [8, 9].

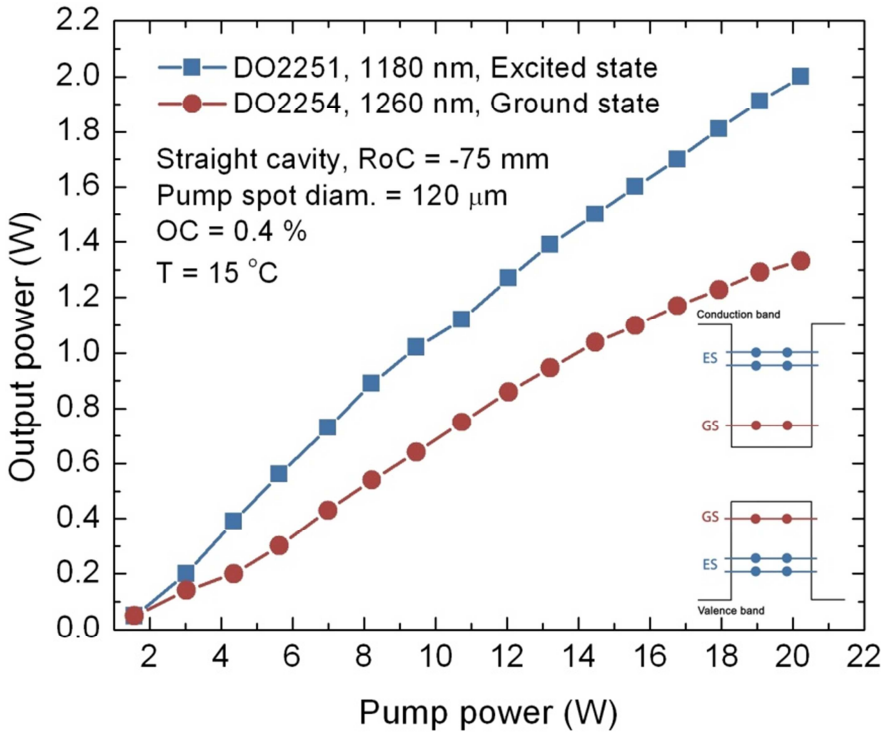

Fig. 3.46. Output power characteristics from QD SDLs operating at GS and ES transitions. The inset shows a schematic picture of GS and ES energy levels in QD.

Table 3.6 summarises the presented QD SDL results in CW regime. Output powers up to 6 W were achieved at 1040 nm (pump limited), 2.25 W at 1180 nm and up to 1.6 W for 1260 nm device. QD SDL operations at GS and ES transitions were compared. It was shown that the first excited state transition supports higher gain in the device as predicted by theory.

Although QD SDLs at 1 µm cannot yet compete with their QW based counterparts in this spectral region, the performance at longer wavelengths is comparable to QW based devices.

Sample No	*Wavelength (nm)*	*CW output power (W)*	*Reference*
DO1845 (without heat spreader)	1040	0.09	[10]
DO1845	1040	6	[4]
DO2251	1180	2.25	[2]
DO2917	1180	1.2	
DO2100	1260	0.055	[7]
DO2254	1260	1.63	[5]

Table 3.6. The summary of presented QD SDL performance results in CW regime. All SDLs were tested using diamond heat spreaders unless otherwise stated.

3.6. Second harmonic generation in quantum dot based semiconductor disk lasers

Following the discussion of CW operation in QD SDLs, a few important intracavity techniques that can be applied to these devices will be introduced. The first applications and the first results of frequency doubled SDLs will be discussed along with the intracavity second harmonic generation principles in SDLs. Finally the experimental results will be presented.

3.6.1. Applications of frequency doubled semiconductor disk lasers

With the proliferation of laser-assisted technologies, the demand for visible coherent light sources is also constantly increasing. Such trends are influenced by various applications employing blue to red emitting lasers such as laser projectors and televisions [11]. For these applications, compact, stable, efficient and cheap laser sources with diffraction limited beam quality and multi-Watt output powers are required for red, green and blue (RGB) colours. The lasers are attractive light sources for such display applications due to several reasons. Firstly, the available emission wavelengths from lasers allow for much wider colour gamut coverage than the competing technologies like cathode ray tubes (CRT), liquid crystal displays (LCD) or LEDs are capable of. Also the better colour saturation is available due to the spectral purity. Better brightness and image contrast are likely to be achievable due to high brightness parameter of laser source [12]. More specific laser display applications can be found in digital cinemas or flight simulators. However, the price of production needs to be reduced for this technology in order to reach a wide consumer market. In this perspective, frequency doubled SDL sources are competing with edge emitters, DPSS lasers and VCSELs.

Another set of applications for visible light lasers lies in medicine. For example red emitting lasers are widely used for photodynamic therapy due to their longer penetration depth into the tissue than shorter wavelengths and photosensitizers available for this spectral region [13, 14]. Yellow emitting lasers are in demand for treatment of retinal vascular diseases in ophthalmology. For example 577 nm lasers are optimized for photocoagulation therapy for patients having diabetic retinopathy or age related macular degeneration [15, 16].

Certain spectroscopic applications also require visible light sources as there are a number of optical transitions in atoms that lie in this spectral region, for example, iodine (503 nm), sodium (589.5 nm), neon (640 nm), calcium (657 and 672 nm), lithium (670.8 nm), strontium (689 nm) [17, 18]. Blue and green multi-Watt output power lasers are used in forensics to detect organic materials based traces [19]. Powerful yellow – orange lasers are needed for laser guide stars [20, 21].

A number of the above mentioned applications already employ SDL sources. The SDL sources are advantageous as they can offer wavelength and power scaling over wide ranges whilst providing good beam quality. The visible spectral region is accessible in SDLs through the second harmonic generation (SHG) using nonlinear crystals with SDLs emitting in the ~0.9 – 1.3 μm region. In visible region SDLs are mainly competing with frequency doubled solid state and dye lasers or indeed other types of semiconductor lasers depending on the required laser properties for certain application. SDLs with direct emission in red region at 674 nm and output powers up to 0.4 W were also demonstrated based on GaInP/AlGaInP QWs [22]. Direct red emission above 700 nm was also demonstrated from InP QDs based SDLs, however, with lower output powers [23].

In terms of CW output power, the SDL sources emitting around 1060nm which are used as a base for green emitting frequency doubled SDLs are quite well developed using well established InGaAs/GaAs quantum well technology providing tens of Watts of output power [24-26]. The wavelengths below and above 532 nm can also be covered by SDL sources. SDLs emitting at 920-980 nm were frequency doubled to the blue region and produced high output powers up to 15 W [25, 27, 28]. UV radiation at 338 nm was achieved by frequency doubling red emitting SDL [29]. Demonstrations of UV generation from SDLs using higher order harmonic generation were also reported [30, 31].

SDLs emitting at 1150 – 1300 nm are required for sources in the yellow – orange – red spectral region. However, this infrared spectral region typically is not achievable using InGaAs/GaAs QWs due to the high compressive strain required to achieve longer emission wavelengths. Highly strained InGaAs/GaAs QWs were used for SDL up to 1170 nm with 7 W of output power [32]. Alternative QW materials for this spectral region include GaAsSb/GaAs and InGaAsN/GaAs compositions [33-35]. Also, AlGaInAs/InP based QWs can emit at 1.3 – 1.55 μm. However, antimonide based compositions typically suffer from weak carrier confinement and high thermal sensitivity. Dilute nitride compositions lead to increased nonradiative recombination as the increased concentration of nitrogen leads to the formation of point defects [2]. An issue related to AlGaInAs/InP composition is the lack of materials for lattice matched DBR fabrication. Monolithic versions of such a device use DBRs with incorporated InP. However, this results in low performance and low thermal conductivity of the DBR limiting the power scaling of the device. As an alternative to the monolithic growth approach, wafer fusion has also been extensively studied in recent years. In this technique, an InP based active region is fused with a separately grown and lattice mismatched DBR based on well-established AlGaAs/GaAs [36-38].

Another alternative to QW based SDLs emitting at 1150 – 1300 nm spectral region is the use of QDs. QDs for this region are based on well-established InGaAs/GaAs materials system. QD based active regions can be monolithically integrated with AlAs/GaAsDBRs. The review and recent results of extended wavelength region from QD based SDLs were presented in a previous chapter. Recently second harmonic generation from these devices in green, orange and red wavelengths have been demonstrated [3, 4,39]. Without the extended wavelength range, QD based frequency doubled SDLs can have additional properties such

as broad tuneability, low threshold or low thermal sensitivity as it has been theoretically predicted. These properties are under investigation at the moment.

3.6.2. Intracavity second harmonic generation in semiconductor disk lasers

Second harmonic generation is a nonlinear process driven by high intensity electric fields in dielectric medium. The nonlinear processes are performed by employing nonlinear crystals which exhibit various properties for different applications and lasers. Frequency doubling can be performed using both, continuous wave and mode-locked lasers. When using pulsed lasers, the SHG is performed outside the cavity by focusing the beam into the crystal. Nonlinear processes are then driven by high peak powers. For CW regime, nonlinear crystals are usually used inside the cavity as most of the oscillating energy is stored there. This is particularly true for QD SDLs as typically output couplers only up to 1 % are used in these devices due to the inherently low gain of QDs. Thus such high-Q cavities are advantageous for intracavity frequency doubling. Another advantage of SDLs as a base for SHG is the absence of so called “green problem”. Large fluctuations in the output of frequency doubled Nd:YAG laser were first observed in 1986, limiting its suitability for some of the applications [40, 41]. The reason for it was the oscillation of several longitudinal modes and their nonlinear interaction in the cavity. The noise of the frequency doubled SDL output is much lower than in solid state lasers due to a short carrier lifetime in semiconductors [42, 43].

In the general case of classical linear optics, the induced dielectric polarization of medium is linearly proportional to the applied electric field E [44]:

$$P = \varepsilon_0 \chi E \tag{3.1}$$

Here ε_0 is permittivity and χ is the electric susceptibility of the medium. The above expression is valid when the external electric field is weak compared to the interatomic fields in the medium. However, when optical intensity is increased, the dependence becomes nonlinear. The above expression can be expanded out into a Taylor series:

$$P = \varepsilon_0\chi^{(1)}E + \varepsilon_0\chi^{(2)}E^2 + \varepsilon_0\chi^{(3)}E^3 + \cdots \tag{3.2}$$

The second and third terms of the above expression describe nonlinear second and third order effects in the medium. Second harmonic generation is described by the second term in (3.2) and it can be seen that it depends on the square of electric field intensity. If the fields in the medium are high enough, the polarization can start an oscillating component with twice the frequency of the incoming wave. However, to achieve efficient frequency conversion, a few important conditions must be fulfilled.

Constructive interference between second harmonic waves needs to be achieved in order to extract useable output power. However, beams of original and doubled frequency travel at different speeds due to the dispersive origin of nonlinear medium. This then leads to the second harmonic waves generated at different points of the crystal to interfere destructively. To avoid this, phase matching techniques are employed in SHG crystals [45]. There are a few different ways to ensure phase matching between original and second harmonic beams.

Birefringent phase matching relies on the intrinsic birefringence properties of the nonlinear crystals. If two waves are in phase, the difference between their wave vectors should be zero. Thus for efficient SHG (in type I phase matching):

$$\Delta k = |2k_\omega - k_{2\omega}| = \left|\frac{4\pi(n_\omega - n_{2\omega})}{\lambda_\omega}\right| = 0 \tag{3.3}$$

In order to fulfil the above expression, n_ω should be equal to $n_{2\omega}$. In crystals used for birefringent phase matching, the refractive index for a given wavelength depends on the electric field polarization for a given direction of propagation [46]. The refractive index changes with the orientation of polarization towards the optical axis of the crystal. The light is subject to the ordinary refractive index n_o if its polarization is perpendicular to optical axis and to the extraordinary refractive index n_e if it is parallel with the optical axis. All other polarizations have both components and depend on the angle θ. The $n_e(\theta)$ in general is expressed as:

$$n_e(\theta) = \frac{n_o n_e}{\sqrt{n_0^2 sin^2(\theta) + n_e^2 cos^2(\theta)}} \tag{3.4}$$

Such notations are valid to uniaxial crystals. If the fundamental and second harmonic waves are polarized in the same direction, it is impossible to achieve $n_\omega = n_{2\omega}$. However, if the waves are polarized orthogonally to each other or if the fundamental wave has ordinary and extraordinary components and the second harmonic is polarized under 45 deg to it, $\Delta k = 0$ can be achieved[46]. The first case is known as type-I and the second as type-II phase matching. Refractive indices for ordinary and extraordinary beams of fundamental and second harmonics in uniaxial crystal are shown in Fig. 3.47. Refractive indices for second harmonic light tend to be higher due to the wavelength dispersion. It can be seen, that axis AA' defines a direction at which $n_\omega = n_{2\omega}$. Thus the most efficient SHG is achieved when the beam travels in such direction through the crystal. Common nonlinear crystals employing birefringence phase matching are lithium triborate (LiB_3O_5 - LBO), barium borate (BaB_2O_4 - BBO), titanyl phosphate ($KTiOPO_4$ - KTP).

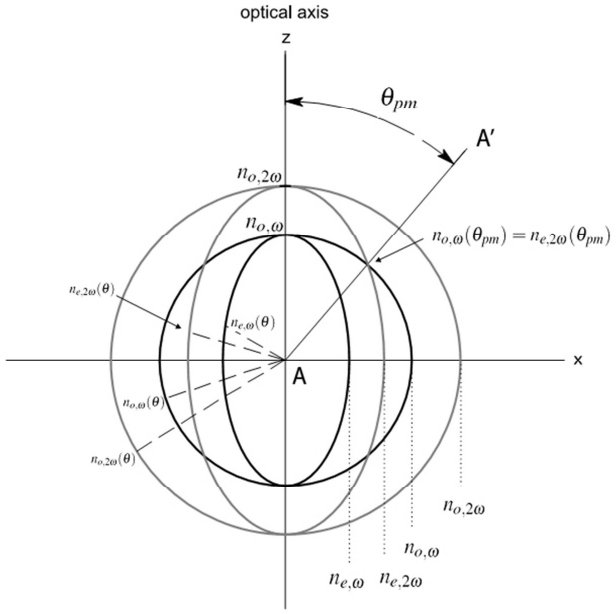

Fig. 3.47. Refractive indices for ordinary and extraordinary beams in uniaxial crystal [46].

Another technique widely used in nonlinear optical elements is called quasi phase matching (QPM). Instead of using the birefringent properties of the crystal, spatially modulated nonlinear properties are used. They periodically reset accumulated phase mismatch, for example, after each two coherence lengths(coherence length is a distance in which the phases of waves separate by π) [46]. The reset is done by either modulating the refractive index or the sign of nonlinearity. In QPM waves can be polarized in the same plane which allows for the exploitation of the highest nonlinearity in the crystal. Furthermore, some additional spectral ranges can be achieved and additional materials can be used in QPM. Periodical changes in such crystals are introduced using periodical poling. This is usually done using high electric fields in ferroelectric nonlinear crystals to change the polarization periodically [47]. Periodically poled lithium niobate ($LiNbO_3$ - LN), lithium tantalate

($LiTaO_3$ - LT) or potassium titanyl phosphate ($KTiOPO_4$ - KTP) are some examples of widely used crystals for quasi phase matching.

Phase matching schemes enable efficient SHG. However, additional parameters of nonlinear crystals help to choose the most suitable ones for specific lasers. Those parameters include transparency, effective nonlinear coefficient, alignment tolerances, walk-off angle, damage threshold, spectral and temperature acceptance and others [46].

3.6.3. Experimental setups for SHG in QD SDLs

The intracavity SHG experiments in QD SDLs were performed using V-shape and W-shape cavity configurations. The same gain elements with diamond intracavity heat spreaders used for previous output power measurement experiments were used. A typical V-shape cavity configuration for intracavity SHG experiment is shown in Fig. 3.48. The cavity is formed using a QD semiconductor chip and two curved mirrors. One of the mirrors served as a folding element and the other one acted as an output coupler. Second harmonic light can also be extracted through both dielectric mirrors depending on their coatings. The nonlinear crystal was positioned in the cavity mode waist for maximum conversion efficiency as it depends on the square of the fundamental power density [17]. The birefringent filter (BRF) was also inserted in the cavity at Brewster's angle. This helps to reduce the spectral width of the fundamental light to suit the spectral acceptance of the crystal which is typically in the range of few nm. In addition it allows for the tuning of the wavelength for optimum operation. Such cavity configuration was used for spectral conversion from the 1040 nm device. The experiments were performed in collaboration with our project partners M Squared Lasers Ltd. A RoC = - 25 mm folding mirror and a

RoC = - 50 mm end mirror were used. The folding mirror was placed 45 mm from the gain chip assembly and 70mm from the end mirror. A 3x3x15 mm lithium triborate (LBO) crystal was placed 13 mm from the 25 mm RoC mirror. A 0.5 mm thick quartz BRF was placed in the short arm. The gain structure was pumped with a 20 W 808 nm pump source with a 200 µm diameter pump spot. The temperature of chip assembly was held at 15 ^{o}C. The output power was measured from both arms [39].

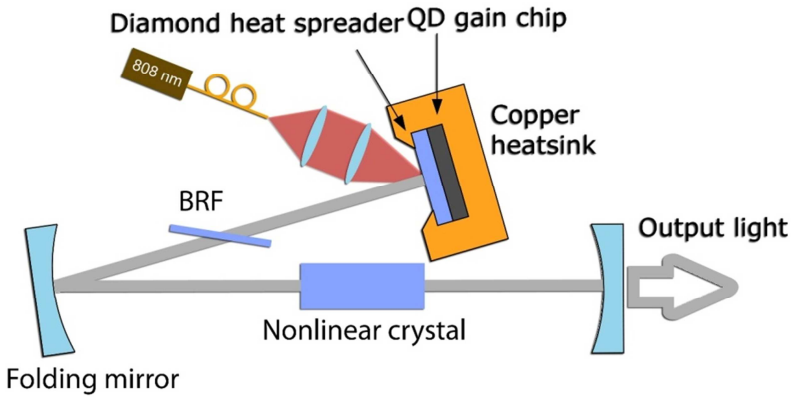

Fig. 3.48. A typical cavity configuration for intracavity second harmonic generation in QD SDLs.

A wavelength tuneability experiment using the same gain chip was also performed. V-shape cavity was used with folding and end mirrors both having RoC = -50 mm. A 3x3x20 mm size LBO crystal was positioned in the cavity along with 1 mm thick quartz BRF. A photo of the working setup is shown in Fig. 3.49.

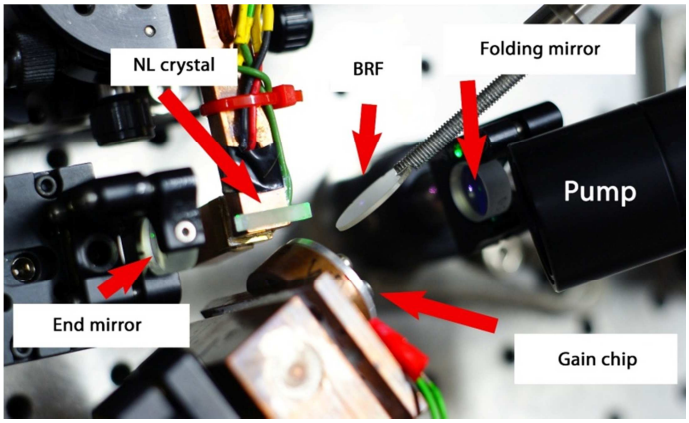

Fig. 3.49. Top view of frequency doubled green emitting QD based SDL.

The SHG experiment with the 1260 nm sample was also performed in V-shape cavity configuration, similar to the experiment with 1040 nm sample, but without the BRF as it was found to work more efficiently due to the high-loss gain chip. The SDL was pumped with 120 µm diameter pump spot. RoC = -50 mm mirror was used as folding element and RoC = -75 mm output coupler was used. A 3x3x10 mm size nonlinear bismuth borate (BiBO) crystal was used for frequency conversion to red spectral region. The output power of resulting light was measured from both cavity arms [4]. A photo of the described setup is shown in Fig. 3.50.

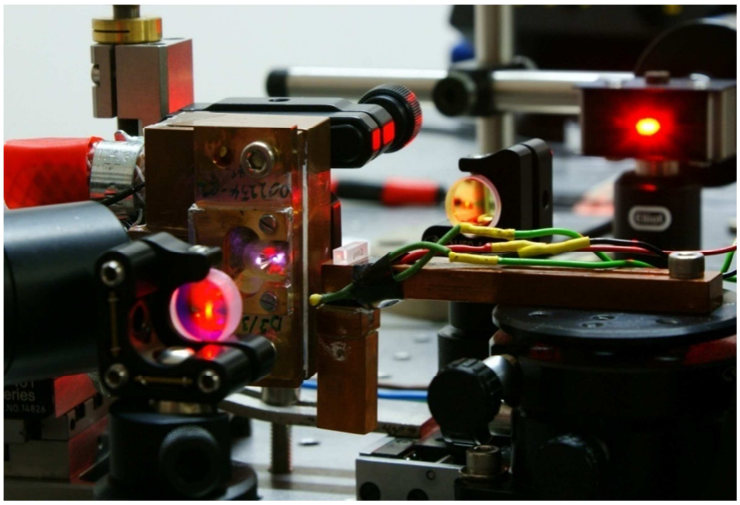

Fig. 3.50. Frequency doubled red emitting QD based SDL.

SHG experiments with the 1180 nm device were performed in collaboration with Tampere University of Technology. It was done in the dual gain chip cavity configuration as a single chip device did not supply enough gain for efficient frequency doubling. A W-shape cavity was used for this experiment. Two gain chips were pumped by two separate diode lasers with 180 µm pump spot diameters. A cavity was formed by two folding mirrors M1 and M2 and the end mirror M3 as it is shown in Fig. 3.51. The 4 mm long nonlinear beta-BaB_2O_4 (BBO) crystal was placed at a cavity waist with a mode diameter of ~180 µm. The frequency doubled output was measured after mirror M2 [4].

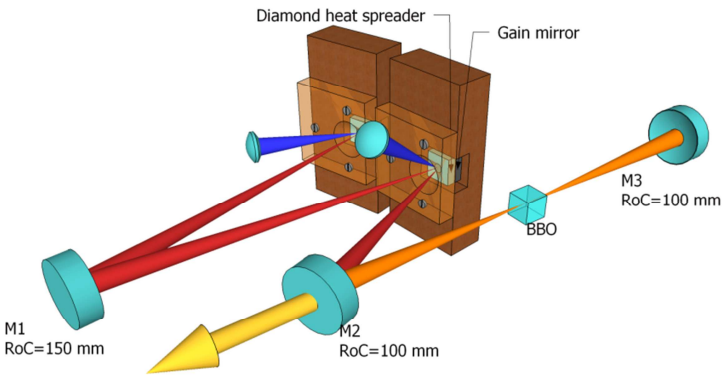

Fig. 3.51. W-shape dual gain chip cavity configuration for SHG in 1180 nm QD SDL.

Table below summarizes the experimental conditions that were used during SHG experiments.

Sample no	Second harmonic wavelength, nm	Cavity configuration	Crystal used	Crystal size, mm
DO1845	514 nm	V shape	LBO	3x3x15
DO1845	517-523 nm	V shape	LBO	3x3x20
DO2251	590 nm	W shape (two gain chips)	BBO	3x3x4
DO2254	624 nm	V shape	BiBO	3x3x10

Table 3.7. Summary of experimental setups used for SHG in QD SDLs

3.6.4. Second harmonic generation results

The output powers and optical spectra measurements of second harmonic light from QD based SDLs described in previous chapter, are presented in this section.

The system was based on a 1040 nm QD SDL which produced nearly 2 W of green light and was limited by the available pump. The overall conversion efficiency from 808 nm pump light to green light was approximately 10% which includes the pump light lost to the reflection from the SDL assembly [39]. It was the most efficient frequency doubled laser demonstrated from our tested samples. The laser operated at 514 nm and therefore it is a potential alternative for the argon ion laser.

As already mentioned, a SHG tuneability experiment was also performed. However, at the time of the experiment, mirrors without antireflective coatings for second harmonic light were only available. Thus, no useful output power could be extracted. The output light spectrum was tuned by rotating the birefringent filter. The output spectrum could be tuned

from 517 nm to 523 nm. The measured output spectra at different points are plotted in Fig. 3.52. The tuneability range should improve within more efficient cavity configuration.

A frequency doubled 1180 nm QD SDL device produced 2.5 W of output power at 590 nm. The total available pump power used from both pump sources was 50 W. To the best of our knowledge, it was the first demonstration of SHG in QD based SDL [3]. The operating wavelength of 590 nm can make this laser source applicable in sodium guide star and certain medical applications.

Up to 340 mW of red light was achieved from a frequency doubled 1260 nm QD SDL device. The device was pumped with up to 15 W of 808 nm light until the thermal rollover was reached. The optical spectrum of it was centred at 624 nm. Pump – output power characteristics of all three described devices are shown in Fig. 3.53 (a). Optical output spectra of fundamental and second harmonic light are shown in Fig. 3.53 (b).

The performance of frequency doubled QD SDLs was comparable to their demonstrated performance in fundamental frequency. Samples DO1845 and DO2251 (in dual gain chip configuration) allowed the generation of multi-Watt output power of green and orange light while sample DO2254 generated few hundred mW of red given its lower gain level as observed before.

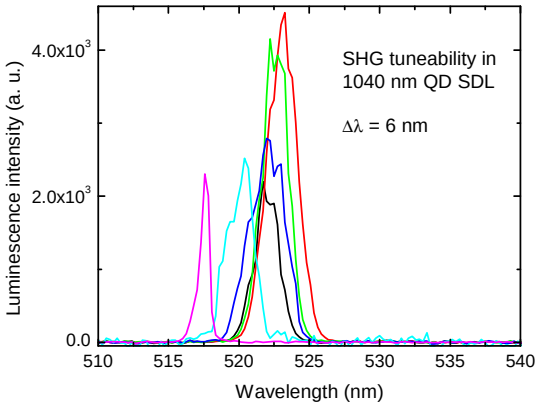

Fig. 3.52. Output spectra at different tuning points of second harmonic light from 1040 nm QD SDL.

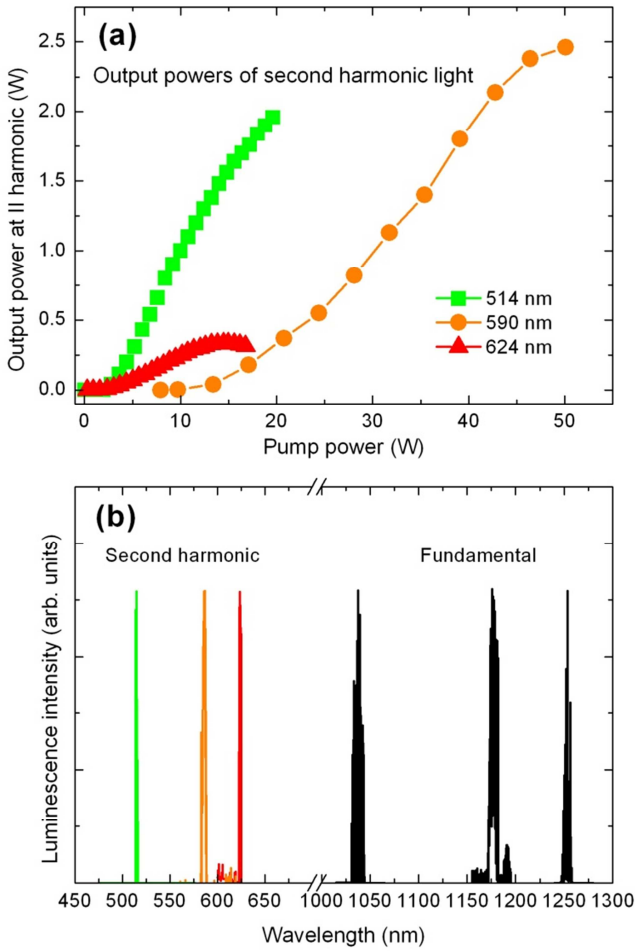

Fig. 3.53. (a) Pump - output power characteristics of frequency doubled QD SDLs tested in our experiments. (b) Normalized optical spectra of fundamental and second harmonic light from tested devices.

3.7. Wavelength tuneability

As already mentioned in the introduction, QD lasers feature a broad gain bandwidth as a result of inhomogeneous broadening which is particularly typical for Stranski-Krastanow QDs [48, 49]. Such a feature can be successfully explored in spectral tuning. Indeed it was demonstrated that spectral tuning of a few hundred nm is achievable in QD based external cavity laser diodes [50, 51]. Tuneability in QD based SDLs at different spectral regions was

measured in our experiments. It was shown that QD SDLs can feature broad tuning ranges of tens of nm [4, 5, 52]. In the following sections wavelength tuning techniques in SDLs will be presented together with main results achieved to date. This will be followed by the presentation of results achieved during the studies.

3.7.1. Wavelength tuning in semiconductor disk lasers

Laser sources featuring broad spectral tuneability ranges always are under intense interest for certain application areas. Broad tuning is often required for spectroscopic [53, 54], interferometry [55, 56], optical fibre communications [57], biological imaging like swept laser sources for optical coherence tomography [58] and other applications. Spectral control of SDL also allows the narrowing and stabilizing the emission spectrum for certain applications, for example, as pump sources for other lasers [59]. That allows for the elimination of thermally induced spectral shift.

The tuneability in QW based SDLs has been explored by a number of groups to date. Tuning ranges up to 50 nm around 1 µm and more than 150 nm around 2 µm were demonstrated. To date results of tuneable SDLs were presented in the introduction chapter, table 1. The structural properties of the listed devices were optimized for tuneability. For example, some of the authors used different thicknesses of QWs in the active region of SDL to broaden the tuning range [60]. Also, multiple gain chips SDLs were used for broader the tuneability[61]. Tuneable micro-lasers based on SDL concept were demonstrated using microelectromechanical systems (MEMS) and fibre assisted tuning [62, 63].

Wavelength selective elements are typically used inside the open cavities of tuneable lasers. These can be dispersive prisms, diffraction gratings or birefringent filters. In first two cases, by rotating the elements, only a narrow width wavelength element can be reflected back into the resonator. The birefringent filter (BRF) employs polarization sensitivity to select the wavelengths. Other elements such as Fabry-Perot etalons can be used for wavelength selection. BRF is usually used in SDL sources due to its simplicity, low losses and easy operation.

A simple birefringent crystal plate with its optical axis being parallel to the surface of the plate can be used as a BRF in linearly polarized lasers like SDLs. Quartz plates are typically used for this purpose. A plate is inserted in the cavity at Brewster's angle to the beam direction. The oscillating modes in the resonator are linearly polarized. After entering the plate, depending on the position of optical axis, the beam is separated into ordinary (o) and extraordinary (e) components. Those two components experience difference phase shifts as the refractive indexes for o and e beams, n_o and n_e are different in quartz [44]. If the phase difference after the plate is equal to $2m\pi$, where m is an integer, the output beam remains unchanged and no losses are introduced, i.e., for the beam to pass through the BRF without any losses, the condition (3.5) must be satisfied.

$$\frac{2\pi}{\lambda}(n_e - n_o)L = 2m\pi \tag{3.5}$$

Here λ is the beam wavelength in vacuum and L is the thickness of the plate along the beam direction. As can be seen, the condition is viable only for a certain wavelength. The wavelength can be tuned by rotating the plate around normal to its surface. In this situation, the value of n_e changes as it depends on the angle between the optical axis and the electric

field vector. As n_e changes, the condition (3.5) is continually satisfied by a different wavelength [44, 64].

A schematic picture of the wavelength tuning principle in SDLs is shown in Fig. 3.54 [65]. As it is shown in the picture, the BRF introduces losses into the resonator. However, for certain frequencies, for which condition (3.5) is satisfied, the minimum of the losses reaches the intrinsic gain of the structure and the laser is forced to operate at that specific frequency. When the BRF is rotated, the minimum position of losses is also shifted across the available longitudinal modes in the resonator. It must be noted, that in real life, the form of losses shown in Fig. 3.54 should be sine wave shapes rather than straight line as shown schematically. The tuning range is mainly limited by the available gain bandwidth and the DBR stopband.

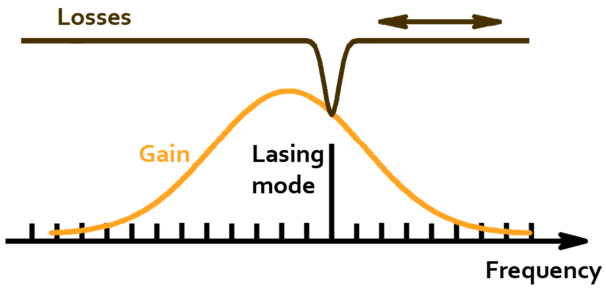

Fig. 3.54. A schematic picture of spectral tuning principle in semicondcutor disk lasers by using an intracavity filter [65].

3.7.2. Wavelength tuning results in QD SDLs

In our experiments, a birefringent quartz plate was used as a spectral filter. The thickness of the plate was 1 mm. The wavelength tuning experiments were performed in a V shape or straight cavity configurations with the BRF inserted at Brewster angle. A typical cavity configuration for wavelength tuneable QD SDL is shown in Fig. 3.55.

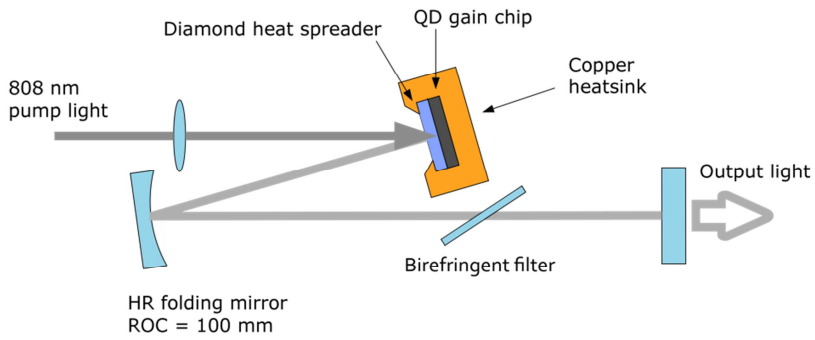

Fig. 3.55. A Schematic drawing of V-shape cavity configuration for wavelength tuneable QD SDL

Sample DO1845 was used for a 1040 nm SDL. By rotating the BRF, the wavelength was tuned over 50 nm around its central wavelength using a 0.75 % output coupling. The optical spectrum of the laser was narrowed to one or just a few modes of the diamond heat spreader modes and typically was narrower than 1 nm. The output power at the central wavelength was almost 4 W and reduced at the wings of the tuning range. Output couplers with different transmission values were also used to extend the tuning range as the outcoupling losses were reduced in the cavity. A 60 nm tuneability range was achieved with a 0.15 % output coupler, however, the output power was reduced to 2.2 W in this case. Wavelength tuning curves for different output couplers are shown in Fig. 3.56.Pump – output power characteristics for this sample were also measured using a 0.75 % output coupler, with and without the BRF inside the resonator. Output power characteristics are shown in Fig. 3.57.It can be seen that the BRF still introduces some losses into the cavity as the maximum output power drops from 4.3 W to 3.6 W after the BRF is inserted.

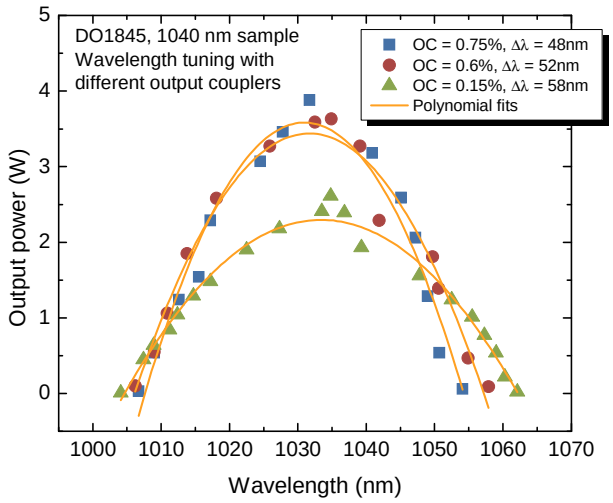

Fig. 3.56. Wavelength tuning curves of 1040 nm QD SDL sample using different output couplers

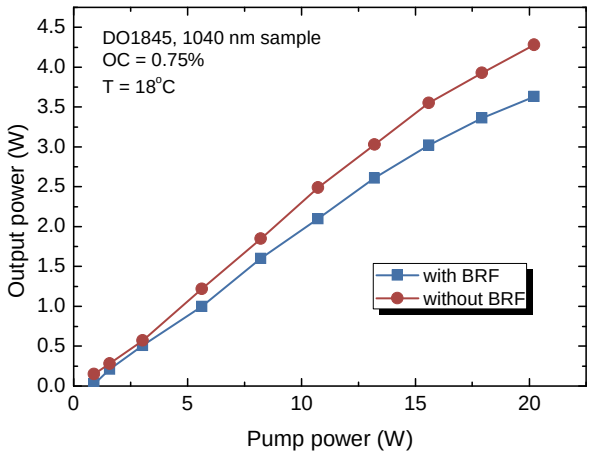

Fig. 3.57. Pump - output power characteristics of 1040 nm QD SDL with and without birefringent filter in the cavity.

Tuning characteristics of the 1180 nm sample were measured in a V- shape cavity configuration with the SDL gain mirror forming one end of the cavity, a RoC = -200mm folding mirror and a plane output coupler forming the other end. The gain mirror was

pumped with 20 W of pump power. With a 0.4 % output coupler, the wavelength was tuned 23 nm around its central wavelength with a maximum output power of 270 mW in the centre of tuning range. After the output coupler was changed to a high reflector, the tuning range was extended to 69 nm allowing the laser to be tuned from 1147 nm to 1210 nm with the output power reaching 80 mW at the centre of tuning range and with a few mW at the wings. The reason of the significant output power drop as compared to the stand alone cavity is not clear.

Wavelength tuneability for the 1260 nm device was measured in a straight cavity configuration using a 0.4 % output coupler. A single mode optical spectrum was tuned over 25 nm around its central wavelength with the output power reaching 550 mW at 1250 nm. Fig. 3.58 shows wavelength tuning characteristics for all three devices. Optical spectra measured at different spectral positions are also shown in the same graph. The points in Fig. 3.58are at the peaks of diamond heatspreader etalon modes. Using a wedged heatspreader or substrate thinning approach would allow for a continuous wavelength tuning.

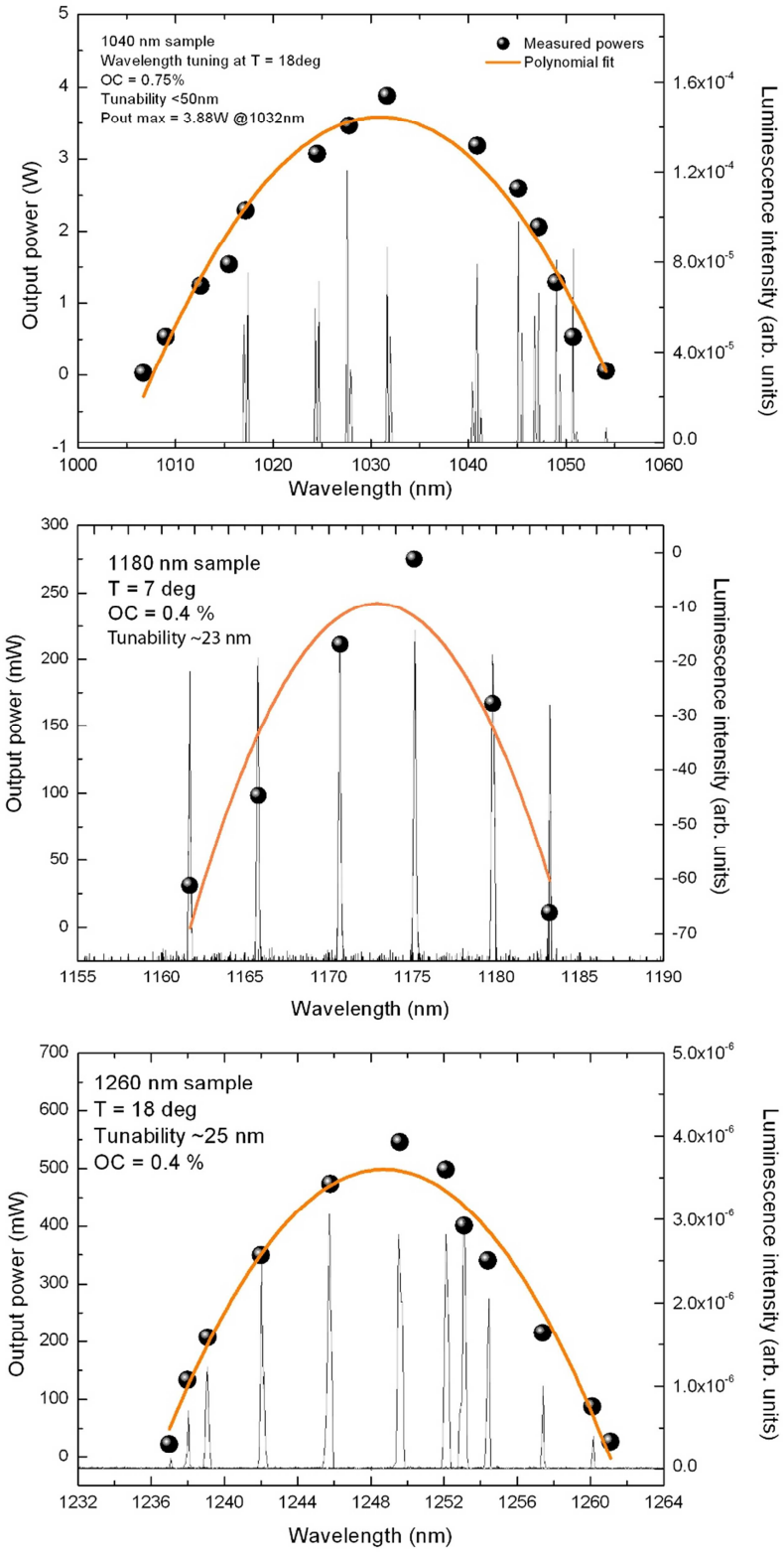

Fig. 3.58. Wavelength tuning characteristics and output spectra of three different wavelength QD SDLs

3.8. Chapter conclusions

In this chapter, the operation of QD based SDLs was explored in continuous wave regime. Devices operating at 1040, 1180 and 1260 nm were used for the experiments. Continuous wave output powers of up to 6 W were achieved for a device emitting at 1040 nm (pump limited) representing most powerful QD SDL to date. An output power of 2.25 W for 1180 nm and up to 1.6 W for 1260 nm devices was achieved. It was demonstrated that the output powers for QD SDLs emitting at 1180 and 1260 nm are comparable to their QW based counterparts. 1180 nm and 1260 nm devices were compared by the optical transition in operation and it was shown that for the design of high power QD SDLs the excited state transition should be considered.

Intracavity second harmonic generation was demonstrated from all three devices giving output powers of 2 W of green, 2.5 W of orange (two chip configuration) and 0.33 W of red light. The ability of frequency conversion broadens the range of QD SDL applications. Future work in this field will include the search for more efficient frequency conversion and exploration of single frequency wavelength tuneability at the second harmonic.

Wavelength tuning capabilities were explored and wide tuneability ranges of 60 nm for 1040 nm, 69 nm for 1180 nm and 25 nm for 1260 nm devices were demonstrated. The results achieved show that the QD based SDLs are comparable to some of their QW based counterparts and might find applications where particular wavelengths or broad tuning ranges are required.

References

[1] A. J. Kemp, G. J. Valentine, J. M. Hopkins, J. E. Hastie, S. A. Smith, S. Calvez, M. D. Dawson, and D. Burns, "Thermal management in vertical-external-cavity surface-emitting lasers: Finite-element analysis of a heatspreader approach," *IEEE Journal of Quantum Electronics,* vol. 41, pp. 148-155, 2005.

[2] J. Rautiainen, I. Krestnikov, M. Butkus, E. U. Rafailov, and O. G. Okhotnikov, "Optically pumped semiconductor quantum dot disk laser operating at 1180 nm," *Optics Letters,* vol. 35, pp. 694-696, 2010.

[3] J. Rautiainen, I. Krestnikov, J. Nikkinen, and O. G. Okhotnikov, "2.5 W orange power by frequency conversion from a dual-gain quantum-dot disk laser," *Optics Letters,* vol. 35, pp. 1935-1937, 2010.

[4] M. Butkus, J. Rautiainen, O. G. Okhotnikov, C. J. Hamilton, G. P. A. Malcolm, S. S. Mikhrin, I. L. Krestnikov, D. A. Livshits, and E. U. Rafailov, "Quantum Dot Based Semiconductor Disk Lasers for 1-1.3 μm," *IEEE Journal of Quantum Electronics*, vol. 17, pp. 1763-1771, 2011.

[5] M. Butkus, C. J. Hamilton, J. Rautiainen, O. G. Okhotnikov, S. S. Mikhrin, I. L. Krestnikov, and E. U. Rafailov, "Broadly tunable 1250 nm quantum dot-based semiconductor disk laser," *IET Optoelectronics,* vol. 5, pp. 165-167, 2011.

[6] M. Butkus, J. Rautiainen, O. G. Okhotnikov, S. S. Mikhrin, I. L. Krestnikov, E. U. Rafailov, "1270 nm Quantum Dot Based Semiconductor Disk Lasers," *22nd International semiconductor lasers conference*, Kyoto, Japan, 2010.

[7] M. Butkus, J. Rautiainen, O. G. Okhotnikov, S. S. Mikhrin, I. L. Krestnikov, and E. U. Rafailov, "Quantum dot semiconductor disk laser operating at 1270 nm," *1st EOS Topical Meeting on Lasers*, Capri, Italy, 2009.

[8] K. Kim, T. B. Norris, S. Ghosh, J. Singh, and P. Bhattacharya, "Level degeneracy and temperature-dependent carrier distributions in self-organized quantum dots," *Applied Physics Letters*, vol. 82, pp. 1959-1961, 2003.

[9] S. W. Osborne, P. Blood, P. M. Smowton, Y. C. Xin, A. Stintz, D. Huffaker, and L. F. Lester, "Optical absorption cross section of quantum dots," *Journal of Physics-Condensed Matter*, vol. 16, pp. S3749-S3756, 2004.

[10] M. Butkus, K. G. Wilcox, J. Rautiainen, O. G. Okhotnikov, S. S. Mikhrin, I. L. Krestnikov, A. R. Kovsh, M. Hoffmann, T. Sudmeyer, U. Keller, and E. U. Rafailov, "High-power quantum-dot-based semiconductor disk laser," *Optics Letters*, vol. 34, pp. 1672-1674, 2009.

[11] J. L. A. Chilla, H. Zhou, E. Weiss, A. L. Caprara, Q. Shou, S. V. Govorkov, M. K. Reed, and L. Spinelli, "Blue & green optically-pumped semiconductor lasers for display," *Projection Displays XI*. vol. 5740, M. H. Wu, Ed., Bellingham: SPIE-Int. Soc. Optical Engineering, pp. 41-47, 2005.

[12] A. Masters and C. Seaton, "Laser-based displays will deliver superior images," *Laser Focus World*, vol. 42, pp. S9-S11, 2006.

[13] L. Brancaleon and H. Moseley, "Laser and non-laser light sources for photodynamic therapy," *Lasers in Medical Science*, vol. 17, pp. 173-186, 2002.

[14] J. Wu, M. S. Feld, and R. P. Rava, "Analytical model for extracting intrinsic fluorescence in turbid media," *Applied Optics*, vol. 32, pp. 3585-3595, 1993.

[15] C. F. Blodi, S. R. Russell, J. S. Pulido, and J. C. Folk, "Direct and feeder vessel photocoagulation of retinal angiomas with dye yellow laser," *Ophthalmology*, vol. 97, pp. 791-797, 1990.

[16] "Optically Pumped Semiconductor Lasers," Coherent Inc., USA, 2010.

[17] S. Calvez, J. E. Hastie, M. Guina, O. G. Okhotnikov, and M. D. Dawson, "Semiconductor disk lasers for the generation of visible and ultraviolet radiation," *Laser & Photonics Reviews,* vol. 3, pp. 407-434, 2009.

[18] C. E. Wieman and L. Hollberg, "Using diode-lasers for atomic physics," *Review of Scientific Instruments,* vol. 62, pp. 1-20, 1991.

[19] "Tracer - portable, compact forensic laser system," Coherent Inc., USA, 2008.

[20] C. A. Denman, P. D. Hillman, G. T. Moore, J. M. Telle, J. E. Preston, J. D. Drummond, and R. Q. Fugate, "Realization of a 50-watt facility-class sodium guidestar pump laser," *Solid State Lasers XIV: Technology and Devices*., vol. 5707, H. J. Hoffman and R. K. Shori, Eds., Bellingham: SPIE-Int. Soc. Optical Engineering, pp. 46-49, 2005.

[21] S. Xie, Y. Bo, J. Xu, Y. Shen, P. Wang, Z. Wang, F. Yang, Q. Peng, D. Cui, J. Zhang, and Z. Xu, "A 7.5 W quasi-continuous-wave sodium D(2) laser generated from single-pass sum-frequency generation in LBO crystal," *Applied Physics B-Lasers and Optics,* vol. 102, pp. 781-787, 2011.

[22] J. E. Hastie, S. Calvez, M. D. Dawson, T. Leinonen, A. Laakso, J. Lyytikainen, and M. Pessa, "High power CW red VECSEL with linearly polarized TEM00 output beam," *Optics Express,* vol. 13, pp. 77-81, 2005.

[23] P. J. Schlosser, J. E. Hastie, S. Calvez, A. B. Krysa, and M. D. Dawson, "InP/AlGaInP quantum dot semiconductor disk lasers for CW TEM00 emission at 716-755 nm," *Optics Express,* vol. 17, pp. 21782-21787, 2009.

[24] J. Lee, S. Lee, T. Kim, and Y. Park, "7 W high-efficiency continuous-wave green light generation by intracavity frequency doubling of an end-pumped vertical

external-cavity surface emitting semiconductor laser," *Applied Physics Letters*, vol. 89, 241107, 2006.

[25] J. Chilla, Q. Z. Shu, H. L. Zhou, E. Weiss, M. Reed, and L. Spinelli, "Recent advances in optically pumped semiconductor lasers - art. no. 645109," *Solid State Lasers XVI: Technology and Devices*. vol. 6451, H. J. Hoffman, R. K. Shori, and N. Hodgson, Eds., Bellingham: SPIE-Int. Soc. Optical Engineering, pp. 45109-45109, 2007.

[26] "Lasers for life sciences," Coherent. Inc., USA, 2011.

[27] J. Y. Kim, S. Cho, S. J. Lim, J. Yoo, G. B. Kim, K. S. Kim, J. Lee, S. M. Lee, T. Kim, and Y. Park, "Efficient blue lasers based on gain structure optimizing of vertical-external-cavity surface-emitting laser with second harmonic generation," *Journal of Applied Physics*, vol. 101, 033103, 2007.

[28] J. Chilla, S. Butterworth, A. Zeitschel, J. Charles, A. Caprara, M. Reed, and L. Spinelli, "High power optically pumped semiconductor lasers," *Solid State Lasers Xiii: Technology and Devices*. vol. 5332, R. Scheps and H. J. Hoffman, Eds., Bellingham: SPIE-Int. Soc. Optical Engineering, pp. 143-150, 2004.

[29] J. E. Hastie, L. G. Morton, A. J. Kemp, M. D. Dawson, A. B. Krysa, and J. S. Roberts, "Tunable ultraviolet output from an intracavity frequency-doubled red vertical-external-cavity surface-emitting laser," *Applied Physics Letters*, vol. 89, 061114, 2006.

[30] Y. Kaneda, J. M. Yarborough, L. Li, N. Peyghambarian, L. Fan, C. Hessenius, M. Fallahi, J. Hader, J. V. Moloney, Y. Honda, M. Nishioka, Y. Shimizu, K. Miyazono, H. Shimatani, M. Yoshimura, Y. Mori, Y. Kitaoka, and T. Sasaki, "Continuous-wave all-solid-state 244 nm deep-ultraviolet laser source by fourth-harmonic

generation of an optically pumped semiconductor laser using CsLiB6O10 in an external resonator," *Optics Letters,* vol. 33, pp. 1705-1707,2008.

[31] Y. Kaneda, M. Fallahi, J. Hader, J. V. Moloney, S. W. Koch, B. Kunert, and W. Stoltz, "Continuous-wave single-frequency 295 nm laser source by a frequency-quadrupled optically pumped semiconductor laser," *Optics Letters,* vol. 34, pp. 3511-3513, 2009.

[32] L. Fan, C. Hessenius, M. Fallahi, J. Hader, H. Li, J. V. Moloney, W. Stolz, S. W. Koch, J. T. Murray, and R. Bedford, "Highly strained InGaAs/GaAs multiwatt vertical-external-cavity surface-emitting laser emitting around 1170 nm," *Applied Physics Letters,* vol. 91, 131114, 2007.

[33] F. Quochi, D. C. Kilper, J. E. Cunningham, M. Dinu, and J. Shah, "Continuous-wave operation of a 1.3 µm GaAsSb-GaAs quantum-well vertical-cavity surface-emitting laser at room temperature," *IEEE Photonics Technology Letters,* vol. 13, pp. 921-923, 2001.

[34] S. Calvez, N. Laurand, H. D. Sun, J. Weda, D. Burns, M. D. Dawson, A. Harkonen, T. Jouhti, M. Pessa, M. Hopkinson, D. Poitras, J. A. Gupta, C. G. Leburn, C. T. A. Brown, and W. Sibbett, "GaInNAs(Sb) surface normal devices," *Physica Status Solidi a-Applications and Materials Science,* vol. 205, pp. 85-92, 2008.

[35] V. M. Korpijarvi, M. Guina, J. Puustinen, P. Tuomisto, J. Rautiainen, A. Harkonen, A. Tukiainen, O. Okhotnikov, and M. Pessa, "MBE grown GaInNAs-based multi-Watt disk lasers," *Journal of Crystal Growth,* vol. 311, pp. 1868-1871, 2009.

[36] J. Rautiainen, J. Lyytikainen, A. Sirbu, A. Mereuta, A. Caliman, E. Kapon, and O. G. Okhotnikov, "2.6 W optically-pumped semiconductor disk laser operating at 1.57 µm using wafer fusion," *Optics Express,* vol. 16, pp. 21881-21886, 2008.

[37] A. Rantamaki, A. Sirbu, A. Mereuta, E. Kapon, and O. G. Okhotnikov, "3 W of 650 nm red emission by frequency doubling of wafer-fused semiconductor disk laser," *Optics Express,* vol. 18, pp. 21645-21650, 2010.

[38] J. Lyytikainen, J. Rautiainen, A. Sirbu, V. Iakovlev, A. Laakso, S. Ranta, M. Tavast, E. Kapon, and O. G. Okhotnikov, "High-power 1.48 µm wafer-fused optically pumped semiconductor disk laser," *IEEE Photonics Technology Letters,* vol. 23, pp. 917-919, 2011.

[39] M. Butkus, C. J. Hamilton, D. Jackson, G. P. A. Malcolm, I. Krestnikov, D. Livshits, and E. U. Rafailov, "Green Second Harmonic Generation in Quantum Dot Semiconductor Disc Lasers," *Laser Optics,* St. Petersburgh, Russia, 2010.

[40] T. Baer, "Large-amplitude fluctuations due to longitudinal mode-coupling in diode-pumped intracavity-doubled nd-yag lasers," *Journal of the Optical Society of America B-Optical Physics,* vol. 3, pp. 1175-1180,1986.

[41] W. P. Risk, T. R. Gosnell, and A. V. Nurmikko, *Compact Blue-Green Lasers,* Cambridge University Press, Cambridge, 2003.

[42] W. Seelert, S. Butterworth, J. Rosperich, C. Walter, R. von Elm, V. Ostroumov, and C. Luebeck, "Optically Pumped Semiconductor Lasers: A new reliable technique for realizing highly efficient visible lasers," *Solid State Lasers XIV: Technology and Devices*. vol. 5707, H. J. Hoffman and R. K. Shori, Eds., Bellingham: SPIE-Int. Soc. Optical Engineering, pp. 33-37, 2005.

[43] A. J. Maclean, A. J. Kemp, S. Calvez, J. Y. Kim, T. Kim, M. D. Dawson, and D. Burns, "Continuous tuning and efficient intracavity second-harmonic generation in a semiconductor disk laser with an intracavity diamond heatspreader," *IEEE Journal of Quantum Electronics,* vol. 44, pp. 216-225, 2008.

[44] O. Svelto, *Principles of Lasers*, 3rd ed., Plenum Press, New York, 1989.

[45] *Semiconductor Disk Lasers: Physics and Technology*, ed. O. G. Okhotnikov, WILEY-VCH Verlag GmbH & Co. KGaA, Weinheim, 2010.

[46] H. Rene, "Intracavity frequency doubling of optically pumped semiconductor disk lasers to the green spectral range," PhD thesis, University of Hamburg, Hamburg, 2008.

[47] K. Fedorova, "Novel semiconductor based broadly tunable light sources," PhD thesis, University of Dundee, Dundee, 2011.

[48] E. U. Rafailov, M. A. Cataluna, and W. Sibbett, "Mode-locked quantum-dot lasers," *Nature Photonics*, vol. 1, pp. 395-401, 2007.

[49] T. D. Germann, A. Strittmatter, U. W. Pohl, D. Bimberg, J. Rautiainen, M. Guina, and O. G. Okhotnikov, "Quantum-dot semiconductor disk lasers," *Journal of Crystal Growth*, vol. 310, pp. 5182-5186, 2008.

[50] K. A. Fedorova, M. A. Cataluna, I. Krestnikov, D. Livshits, and E. U. Rafailov, "Broadly tunable high-power InAs/GaAs quantum-dot external cavity diode lasers," *Optics Express*, vol. 18, pp. 19438-19443, 2010.

[51] P. M. Varangis, H. Li, G. T. Liu, T. C. Newell, A. Stintz, B. Fuchs, K. J. Malloy, and L. F. Lester, "Low-threshold quantum dot lasers with 201 nm tuning range," *Electronics Letters*, vol. 36, pp. 1544-1545, 2000.

[52] M. Butkus, C. J. Hamilton, G. P. Malcolm, I. Krestnikov, D. Livshits, and E. U. Rafailov, "Wavelength Tuning In Quantum Dot Semiconductor Disc Lasers," *22nd International Semiconductor Laser Conference*, Kyoto, Japan, 2010.

[53] A. Garnache, A. A. Kachanov, F. Stoeckel, and R. Houdre, "Diode-pumped broadband vertical-external-cavity surface-emitting semiconductor laser applied to

high-sensitivity intracavity absorption spectroscopy," *Journal of the Optical Society of America B-Optical Physics,* vol. 17, pp. 1589-1598, 2000.

[54] S. C. Woodworth, D. T. Cassidy, and M. J. Hamp, "Sensitive absorption spectroscopy by use of an asymmetric multiple-quantum-well diode laser in an external cavity," *Applied Optics,* vol. 40, pp. 6719-6724, 2001.

[55] N. Kuramoto and K. Fujii, "Volume determination of a silicon sphere using an improved interferometer with optical frequency tuning," *IEEE Transactions on Instrumentation and Measurement,* vol. 54, pp. 868-871, 2005.

[56] G. Galzerano, G. Mana, and E. Massa, "On the effect of broadband emission in external-cavity diode-laser interferometry," *Measurement Science & Technology,* vol. 18, pp. 1338-1342, 2007.

[57] S. J. B. Yoo, "Wavelength conversion technologies for WDM network applications," *Journal of Lightwave Technology,* vol. 14, pp. 955-966, 1996.

[58] B. J. Stevens, D. T. D. Childs, K. M. Groom, M. Hopkinson, and R. A. Hogg, "All semiconductor swept laser source utilizing quantum dots," *Applied Physics Letters,* vol. 91, 121119, 2007.

[59] L. Fan, M. Fallahi, J. Hader, A. R. Zakharian, M. Kolesik, J. V. Moloney, T. Qiu, A. Schulzgen, N. Peyghambarian, W. Stolz, S. W. Koch, and J. T. Murray, "Over 3 W high-efficiency vertical-external-cavity surface-emitting lasers and application as efficient fiber laser pump sources," *Applied Physics Letters,* vol. 86, 211116, 2005.

[60] J. Paajaste, S. Suomalainen, R. Koskinen, A. Harkonen, M. Guina, and M. Pessa, "High-power and broadly tunable GaSb-based optically pumped VECSELs emitting near 2 mu m," *Journal of Crystal Growth,* vol. 311, pp. 1917-1919, 2009.

[61] L. Fan, M. Fallahi, A. R. Zakharian, J. Hader, J. V. Moloney, R. Bedford, J. T. Murray, W. Stolz, and S. W. Koch, "Extended tunability in a two-chip VECSEL," *IEEE Photonics Technology Letters*, vol. 19, pp. 544-546, 2007.

[62] F. Riemenschneider, M. Maute, H. Halbritter, G. Boehm, M. C. Amann, and P. Meissner, "Continuously tunable long-wavelength MEMS-VCSEL with over 40-nm tuning range," *IEEE Photonics Technology Letters*, vol. 16, pp. 2212-2214, 2004.

[63] N. Laurand, B. Guilhabert, E. Gu, S. Calvez, and M. D. Dawson, "Tunable single-mode fiber-VCSEL using an intracavity polymer microlens," *Optics Letters*, vol. 32, pp. 2831-2833, 2007.

[64] L. Fan, "Tunable high-power high-brightness vertical-external-cavity surface-emitting lasers and their applications," PhD thesis, University of Arizona, Tucson, 2006.

[65] Encyclopedia of laser physics and technology (2009), Wavelength tuning, URL: *http://www.rp-photonics.com/wavelength_tuning.html* [02 July 2012].

4. Quantum dot use in mode – locked semiconductor disk lasers

There are several techniques in photonics to force lasers to operate in a pulsed regime - gain or Q-switching, cavity dumping and active or passive mode-locking. Passive mode-locking is a standard technique for semiconductor disk lasers (SDLs). Semiconductor saturable absorber mirrors (SESAMs) are used as passive elements to mode-lock the laser. QDs introduced in SESAMs have enabled a number of new properties in this type of absorbers. In this chapter a short description of mode-locking principles will be presented with the

focus on SDL technology. Also, properties of SESAMs and the use of QD structures will be discussed. SDL mode-locking results achieved using QD based SESAM will be presented.

4.1. Principles of mode-locking semiconductor disk lasers

In the continuous wave regime, many of the longitudinal modes that are supported by the active material gain and cavity design operate simultaneously in the resonator. Those modes operate independently. However, the situation changes when a saturable absorber is inserted in the cavity. A key property of a saturable absorber that enables it to be used for mode-locking is the intensity dependent absorption coefficient, i.e., the saturable absorber introduces nonlinear losses in the cavity – optical losses decrease as the intensity of the oscillating light increases. Thus such an absorber transmits more intense pulses while absorbing weak ones [1]. In this situation the oscillating light tends to operate in pulses as high peak power tends to bleach the absorber faster. The frequencies of oscillating modes in the cavity are equally spaced by:

$$\Delta\omega = 2\pi c/l \tag{4.1}$$

Where l is the optical roundtrip length in the cavity and c is the speed of light. If there are n modes in the cavity, then the total optical field can be described as:

$$E(t) = \sum_n E_n \exp i[(\omega_0 + n\Delta\omega)t + n\Delta\varphi] \tag{4.2}$$

Here ω_0 is the centre frequency of the output, E_n is the amplitude of the n-th mode and $\Delta\varphi$ is the phase difference between adjacent modes [2]. Fig. 4.59 shows the interference effect of three modes with the same amplitude and $\Delta\varphi$=0. Part (b) shows interference results of

higher number of modes with the same phase. It can be seen, that a higher number of interfering modes leads to shorter pulse durations. A broad gain bandwidth is required to support the high number of modes that would contribute in the mode-locking. This is well expressed in the Fourier analysis where it is shown that the product of the pulse duration $\Delta\tau$ and the frequency bandwidth $\Delta\upsilon = c\Delta\lambda/\lambda^2$ of the pulse is equal to a constant value for a given pulse shape [2, 3]:

$$\frac{c}{\lambda^2}\Delta\lambda \times \Delta\tau = const \tag{4.3}$$

Here c is the speed of light, λ is the central wavelength in the optical spectrum of the pulse and Δλ is the full-width at half-maximum value of the spectrum. The constant described by (4.3) is known as a time-bandwidth product. For Gaussian-shape pulses the value of the constant is 0.44 and for $\text{sech}^2 t$ pulses it is equal to 0.315. If the parameters of the pulse satisfy (4.3), it is said that the pulse is transform limited, i.e, it is the shortest pulse obtainable in the given laser source. Typically, to achieve 100 fs pulse in the near infrared spectral range, a spectral bandwidth of about 10 nm is required.

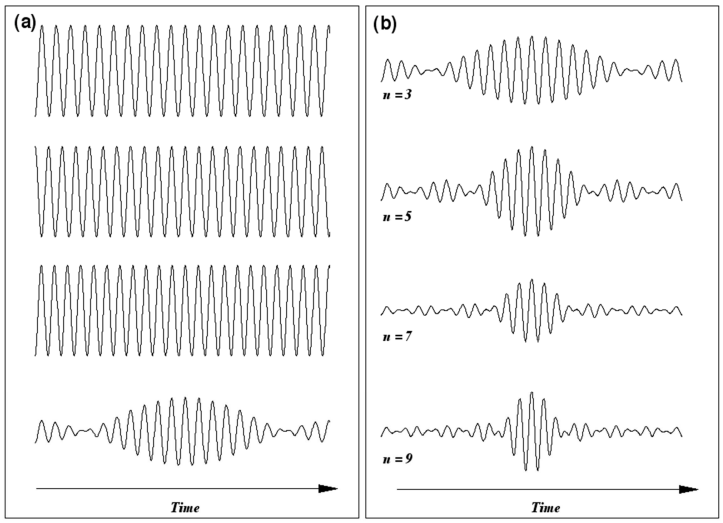

Fig. 4.59. Pulse formation by interference of different number of phase locked modes in the laser cavity [2].

When oscillating waves are locked in phase, the power distribution in the cavity changes dramatically. In the CW regime, the output power from the laser is typically constant during the time. However, when pulses are formed during the mode-locking, the main power is concentrated in the time of pulse durations and can be hundreds or thousands of times larger than the average power P_{av} of the mode-locked laser. This is especially true if the pulse duration is substantially shorter than the cavity round-trip time. The table below shows the general expressions for various pulse parameters such as peak and average power, pulse energy and repetition rate. Fig. 4.60 below also shows a schematic drawing of a laser mode-locked using a saturable absorber for visualisation.

Pulse repetition rate	$f_r = \frac{c}{2nd}$
Pulse energy	$E_p = \frac{P_{av}}{f_r}$
Pulse peak power	$P_{peak} = \frac{E_p}{\Delta\tau} = \frac{P_{av}}{f_r}\frac{1}{\Delta\tau}$

Table 4.8. Various expressions for laser pulse parameters.

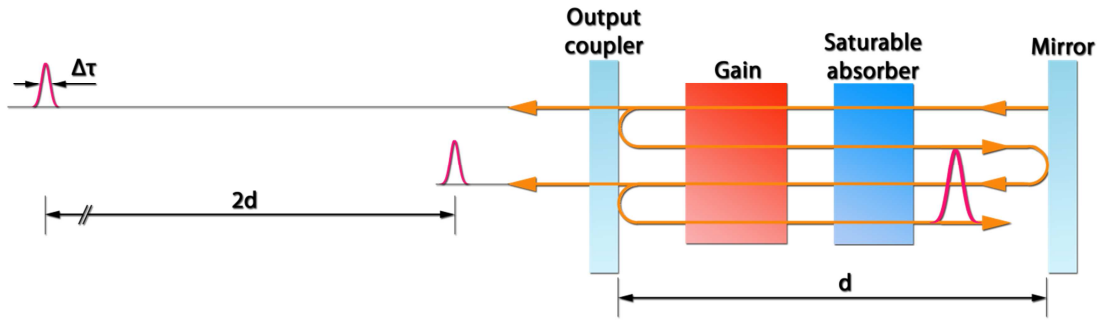

Fig. 4.60. A schematic drawing of mode-locked mechanism in laser with saturable absorber.

Mode-locking of semiconductor disk lasers was successfully demonstrated with a number of different parameters [4]. High average and peak powers, ultrafast pulses and high

repetition rates were reported as already discussed in the introduction chapter of this thesis [5-9]. The versatility of all these parameters makes mode-locked SDLs as an attractive feature for on demand applications.

To date, semiconductor saturable absorber mirrors (SESAMs) have been used to passively mode-lock SDL sources [10]. Similarly to the schematic laser cavity shown in Fig. 4.60, a mode-locked SDL also consists of the gain element and the saturable absorber combined with additional optics. The formation of pulses in this configuration is supported by the interplay between the gain which is provided by SDL chip and the losses provided by the SESAM. Just before the start of lasing, the losses in the cavity are held slightly higher than the gain as the saturable absorber mirror does not provide enough reflectivity. As soon as the absorber is saturated, the absorbing part of it becomes transparent to the incoming wave and the reflectivity increases to the value provided by DBR part of the SESAM. Then a short time period is opened during which the gain is higher than cavity losses and the accumulated energy is released in a form of a light pulse.

There are several distinct mechanisms of pulse formation in mode-locked lasers depending on the type of the SESAM used. One of the key parameters of the saturable absorber is its recovery time, i.e., how fast the absorber can return to its initial state of unsaturated regime. Two main types of absorbers – fast and slow are used regarding this feature. Typical pulse formation mechanisms for such absorbers are shown in Fig. 4.61 [11]. Fast saturable absorbers have a recovery time shorter than the emitted light pulse. Meanwhile slow absorbers require more time to recover than the pulse duration.

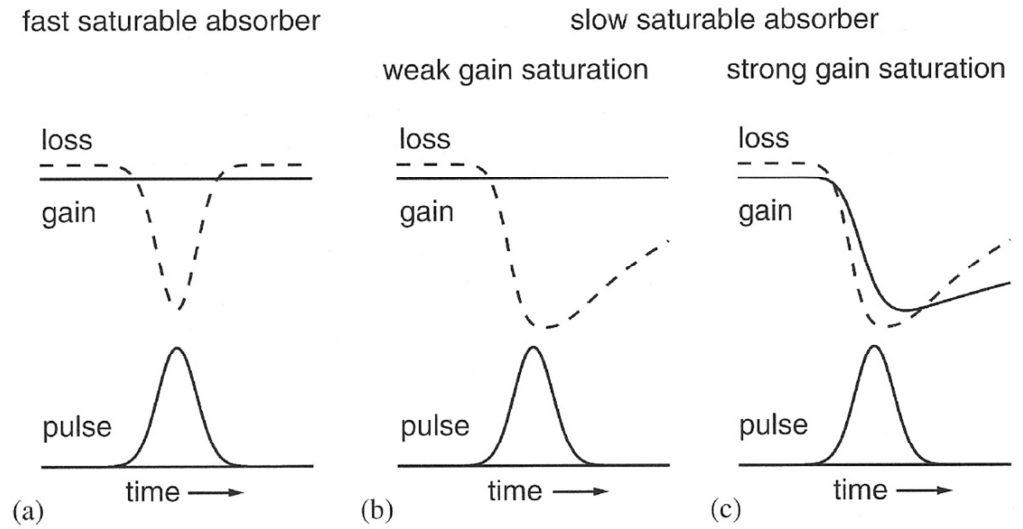

Fig. 4.61. Pulse formation mechanisms using fast and slow saturable absorbers [11].

With fast saturable absorber (Fig. 4.61 a), the positive net gain window is closed immediately after the end of the formed pulse as the loss is modulated similarly as the pulse shape. A good example of such behaviour is a Kerr-lens mode-locked Ti:Sapphire laser [12, 13]. Here nonlinear processes in the Kerr lens form an effective saturable absorber although no physical saturable absorbers are used in typical configuration of Ti:Sapphire laser [14, 15]. Kerr-lens mode-locking in Ti:Sapphire gain material allowed has allowed for the demonstration of pulses with durations of only a few femtoseconds.

Two separate cases are usually distinguished in the case of slow saturable absorber – with weak and strong gain saturation (Fig. 4.61 b, c). Those are also often referred to as with and without dynamic gain saturation depending on the change of the saturated gain level during the time [4]. When gain in the cavity is saturated weakly compared to some other types of gain media, the net gain window remains open after the formation of pulse. Such a situation is typical for ion doped solid state mode-locked lasers where the upper state lifetime is longer (up to miliseconds time scale) than the cavity roundtrip time and gain thus remains

constant. However, even in this situation, pulses much shorter than the gain window can be formed. The pulse formation in such regime can be stabilised by soliton mode-locking [16]. Mode-locking in this regime without soliton shaping was also demonstrated [17].

Different pulse formation dynamics occur when slow absorbers are used with strong gain saturation (Fig. 4.61 c). Saturable absorber assisted mode-locking is typical for gas and semiconductor lasers [11]. In such media, the upper state lifetime of carriers is comparable to the cavity roundtrip time and thus the gain level changes along with losses. The losses in this case decrease and increase faster than the gain and the positive net gain window is closed after the formation of pulse [11]. However, in order for losses to drop more rapidly, the absorber must be saturated faster, i.e., at lower pulse energies than the gain element. This condition is very important for semiconductor disk lasers given that the saturable absorber and gain element are both based on the same material. Thus, the condition below must be satisfied for stable mode-locking:

$$\frac{E_{sat,abs}}{E_{sat,gain}} \ll 1 \tag{4.4}$$

However, the above condition puts some limitations on the parameters of saturable absorber and cavity configuration.

The discussion above concerning pulse formation in different regimes of saturable absorber only considers the effect of gain saturation level and losses in the cavity. However, there are more factors that contribute to the formation and shaping of the laser pulses. These include group delay dispersion, gain filtering, i.e., the gain supported bandwidth, noise, saturation of absorber and gain to name but a few [11].

So far, slow saturable absorbers with dynamic gain saturation have been used in mode-locked SDLs. Although some mode-locking with fast saturable absorbers have also been demonstrated in the technique known as Stark mode-locking [18].

The next section will discuss semiconductor saturable absorbers in more detail along with their parameters that are desirable for stable mode-locking in SDLs.

4.2. Properties of SESAMs

As already mentioned in the previous section, the introduction of SESAMs was a big step forward in stabilising, enhancing and simplifying mode-locking in a several types of lasers. It is a key element in mode-locking SDL due to its robustness, simplicity and the opportunity to modify various parameters according to the needs of specific laser. Typically a SESAM consists of a DBR designed for laser wavelength. A number of QD or QW layers are grown on the top of it in a manner similar to that used in the growth of the gain region of SDL. Some SESAMs work in transmission mode and can be grown without DBR layers. There is a set of SESAM parameters that mainly determines its properties in mode-locking such as:

- Modulation depth ΔR
- Nonsaturable losses ΔR_{ns}
- Saturation fluence F_{sat}
- Saturable absorber recovery time τ

The first three parameters define the properties of the nonlinear reflectivity of the SESAM. Nonlinear reflectivity is typically measured by sending a pulse of mode-locked laser to the SESAM and measuring the reflected pulse energy as a function of the energy of incident

pulse. The reflectivity can then be plotted against the calculated pulse fluence. Pulse fluence F_p is equal to pulse energy density, i.e., E_p divided by $1/e^2$ mode area A_{abs} on the SESAM:

$$F_p = \frac{E_p}{A_{abs}} \tag{4.5}$$

A characteristic curve of nonlinear reflectivity of the SESAM is shown in Fig. 4.62 with the main SESAM parameters being marked [15]. It can be seen, that the modulation depth shows the reflectivity difference between a saturated and unsaturated SESAM. Nonsaturable losses describe unwanted loss in the SESAM which originate from nonsaturable absorption, scattering or transmission through the DBR part. Nonsaturable losses are desired to be as low as possible and the tolerance is defined by the available gain in the cavity. For example, those losses should be << 1% for QD based SDLs, as typically an output coupling of less than 1% is used. The saturation fluence shows the pulse fluence at which the SESAM is saturated. It is measured at the 1/e value of the full saturation as can be seen from the graph.

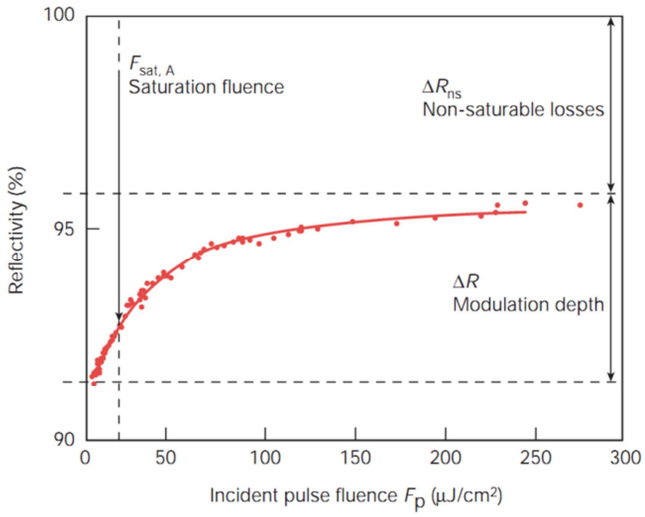

Fig. 4.62. Typical nonlinear reflectivity curve of SESAM and its parameters [15].

The last mentioned parameter, recovery time, is related to the dynamics of carriers in time and shows how fast the saturated SESAM can recover to its initial state. To measure the recovery time, the pump probe technique is used. In this technique, a pulse of a mode-locked laser is split into two pulses with power ratio of ~10:1. The powerful pump pulse then hits the SESAM sample to fully saturate it. Electron – hole pairs are created after the absorption of the light pulse. The probe pulse then also hits the same spot on the sample and its reflected part is measured. A delay line is used to delay the probe pulse in time in accordance with pump. The reflectivity is then measured at different times after the saturation of the SESAM. Reflectivity or the change in the transmission is then plotted as a function of time. Such pump – probe technique allows for the measurement of SESAM recovery dynamics after it is saturated by the pulse with sub-picosecond time precision. A sample graph of such a measurement is shown in Fig. 4.63[19]. Data presented in the graph were measured for a QD based SESAM designed for 1040 nm. As can be seen in the graph, decay with two time constants, fast and slow, is observable. These dynamics are typical for QD based absorbers and can be described by bi-exponential decay [11]:

$$\Delta T(\tau) = A_{slow} e^{-\tau/\tau_{slow}} + A_{fast} e^{-\tau/\tau_{fast}} \tag{4.6}$$

Here A_{slow} and A_{fast} are the amplitudes of both components ($A_{slow} + A_{fast} = 1$) and τ_{slow} and τ_{fast} are the time constants of the corresponding decay parts. Different decay rates reflect on different mechanisms in the SESAM recovery dynamics. The fast decay which occurs in sub-picosecond time scale in the given example is due to the transitions in the QDs. Meanwhile the longer decay typically is in the order of 100 ps and is associated with carrier recombination [19, 20]. Such behaviour of SESAM decay is advantageous for mode-locking applications as the fast part of the recovery is responsible for shaping the

pulse and longer decay reduces the saturation fluence of the SESAM. More extended discussion about the properties of QD based SESAMs will be given in section 4.4.

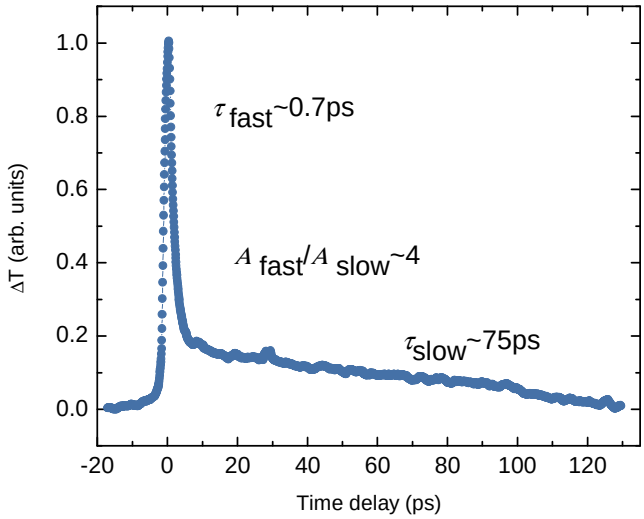

Fig. 4.63. Pump – probe measurement techniques for QD based saturable absorber [19].

The fast dynamics of such saturable absorbers is not an intrinsic property of semiconductors as carrier dynamics in bulk semiconductor lie in the range of nanoseconds. However the technique of semiconductor saturable absorbers have made ultrafast dynamics possible. There are several techniques for surpresing the decay time. One of the most often used for GaAs based SESAMs is low temperature growth. The density of material defects is increased during such procedure. They then serve as nonradiative mid-gap recombination centres and thus can reduce the carrier concentration decay rates [21]. Techniques like impurity doping or particle bombardment are also used to reduce recovery times in SESAMs [22-24].

All these techniques have enabled fast modulation of SESAMs possible. However, it must be noted that all the techniques incorporating defect states come to the cost of increased level of nonsaturable losses.

A typical SESAM works on a standalone basis and is ready to use when cleaved from the wafer. However, there are SESAMs that can be controlled electrically. They are often referred as a *p-n* junction SESAMs and have layers doped both by acceptors and donors [25, 26]. Such doping allows direct electrical control in the active region of the SESAM and enables the control of modulation depth and recovery time of the SESAM [27, 28]. Although such electrical control of the saturable absorber needs an additional power source, it adds a great deal of flexibility to the laser. It allows for the switching between CW and mode-locked regimes as well as allows the tuning of the pulse duration. It can be fully exploited for applications such as optical trapping and manipulation, multiphoton microscopy or nanosurgery where variable laser parameters are required [29-31]. So far p-n junction SESAMs have been used to mode-lock fiber and solid state lasers [26, 32, 33]. A similar principal for mode-locking control is also used in mode-locked monolithic laser diodes where a reverse bias is applied to the absorber section of the device [34]. One part of our ongoing work is also targeted at the mode-locking of SDLs using p-n junction SESAMs. This would add additional variable or tuneable parameters for such laser source.

4.3. Design of the SESAMs

The structure of a semiconductor saturable absorber mirror is quite similar to the structure of an SDL gain chip. The DBR for the design wavelength is first deposited on the semiconductor substrate. The absorber region of the SESAM is deposited on top of it.

Compared to the SDL active region, a SESAM typically has less layers of QDs or QWs. Light reflection from the DBR and semiconductor air interface creates a standing wave effect in the absorber region. QD or QW layers are positioned at the antinodes of such standing wave to create a resonant periodic structure using spacer layers [35]. A carrier blocking layer is usually not used in SESAMs in order to allow faster carriers recombination and the top of the SESAM is covered by GaAs layer. The thickness of the absorber section can again be adjusted to be in resonance or antiresonance with the design wavelength. The flexibility of this feature leads to different properties of the SESAM affecting the enhancement factor in the subcavity, field intensity at the semiconductor-air interface, operational bandwidth and dispersion value [36].

Fig. 4.64 shows two sample structures of a SESAM. The refractive index pattern and field enhancement are shown in the graphs [11]. The left part of the structure shows part of the DBR followed by the absorber section containing a single QW. Part (a) represents the case of an antiresonant structure and (b) shows a resonant type of SESAM [11].

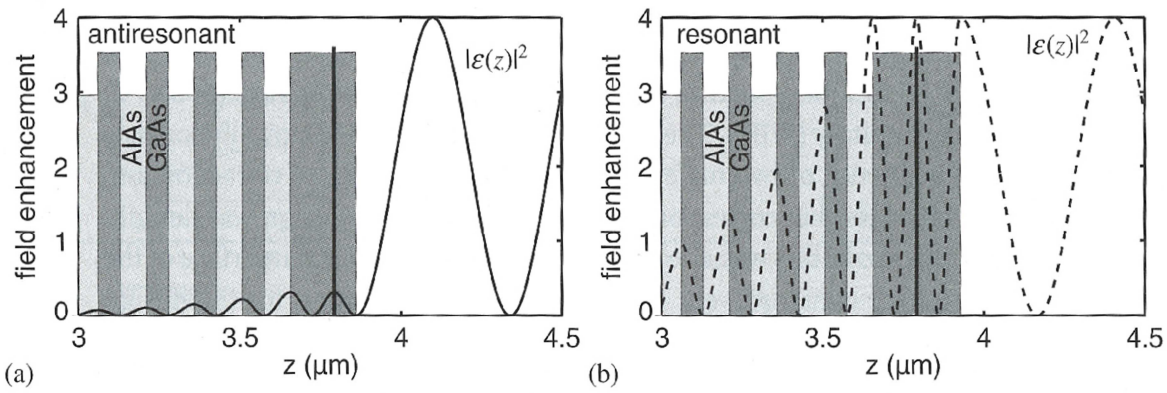

Fig. 4.64. Two sample structures of (a) antiresonant and (b) resonant type SESAMs [11].

Field enhancement factor $\Gamma = |\varepsilon(z)|^2$ depicted in the graphs above is directly proportional to the intensity of the standing electric field wave in the subcavity and thus has an

important influence on the SESAM parameters. Here ε is electric field normalized to 1 for the incident wave. For low field enhancement, the modulation depth is low, but the saturation fluence is high because more energy is needed to bleach the absorber. In the resonant case with higher field enhancement, the saturation fluence is much lower, and the modulation depth is high, i. e., modulation depth ΔR is directly proportional and saturation fluence F_{sat} is inversely proportional to the enhancement factor. If the enhancement factor is changed in a given QW SESAM, the product of $\Delta R \times F_{sat}$ remains constant and represents the energy needed to fully saturate the absorber [11, 37].

Furthermore, similarly to the gain chips, a resonant SESAM structure also has a lower threshold damage value. An antiresonant structure is less sensitive to spectral shifts in the laser and thus has larger tolerances in the growth process.

When the duration of the pulses is in the order of a few picoseconds or less, dispersion control also plays an important role. Group delay dispersion (GDD) originating from light matter interaction is again different for different type of the SESAMs as it is shown in Fig. 4.65. Here the software calculated GDD as a function of operating wavelength is shown for resonant and antiresonant SESAMs designed for 1040 nm. It can be seen that the GDD shows much less fluctuations around the design wavelength in the antiresonant case as compared to the resonant SESAM. In the case of SDL mode-locking, resonant type SESAMs are often used due to their low saturation fluence and sufficient modulation depth. In order to keep their dispersion to a minimum around the design wavelength, SESAMs with AR coating on the top of the structure are sometimes used. For it, a single quarter-wave thick layer of dielectric is often used. It allows the GDD to act as if it were in the antiresonant case. However, it reduces the enhancement factor, although it is then still higher than in the classical antiresonant design SESAM [38, 39]. In order to introduce a

specific amount of dispersion, for example, for dispersion compensation, dispersive SESAMs can also be used [40].

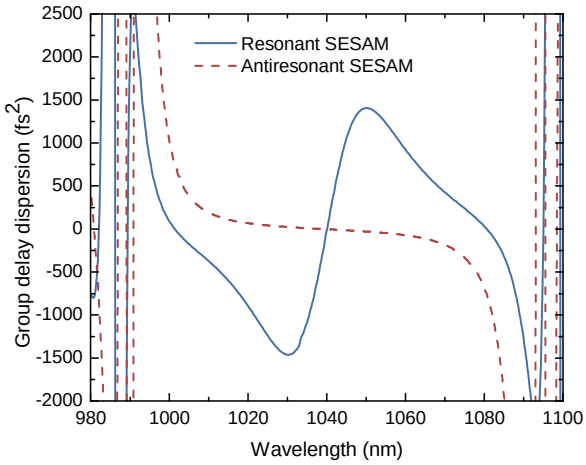

Fig. 4.65. Calculated group delay dispersion curves for resonant and antiresonant SESAMs.

4.4. QD based SESAMs

Similarly to SDL gain elements, most of the semiconductor saturable absorbers were first based on QW structures. In mode-locked SDLs, a similar type of material was typically used for both gain chip and SESAM. However, as was discussed in previous chapters, the SESAM must be saturated at lower pulse fluences in order to achieve stable mode-locking. Thus, the light on the SESAM needs to be focused into a smaller spot than it is on the gain chip. This ultimately limits the cavity size and the achievable repetition rate. Other ways to decrease the saturation fluence of the SESAM are often required. However, the reduction of saturation fluence comes to the cost of increased modulation depth as the product of these two parameters is constant (F_{sat} x ΔR = const) [11]. Too large modulation depth should be avoided in SDL mode-locking as the available gain then cannot overcome the existing loss

level in the cavity. As it was mentioned before, the product of these two SESAM parameters represents the energy value needed to saturate the absorber. Thus it is proportional to the number of energy states in the absorbing material it needed to fill.

A solution to this problem was brought by QD based SESAMs [19]. It was shown that saturation fluence and modulation depth can be controlled independently in semiconductor QDs based absorbers [41]. This became possible as QDs exhibit a discrete density of states function which is proportional to the dot density. Thus the modulation depth can basically be controlled by the density of quantum dots in the structure which depends on the number of states that need to be filled up in order to achieve the transparency in the absorber region of SESAM. It was shown that the dot density during the growth is determined by a set of parameters including substrate temperature, growth rate, gas pressure and monolayer coverage. A sample graph illustrating InGaAs dot density dependence on the growth rate is shown in Fig. 4.66 [19]. Meanwhile the saturation fluence can be controlled by field enhancement in the sub-cavity, as was discussed in the previous chapter. QD based SESAMs with saturation fluences of less than 10 to a few tens of $\mu J/cm^2$ were demonstrated while typical QW based absorbers usually feature saturation fluencies a few times higher [19, 41].

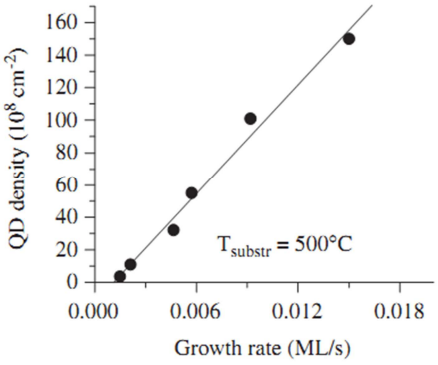

Fig. 4.66. Quantum dots density dependence on the growth rate with fixed substrate temperature [19].

QD SESAMs have brought an innovative approach to parameter control and allowed for the realization of low saturation fluence SESAMs with appropriate amount of modulation depth. This has loosened the requirements for mode-locked SDL cavity configurations, as similar mode sizes on both the gain chip and the SESAM could be used. It has resulted in the increased repetition rate values that have reached 50 GHz by using a miniature cavity with a total length of 3 mm [9]. Also, the devices with monolithically integrated gain and SESAM elements have been demonstrated, called MIXSELs – mode-locked integrated external cavity surface emitting lasers [42]. To date such devices have demonstrated 6.4 W of average output power with 28 ps pulse duration and 2.5 GHz repetition rate [43].

Another advantage that came along with QD based SESAMs was ultrafast recovery dynamics as has been already mentioned in the chapter about SESAM parameters. Not long after the first demonstrations of QD SESAMs, their fast-part recovery time of subpicosecond values were reported [44]. These were successfully used to mode-lock a number of different lasers [19, 45].

Excluding the previously mentioned high repetition rate mode-locking and MIXEL demonstrations, mode-locking SDLs with QD based SESAMs is a partially unexplored research area. The first mode-locked SDL using a QD absorber to demonstrate sub-picosecond pulse durations was achieved recently [46]. The results of this demonstration will be discussed more widely in the following chapter. Not long after this, an all-QD based mode-locked SDL was demonstrated [47]. After that improved results with average output power of more than 1 W at 970 nm were also reported [38]. However, these experiments were performed at an operating temperature of -20 ^{o}C. All QD based mode-locked SDLs potentially can have advantageous features supported by QD based gain and saturable absorption. Work is being done at the moment to try to incorporate spectral tuneability in

the mode-locked QD SDL as well as trying to mode-lock SDL devices at 1040 - 1260 nm wavelengths.

4.5. Mode-locking results

A QW based SDL mode-locked using a QD based saturable absorber mirror will be presented in this section. To the best of our knowledge, at the time of the publication of these results it was the first demonstration of SDL mode-locked using QD SESAM with femtosecond light pulses. First, the structural details of gain and SESAM parts will be described followed by the experimental part. The results achieved will be presented after.

The gain structure used for this work was an MBE grown, 6 QW anti-resonant step-index structure with a design wavelength of 1040 nm and consists of a 27.5 pair GaAs/AlAs DBR, a 7λ/2 micro-cavity containing pump absorbing GaAs spacers and 6 $In_{0.25}Ga_{0.75}As$ quantum wells, positioned at the antinodes of the standing wave and distributed in a non-uniform manner to produce a uniform carrier density in each well as the intensity of pump light decays exponentially after entering the medium. The structure was completed by a λ/4 AlAs window layer and an 8 nm GaAs cap to protect the structure from oxidation. This gain structure ensures that the gain bandwidth is broad, and is not filtered by the microcavity formed between the air-semiconductor interface and the DBR. Fig. 4.67 shows a bandgap profile and the optical standing wave of the structure.

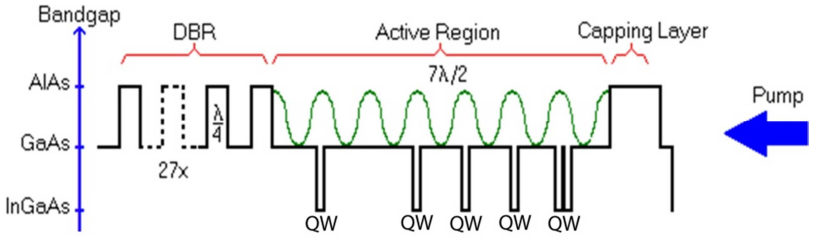

Fig. 4.67. Bandgap profile of the QW SDL semiconductor part.

The QD SESAM, grown by MBE, consists of a highly reflecting 25-pair $Al_{0.9}Ga_{0.1}As/GaAs$ distributed Bragg reflector (DBR) centred at a wavelength of 1070 nm and a 2λ GaAs sub-cavity with a design wavelength of 1050 nm containing 3 groups of 3 layers of InAs/GaAs quantum dots grown in the S-K regime and positioned at the antinodes of the field. A schematic structure of the SESAM used along with the reflectivity and luminescence spectra is shown in Fig. 4.68. The surface quantum dot density was measured to be $\sim 5x10^{10} cm^{-2}$ and the lateral size of a dot was about 7 nm. This SESAM has previously been used to mode-lock a Yb:KGW solid state laser, producing pulses as short as 114 fs [45]. Nonlinear reflectivity of the SESAM was previously measured and a saturation fluence value of 25 $\mu J/cm^2$, modulation depth of 2.35 % and nonsaturable losses of 0.2 % were reported. The measurement was performed using Yb:KYW femtosecond laser. The energy of the incident and reflected light pulses was measured. As the pulse energy of the incident light was increased, the absorber was saturated and larger part of the light was reflected. The graph of nonlinear reflectivity measurement is shown in Fig. 4.69 [45].

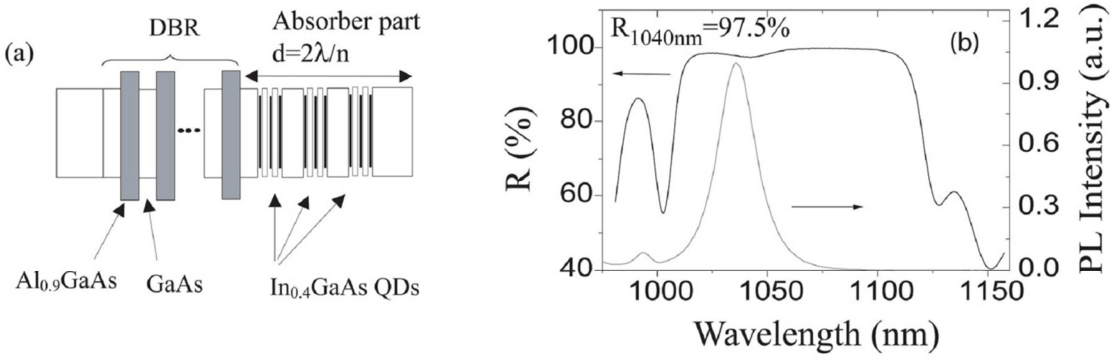

Fig. 4.68. A schematic structure of QD SESAM used in the experiments is shown in (a) part and reflectivity and luminescence spectra are shown in (b).

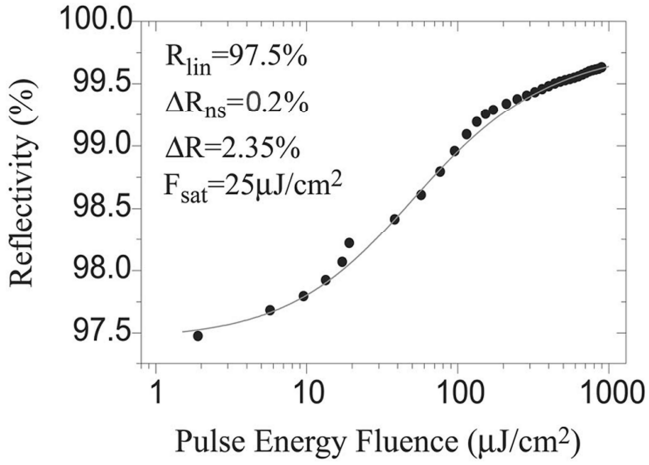

Fig. 4.69. Nonlinear reflectivity measurement of the SESAM used in the experiments [45].

The mode-locked SDL utilised a Z cavity, with the gain structure acting as one folding mirror and the QD-SESAM acting as an end mirror. A 75 mm radius of curvature with 0.6 % transmission output coupler formed the other end of the cavity and a 38 mm radius of curvature high reflector provided the second folding mirror. A diagram of the mode-locked SDL cavity is shown in Fig. 4.70. The laser had a fundamental repetition rate of 895.5 MHz. The laser mode radii on the gain medium and SESAM were 60 µm and 22.5 µm respectively, giving an area ratio of 7. The gain medium and SESAM were mounted on temperature controlled copper mounts. No post growth processing was performed on the

gain structure; therefore the maximum output power was limited by the temperature increase in the active region. The gain structure was optically pumped by up to 1.3 W at a wavelength of 808 nm from a multimode fibre-coupled diode laser. First, the cavity was aligned using three external dielectric mirrors without a SESAM. After the CW operation was observed, the end mirror was changed to a QD SESAM. The mode-locked output was characterised using a commercially available RF spectrum analyser, an optical spectrum analyser and an intensity autocorrelator.

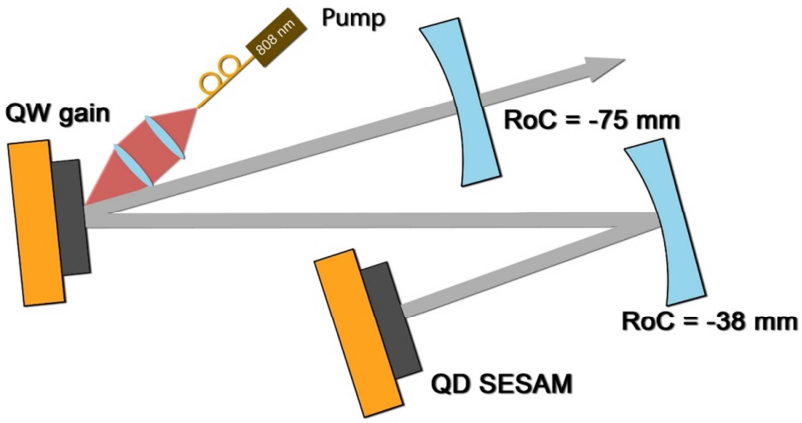

Fig. 4.70. A scheme of the mode-locked SDL Z-shape cavity.

The laser output was a near-circularly symmetric TEM_{00} beam with average output power up to 60 mW during the mode-locked operation, limited by thermal roll-over. The shortest pulse was observed when the QD-SESAM was at a temperature of 20 ^{0}C and the quantum well gain structure was at 0.9 ^{0}C. The incident pump power was 0.93 W and the output power under these conditions was measured to be 45.5 mW. The pulse fluence on the SESAM was calculated to be 530 μJ/cm^2. The optical spectrum and RF spectrum of the mode-locked laser are shown in Fig. 4.71 and the autocorrelation trace is shown in Fig. 4.72. The pulses had a near Gaussian profile and the measured autocorrelation width yielded a pulse duration of 870 fs at full width half maximum (FWHM). The optical

spectrum had a width of 2 nm FWHM leading to the pulse being 1.14 times Fourier limited. The minimum pulse duration was obtained when the laser wavelength was tuned such that the net dispersion introduced by the gain and SESAM was near zero. Fig. 4.73 shows the calculated group delay dispersion (GDD) introduced by the gain and the SESAM in this cavity configuration (double pass of gain, single pass of SESAM per roundtrip) over the wavelength range 1020-1040 nm. It can be seen that at a wavelength close to 1027.5 nm the net GDD is zero. However, the net dispersion becomes positive at shorter wavelengths and negative at longer wavelengths. The slight chirp remaining when the minimum pulse duration is observed is thought to be due to self-phase modulation in the SESAM.

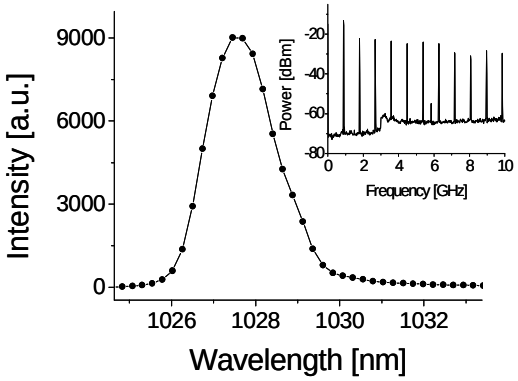

Fig. 4.71. Optical spectrum of the mode-locked SDL. RF spectrum trace is shown in the inset.

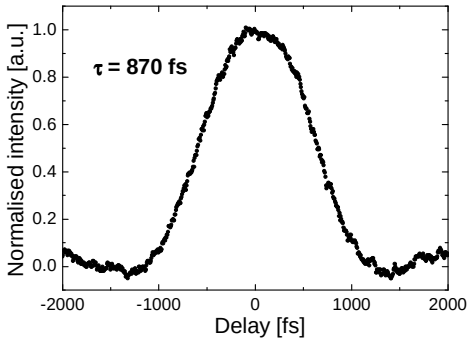

Fig. 4.72. Autocorrelation trace of the mode-locked laser pulses.

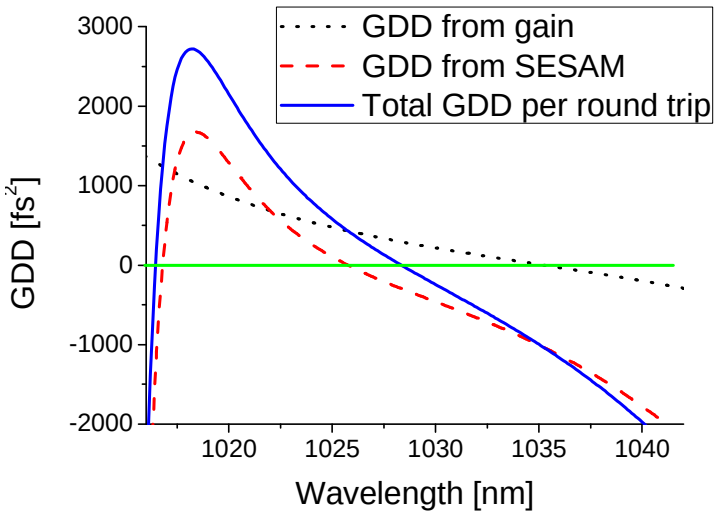

Fig. 4.73. Calculated group delay dispersion values in the mode-locked SDL cavity.

The mode-locking characteristics were also observed as the SESAM was temperature tuned over a heat sink temperature ranging from -10 to 85 ^{o}C. Stable mode-locking was obtained over the entire temperature range; the pulse duration increased to 2 ps at 85 ^{o}C, and reached a minimum at 20 ^{o}C before increasing again to 1.5 ps at -10 ^{o}C. Fig. 4.74 shows the pulse duration and magnitude of the roundtrip GDD versus SESAM temperature. As the SESAM temperature was varied the pulse length varies due to the temperature induced change in the subcavity length of the SESAM, hence the change in net roundtrip dispersion. However, the relative pulse duration insensitivity to quantum dot SESAM temperature is important as it shows that the mode-locking mechanism employed here is robust to temperature variations.

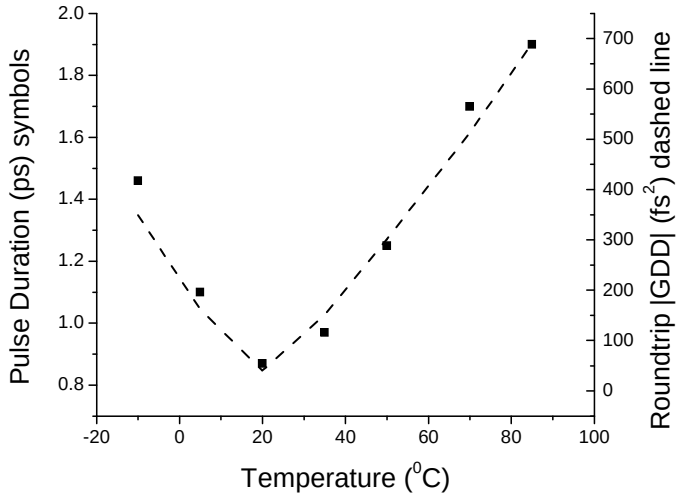

Fig. 4.74. Dependence of pulse duration (symbol) and magnitude of GDD versus SESAM temperature

4.6. Chapter conclusions

In conclusion, the main principles of SDL passive mode-locking using SESAM elements were discussed. Introduction of QDs in mode-locked SDLs was reviewed. In the experimental section, the first sub-picosecond pulse demonstration from mode-locked SDL using QD based SESAM was reported. Also, work is being done in the area of mode-locked all QD based SDLs trying to improve recently reported results and to explore new features provided by QD structures. Work to mode-lock SDLs using p-n junction SESAMs is also planned. A successful demonstration potentially would allow an additional degree of freedom in mode-locked SDLs.

References

[1] B. E. A. Saleh and M. C. Teich, *Fundamentals of Photonics*, Second Edition, John Wiley & Sons, Inc., New Jersey, US, 2007.

[2] D. T. Reid, "Ultrafast photonics," lectures notes, Heriot-Watt University, Edinburgh, UK, 2006.

[3] M. A. Cataluna, "Ultrashort-pulse generation from quantum-dot semiconductor diode lasers," PhD thesis, University of St Andrews, St Andrews, 2007.

[4] U. Keller and A. C. Tropper, "Passively modelocked surface-emitting semiconductor lasers," *Physics Reports-Review Section of Physics Letters*, vol. 429, pp. 67-120, 2006.

[5] A. H. Quarterman, K. G. Wilcox, V. Apostolopoulos, Z. Mihoubi, S. P. Elsmere, I. Farrer, D. A. Ritchie, and A. Tropper, "A passively mode-locked external-cavity semiconductor laser emitting 60-fs pulses," *Nature Photonics*, vol. 3, pp. 729-731, 2009.

[6] A. H. Quarterman, A. Perevedentsev, K. G. Wilcox, V. Apostolopoulos, H. E. Beere, I. Farrer, D. A. Ritchie, and A. C. Tropper, "Passively harmonically mode-locked vertical-external-cavity surface-emitting laser emitting 1.1 ps pulses at 147 GHz repetition rate," *Applied Physics Letters*, vol. 97, 251101, 2010.

[7] A. Aschwanden, D. Lorenser, H. J. Unold, R. Paschotta, E. Gini, and U. Keller, "2.1-W picosecond passively mode-locked external-cavity semiconductor laser," *Optics Letters*, vol. 30, pp. 272-274, 2005.

[8] K. G. Wilcox, A. H. Quarterman, H. Beere, D. A. Ritchie, and A. C. Tropper, "High Peak Power Femtosecond Pulse Passively Mode-Locked Vertical-External-Cavity

Surface-Emitting Laser," *IEEE Photonics Technology Letters,* vol. 22, pp. 1021-1023, 2010.

[9] D. Lorenser, D. Maas, H. J. Unold, A. R. Bellancourt, B. Rudin, E. Gini, D. Ebling, and U. Keller, "50-GHz passively mode-locked surface-emitting semiconductor laser with 100-mW average output power," *IEEE Journal of Quantum Electronics,* vol. 42, pp. 838-847, 2006.

[10] S. Hoogland, S. Dhanjal, A. C. Tropper, J. S. Roberts, R. Haring, R. Paschotta, F. Morier-Genoud, and U. Keller, "Passively mode-locked diode-pumped surface-emitting semiconductor laser," *IEEE Photonics Technology Letters,* vol. 12, pp. 1135-1137, 2000.

[11] T. Sudmeyer, D. Maas, and U. Keller, "Mode-Locked Semiconductor Disk Lasers," in *Semiconductor Disk Lasers: Physics and Technology*, O. G. Okhotnikov, Ed., Wiley-VCH Verlag GmbH & Co., Darmstadt, pp. 213-261, 2010.

[12] D. E. Spence, P. N. Kean, and W. Sibbett, "60-fsec pulse generation from a self-mode-locked Ti-sapphire laser," *Optics Letters,* vol. 16, pp. 42-44, 1991.

[13] R. Ell, U. Morgner, F. X. Kartner, J. G. Fujimoto, E. P. Ippen, V. Scheuer, G. Angelow, T. Tschudi, M. J. Lederer, A. Boiko, and B. Luther-Davies, "Generation of 5-fs pulses and octave-spanning spectra directly from a Ti : sapphire laser," *Optics Letters,* vol. 26, pp. 373-375, 2001.

[14] F. Salin, J. Squier, and M. Piche, "Mode-locking of Ti-Al_2O_3 lasers and self-focusing - a Gaussian approximation," *Optics Letters,* vol. 16, pp. 1674-1676, 1991.

[15] U. Keller, "Recent developments in compact ultrafast lasers," *Nature,* vol. 424, pp. 831-838, 2003.

[16] G. J. Spuhler, L. Krainer, E. Innerhofer, R. Paschotta, K. J. Weingarten, and U. Keller, "Soliton mode-locked Er: Yb: glass laser," *Optics Letters,* vol. 30, pp. 263-265,2005.

[17] R. Paschotta, R. Haring, A. Garnache, S. Hoogland, A. C. Tropper, and U. Keller, "Soliton-like pulse-shaping mechanism in passively mode-locked surface-emitting semiconductor lasers," *Applied Physics B-Lasers and Optics,* vol. 75, pp. 445-451, 2002.

[18] K. G. Wilcox, Z. Mihoubi, G. J. Daniell, S. Elsmere, A. Quarterman, I. Farrer, D. A. Ritchie, and A. Tropper, "Ultrafast optical Stark mode-locked semiconductor laser," *Optics Letters,* vol. 33, pp. 2797-2799, 2008.

[19] A. A. Lagatsky, C. G. Leburn, C. T. A. Brown, W. Sibbett, S. A. Zolotovskaya, and E. U. Rafailov, "Ultrashort-pulse lasers passively mode locked by quantum-dot-based saturable absorbers," *Progress in Quantum Electronics,* vol. 34, pp. 1-45, 2010.

[20] F. Quochi, M. Dinu, J. Shah, L. N. Pfeiffer, K. W. West, and P. M. Platzman, "Ultrafast carrier activation in resonantly excited 1.3 µm InAs/GaAs quantum dots at room temperature," *Physical Review B,* vol. 65, pp. 179-180, 2002.

[21] S. D. Benjamin, H. S. Loka, A. Othonos, and P. W. E. Smith, "Ultrafast dynamics of nonlinear absorption in low-temperature-grown GaAs," *Applied Physics Letters,* vol. 68, pp. 2544-2546, 1996.

[22] A. Marceaux, S. Loualiche, O. Dehaese, and B. Lambert, "High-speed 1.55 mu m Fe-doped multiple-quantum-well saturable absorber on InP," *Applied Physics Letters,* vol. 78, pp. 4065-4067, 2001.

[23] R. Takahashi, Y. Kawamura, T. Kagawa, and H. Iwamura, "Ultrafast 1.55 μm photoresponses in low-temperature-grown InGaAs/InAlAs quantum-wells," *Applied Physics Letters,* vol. 65, pp. 1790-1792, 1994.

[24] Y. Silberberg, P. W. Smith, D. A. B. Miller, B. Tell, A. C. Gossard, and W. Wiegmann, "Fast nonlinear optical-response from proton-bombarded multiple quantum well structures," *Applied Physics Letters,* vol. 46, pp. 701-703, 1985.

[25] S. Zolotovskaya, "Novel semiconductor-based laser systems and their applications," PhD thesis, Department Electronic Engineering & Physics, University of Dundee, Dundee, 2010.

[26] A. A. Lagatsky, E. U. Rafailov, W. Sibbett, D. A. Livshits, A. E. Zhukov, and V. M. Ustinov, "Quantum-dot-based saturable absorber with p-n junction for mode-locking of solid-state lasers," *IEEE Photonics Technology Letters,* vol. 17, pp. 294-296, 2005.

[27] X. M. Liu, E. U. Rafailov, D. Livshits, and D. Turchinovich, "Quantum well saturable absorber mirror with electrical control of modulation depth," *Applied Physics Letters,* vol. 97, 051103, 2010.

[28] S. A. Zolotovskaya, M. Butkus, R. Häring, A. Able, W. Kaender, I. L. Krestnikov, D. A. Livshits, and E. U. Rafailov, "p-i-n junction quantum dot saturable absorber mirror: electrical control of ultrafast dynamics," *Optics Express,* vol. 20, pp. 9038-9045, 2012.

[29] A. Ashkin, J. M. Dziedzic, and T. Yamane, "Optical trapping and manipulation of single cells using infrared-laser beams," *Nature,* vol. 330, pp. 769-771, 1987.

[30] B. Agate, C. T. A. Brown, W. Sibbett, and K. Dholakia, "Femtosecond optical tweezers for in-situ control of two-photon fluorescence," *Optics Express,* vol. 12, pp. 3011-3017, 2004.

[31] K. Konig, I. Riemann, P. Fischer, and K. H. Halbhuber, "Intracellular nanosurgery with near infrared femtosecond laser pulses," *Cellular and Molecular Biology,* vol. 45, pp. 195-201, 1999.

[32] A. Isomaki, A. Vainionpaa, S. Suomalainen, and O. G. Okhotnikov, "Self-starting mode-locked fiber laser using biased semiconductor absorber mirror," in *Lasers and Applications*. vol. 5958, K. M. Abramski, A. Lapucci, and E. F. Plinski, Eds., Bellingham: SPIE-Int. Soc. Optical Engineering, 2005.

[33] B. Stormont, E. U. Rafailov, I. G. Cormack, A. Mooradian, and W. Sibbett, "Extended-cavity surface-emitting diode laser as active mirror controlling modelocked Ti:sapphire laser," *Electronics Letters,* vol. 40, pp. 732-734, 2004.

[34] E. U. Rafailov, M. A. Cataluna, and W. Sibbett, "Mode-locked quantum-dot lasers," *Nature Photonics,* vol. 1, pp. 395-401, 2007.

[35] M. Y. A. Raja, S. R. J. Brueck, M. Osinski, C. F. Schaus, J. G. McInerney, T. M. Brennan, and B. E. Hammons, "Resonant periodic gain surface-emitting semiconductor-lasers," *IEEE Journal of Quantum Electronics,* vol. 25, pp. 1500-1512, 1989.

[36] U. Keller, "Semiconductor nonlinearities for solid-state laser modelocking and Q-switching," *Nonlinear Optics in Semiconductors II,* vol. 59, pp. 211-286, 1999.

[37] L. R. Brovelli, M. Lanker, U. Keller, K. W. Goossen, J. A. Walker, and J. E. Cunningham, "Antiresonant fabry-perot quantum-well modulator to actively

modelock and synchronize solid-state lasers," *Electronics Letters,* vol. 31, pp. 381-382, 1995.

[38] M. Hoffmann, O. D. Sieber, V. J. Wittwer, I. L. Krestnikov, D. A. Livshits, Y. Barbarin, T. Sudmeyer, and U. Keller, "Femtosecond high-power quantum dot vertical external cavity surface emitting laser," *Optics Express,* vol. 19, pp. 8108-8116, 2011.

[39] G. J. Spuhler, K. J. Weingarten, R. Grange, L. Krainer, M. Haiml, V. Liverini, M. Golling, S. Schon, and U. Keller, "Semiconductor saturable absorber mirror structures with low saturation fluence," *Applied Physics B-Lasers and Optics,* vol. 81, pp. 27-32, 2005.

[40] D. Kopf, G. Zhang, R. Fluck, M. Moser, and U. Keller, "All-in-one dispersion-compensating saturable absorber mirror for compact femtosecond laser sources," *Optics Letters,* vol. 21, pp. 486-488, 1996.

[41] D. Maas, A. R. Bellancourt, M. Hoffmann, B. Rudin, Y. Barbarin, M. Golling, T. Sudmeyer, and U. Keller, "Growth parameter optimization for fast quantum dot SESAMs," *Optics Express,* vol. 16, pp. 18646-18656, 2008.

[42] A. R. Bellancourt, Y. Barbarin, D. Maas, M. Shafiei, M. Hoffmann, M. Golling, T. Sudmeyer, and U. Keller, "Low saturation fluence antiresonant quantum dot SESAMs for MIXSEL integration," *Optics Express,* vol. 17, pp. 9704-9711, 2009.

[43] B. Rudin, V. J. Wittwer, D. Maas, M. Hoffmann, O. D. Sieber, Y. Barbarin, M. Golling, T. Sudmeyer, and U. Keller, "High-power MIXSEL: an integrated ultrafast semiconductor laser with 6.4 W average power," *Optics Express,* vol. 18, pp. 27582-27588, 2010.

[44] E. U. Rafailov, S. J. White, A. A. Lagatsky, A. Miller, W. Sibbett, D. A. Livshits, A. E. Zhukov, and V. M. Ustinov, "Fast quantum-dot saturable absorber for passive mode-locking of solid-state lasers," *IEEE Photonics Technology Letters*, vol. 16, pp. 2439-2441, 2004.

[45] A. A. Lagatsky, F. M. Bain, C. T. A. Brown, W. Sibbett, D. A. Livshits, G. Erbert, and E. U. Rafailov, "Low-loss quantum-dot-based saturable absorber for efficient femtosecond pulse generation," *Applied Physics Letters*, vol. 91, 231111, 2007.

[46] K. G. Wilcox, M. Butkus, I. Farrer, D. A. Ritchie, A. Tropper, and E. U. Rafailov, "Subpicosecond quantum dot saturable absorber mode-locked semiconductor disk laser," *Applied Physics Letters*, vol. 94, 251105, 2009.

[47] M. Hoffmann, Y. Barbarin, D. Maas, A. R. Bellancourt, M. Shafiei, M. Golling, T. Sudmeyer, U. Keller, I. L. Krestnikov, S. S. Mikhrin, A. R. Kovsh “All Quantum Dot Modelocked Vertical External Cavity Surface Emitting Laser”, *CLEO/QELS*, Munich, Germany, 2009.

5. Electrically pumped VECSELs

So far, the QD based SDLs reviewed all used an optical pumping scheme. However, for some applications, it is considered to be one of the largest drawbacks for this type of laser. For further miniaturization and cost reduction, a different approach is required. Direct electrical pumping is primarily associated with semiconductor laser diodes. However, as was already mentioned in the introduction chapter, so far it has not proved an efficient way to pump SDLs. The main reason for this are the difficulties of uniform large area pumping, which is the main factor when combining good beam quality and high output power. However, the research in this sector has also progressed. In this final experimental chapter, we will discuss the development of electrically pumped VECSELs and the issues related to them. Experimental results obtained in the testing of such devices in both the continuous wave and mode-locking regimes are presented.

5.1. Development of electrically pumped VECSELs

Part of these studies was devoted to experimental testing of EP-VECSELs. The development and testing of such devices based on both quantum wells (QWs) and ultimately on quantum dots (QDs) as a gain medium was also a part of the FAST-DOT project. However, to date, the devices with only QW gain medium were reported. Analogous optically pumped devices have already demonstrated high output powers with diffraction limited beam quality, which is enabled by the nature of optical pumping [1, 2]. However, the additional pump light source is one of the cumbersome parts of such devices and thus the development of direct electrically pumped VECSELs would significantly reduce the size and cost of the device. Meanwhile, the external cavity configuration still

allows such intracavity techniques as mode-locking, intracavity frequency conversion or spectral filtering to be exploited. EP-VECSELs potentially can be widely used with applications where Watt level CW output power or mode-locked sources with picosecond pulses are required.

Novalux Corporation reported cw wave EP-VECSELs with output powers of 1 W at 980 nm in 2003 [3]. Second harmonic generation and mode-locking were also demonstrated in these devices [4-7]. EP-VECSELs were also demonstrated at longer wavelengths, specifically at 1.55 µm and 2.3 µm [8, 9]. However, more research and development needs to be done in order to make these devices ready for market. As most of the work on these devices was concentrated around 1 µm spectral region, the discussions below concern InGaAs/GaAs material system and AlGaAs/GaAs based DBRs.

In most cases, the design of optically pumped SDLs includes the calculation of the correct distributed Bragg reflector (DBR) with required reflectivity and the active region with the desired number of QW or QD layers and their positioning, as was shown in the introduction chapter. Such parameters as power scaling can then be modified separately, i.e. by changing area of external pump spot on the device. Also, such devices avoid the need for doping and electrical contacts which makes the growth and fabrication processes simpler. In the case of EP-VECSELs the design is more complicated as the tradeoffs between optical and electrical parameters need to be made [10, 11].

A typical EP-VECSEL consists of a p-doped highly reflective bottom DBR. A number of quantum wells are inserted above it. The QWs are positioned at the antinodes of the optical standing wave to achieve the maximum gain. A partially reflective (typically 70-80 %) n-doped DBR is deposited above the QWs. This is used to reduce the operation threshold and

enhance the gain of the device as the typical gain of the VECSEL configuration is relatively low compared with edge emitters, due to the thin interaction path of light and active region. However, it must be noted that the existence of the second DBR creates a Fabry-Perot etalon effect thus limiting the gain bandwidth and the minimum achievable pulse duration in mode-locking operation. On top of the n-DBR goes n-doped current spreading layer. It is a relatively thick (up to 100 μm) material layer featuring high mobility for charge carriers and low optical absorption. The current spreading layer is used to uniformly confine the current in the active region in order to achieve the highest power in TEM_{00} mode. To pump the EP-VECSEL, two contacts on the bottom and the top of the device are used. The bottom contact has a disk form and it refines the mode size of the device as the holes in p-doped DBR have low mobility and are confined above the bottom contact. The top contact has a ring shape and defines the circular aperture through which the light is extracted. The top aperture is typically slightly larger (few tens of microns) than the bottom disk contact. The output aperture of the device is also often AR coated to reduce the reflection losses and to avoid the formation of second Fabry-Perot etalon in the subcavity. External dielectric mirrors are used to control the transverse mode. A schematic cross-section of the semiconductor part of the EP-VECSEL is shown in Fig. 5.75.

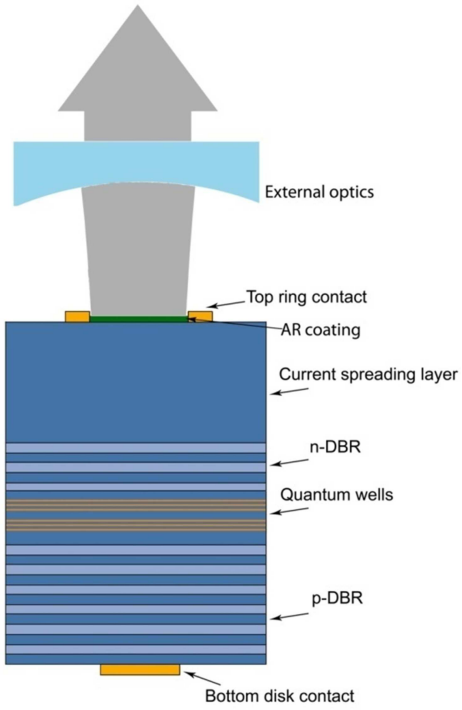

Fig. 5.75. A schematic cross section view of EP-VECSEL.

The overall design of the EP-VECSEL includes finding the tradeoffs between many competing parameters. For example, in the p-doped DBR, low hole mobility leads to high resistivity of the layers hence, increases Joule heating and degrades the device performance. If the number of quarter wave thick layers is reduced, the high reflectivity value is sacrificed. Also, in such a case heavier doping must be used which then increases the losses due to free carrier absorption. This is particularly the case when doping levels exceed 10^{18} cm^{-3}. Mole fraction grading at the layer interfaces were found as an optimal solution to reduce the resistivity [10]. The n-doped DBR is slightly less demanding, as it features lower resistivity and layers with or without grading can be grown. Typically, doping concentrations for the p- and n-doped DBR are in the order of 10^{18} cm^{-3}, and in the order of 10^{17} - $10^{18}cm^{-3}$ for the current spreading layer [12]. Typical bottom disk diameters lie in the

range of ~100 µm as it was shown that a sufficiently uniform carrier distribution is possible with such bottom contact sizes. A sample near-field electroluminescence profile measurements performed by project partners are shown in Fig.5.76 [11]. Data are shown for different bottom contact diameters. The measured profiles reflect the carriers' distribution across the emitter. It can be seen that with sizes above 100 µm, the intensity at the edges of the profile is increased, showing lower carrier concentration in the centre of the device.

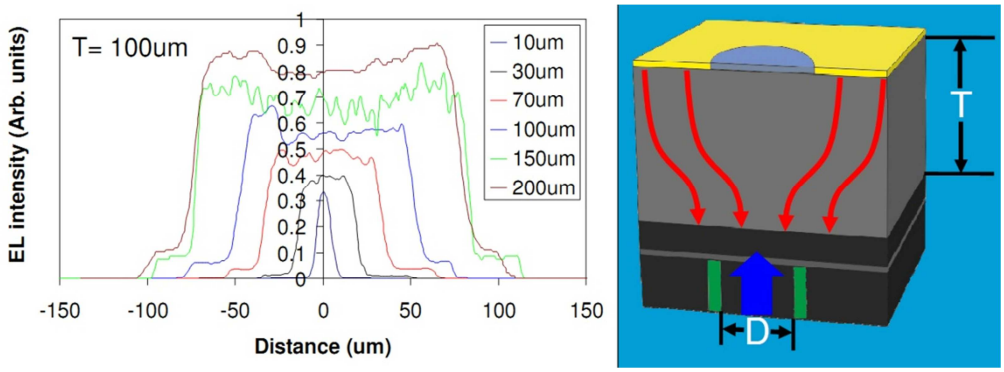

Fig.5.76. Near field elctroluminescence profile measurements of EP-VECSEL with different bottom contact diameters[11].

Although EP-VECSELs were already offered for the market [13], they are still mainly in the research stage. Also, to the best of our knowledge, no QD based EP-VECSELs were demonstrated at the time of this thesis. The incorporation of QDs would allow the extension of wavelength coverage to 1.1-1.3 µm. It could potentially lower the threshold of such devices and improve the overall efficiency. The main remaining issue is that QDs exhibit relatively low gain as compared with QW structures. This obstacle usually is overcome by growing a number of layers (few tens) of QDs in order to increase the net gain. This approach was successfully demonstrated in optically pumped SDLs [2]. However, if the multilayer approach is used, the active region becomes unsuitably thick for EP-VECSELs.

This results in problems with carrier transport uniformity. Secondly, QD lasers are much more sensitive to cavity losses. Thus, further optimizations of QDs and EP-VECSEL technology are required to produce QD based EP-VECSELs.

5.2. EP-VECSEL samples

EP-VECSEL samples from two partners were tested. A set of 18 EP-VECSEL devices with different designs was received from Philips. Experimental testing involved different designs of EP-VECSELs. Supplied samples had different sizes of the top aperture contact of 100, 140 and 150 µm. Also, they had three different thicknesses of the n-doped DBR with 9, 11 and 13 pairs of quarter wave-thick layers.

One EP-VECSEL device was also received from the University of Sheffield for experimental testing. The device was grown on the n-doped GaAs substrate in a reverse order. It had 32 pairs of graded GaAs/$Al_{0.8}Ga_{0.2}As$ p-doped DBR. The active region consisted of 6 quantum wells spaced by $Ga_{0.9}AsP_{0.1}$ layers. N-DBR had 12 pairs of graded GaAs/$Al_{0.8}Ga_{0.2}As$. The device had a 100 µm diameter ring contact. A schematic drawing of the device is shown in Fig. 5.77. All samples were designed for 980 nm emission.

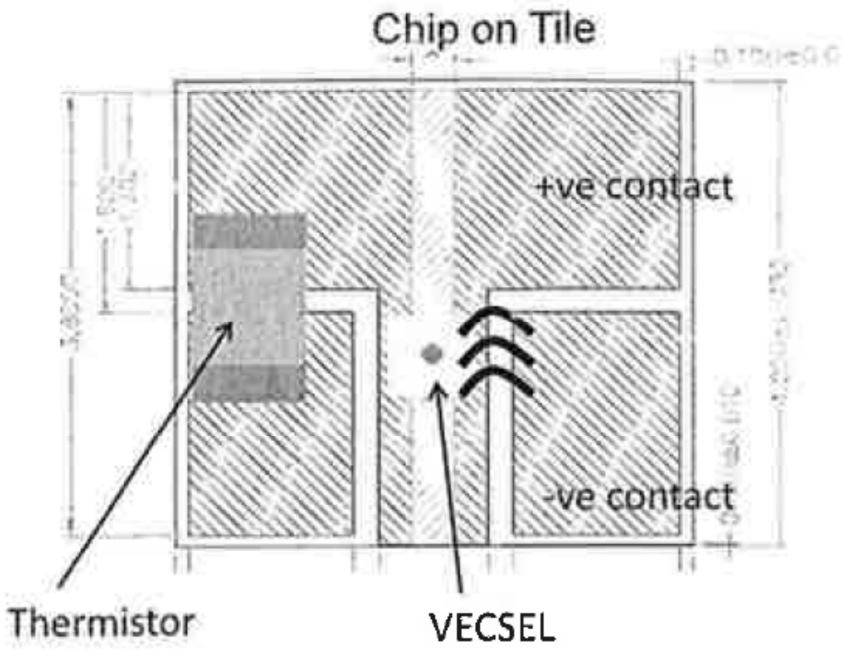

Fig. 5.77. Schematic drawing of EP-VECSEL sample (top view).

5.3. Experimental testing of EP-VECSEL samples

The EP-VECSEL samples were tested in both CW and mode-locked operation. Experimental conditions and the performance of the devices will be described in the subsequent sections.

5.3.1. Testing in CW regime

The devices were first tested in the CW regime to observe the maximum achievable output power. For these experiments, devices were attached to larger copper heatsinks. The temperature of the heatsink was thermoelectrically controlled. A straight external cavity was formed by using RoC = -25mm output couplers with 1%, 2%, 4% and 10%

transmissions. The optimum transmission was found for each sample. The devices from the first set that demonstrated the best performance are listed in the table below.

Sample No.	**Aperture diam., µm**	**Number of pairs in n-DBR**	**Maximum output power (mW)**	**Output coupler used**	**Temperature (^{0}C)**	**Pump current (mA)**
95_44	100	13	60	10%	15	~430
50_44	100	13	52	10%	15	~370
53_14	100	9	40	4%	15	~370
47_14	100	9	35	4%	15	~320

Table 5.9. The list of best performing EP-VECSELs.

A maximum output power up to 60 mW was achieved from the device with 100 µm aperture and a 13-pair n-DBR. In general, devices with 100 µm aperture demonstrated the best performance, which suggests that this is the optimum size of ring contact aperture for such devices. Current-light performances for a few of these devices are shown in Fig. 5.78 and Fig. 5.79. The devices were pumped with a current up to 400 mA until they reached thermal rollover. The threshold current for the devices were around 60 mA. The data shown were measured with a heatsink temperature of 15 ^{o}C. The output spectrum of the samples was centered around 980 nm. A sample spectrum of 95_44 sample is shown in Fig. 5.80.

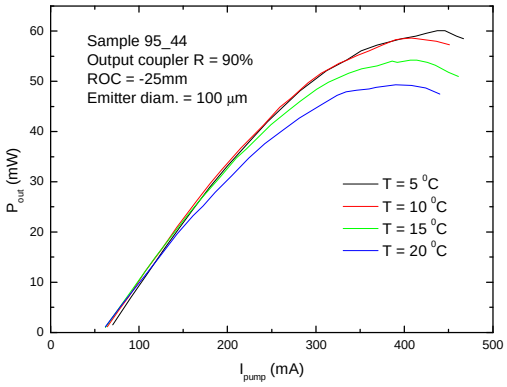

Fig. 5.78. Current-light characteristics at different temperatures in cw for the 95_44 device from Philips.

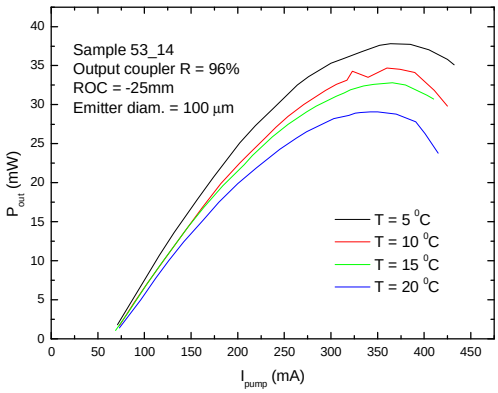

Fig. 5.79. Current-light characteristics at different temperatures in cw for the 53_14 device from Philips.

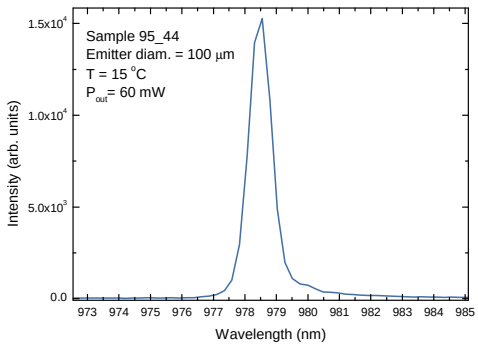

Fig. 5.80. Optical spectrum of the 95_44 EP-VECSEL sample.

For the sample from the University of Sheffield, 10% output coupling was used and it was tested in the same cavity configuration as with the previous samples. Fig. 5.81 shows the current-light characteristics of the device and the optical spectra at different temperatures are shown in Fig. 5.82. An output power up to 45 mW in the cw regime was achieved. The device operated at 980 nm at room temperature.

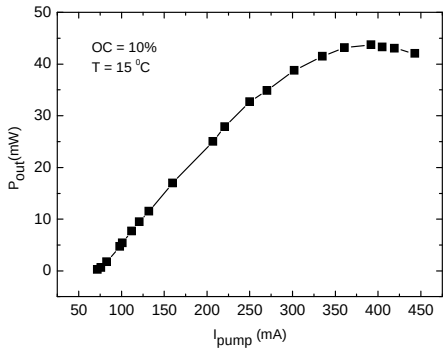

Fig. 5.81. Current-light characteristic in the CW regime from the device manufactured in Sheffield.

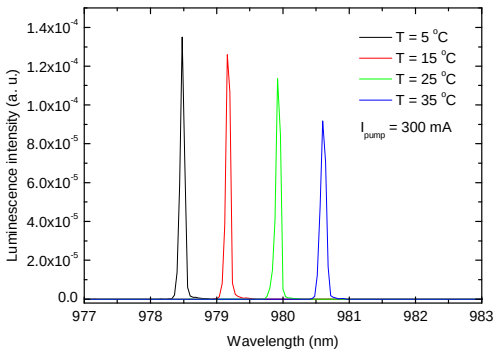

Fig. 5.82. Optical spectra of EP-VECSELs at different heatsink temperatures.

5.3.2. Mode-locking experiments

The samples were also tested in the mode-locked regime. Slightly different experimental configurations were used for different samples. From the set of Philips manufactured samples, 95_44 was used for the experiments. A straight cavity configuration was employed for the mode-locking test. The luminescence from the sample was focused on the SESAM output coupler using a 10X aspherical lens as shown in Fig. 5.83. A commercially available SESAM working as a partly reflecting mirror was used for mode-locking. The SESAM was designed for λ = 980 nm and had a saturated transmission of ~6%.

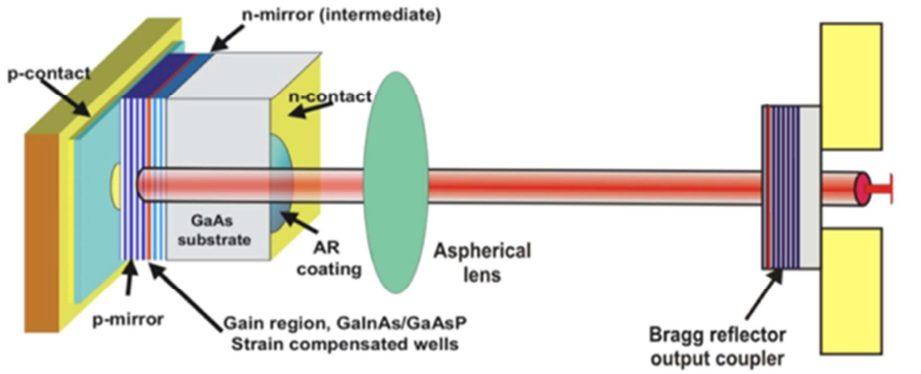

Fig. 5.83. A schematic drawing of a cavity to mode-lock EP-VECSEL from Philips.

Mode-locking was observed using a fast photodetector and radio frequency spectrum analyzer. In this configuration, pulsed operation with a repetition rate of 1.9 GHz was observed. Fig. 5.84 shows the recorded RF spectrum plot and several harmonics with resolution bandwidth of 10 MHz. The average output power was 8 mW at room temperature. A fast oscilloscope was used to measure the pulse duration. For this, the light was split by a beamsplitter and two separate photodetectors with 15 ps pulse response time were used for trigger and signal channels in the oscilloscope. The measured pulse duration was 270 ps. The trace of the measured pulses is shown in Fig. 5.85.

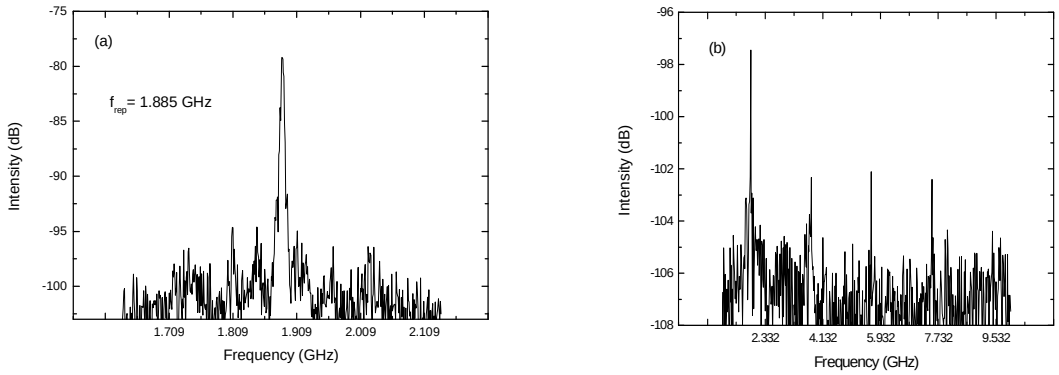

Fig. 5.84. Single line RF spectrum of the mode-locked device is shown in (a), and (b) shows the same spectrum with a few harmonics.

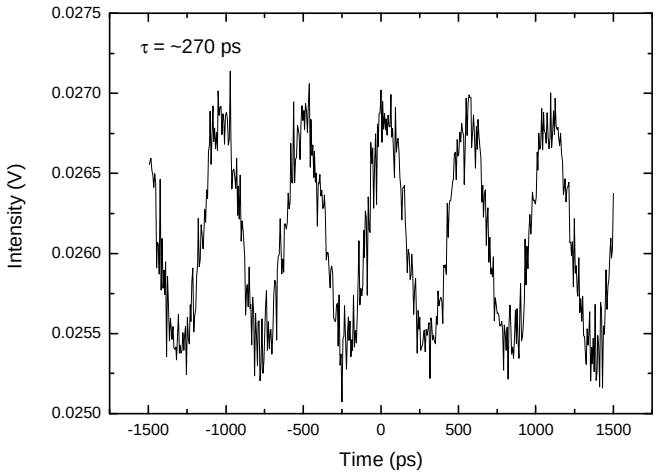

Fig. 5.85. Trace of the pulsed output from a mode-locked EP-VECSEL sample 94_44 showing pulse duration of 270 ps.

Later, mode-locking experiments with a Sheffield manufactured EP-VECSEL sample were performed. This time, the experiment was done in a Z-shape cavity configuration. A schematic of such a cavity is shown in Fig. 5.86. An RoC = -50 mm mirror was used as the output coupler, while an RoC = -25mm folding mirror was used to focus the light onto the SESAM. For these experiments, a QD based SESAM was used. It was designed for 980 nm wavelength and featured 2% modulation depth.

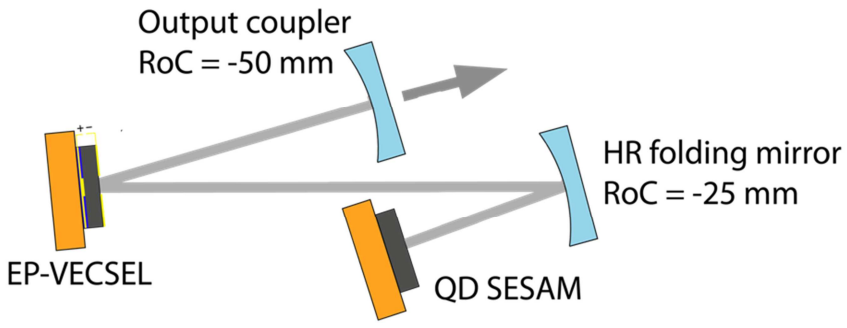

Fig. 5.86. A schematic drawing of the Z-shape cavity configuration for a mode-locked EP-VECSEL.

The signal from the mode-locked device was observed using a fast photodiode and a radio frequency spectrum analyzer. Mode-locking was first observed at ~1.49 GHz with an output power of 1mW while 330 mA current was applied and 2% output coupling was used. An output power up to 8 mW was achieved with 10% output coupling, however, mode-locking was unstable at this point. The experiment was performed while keeping the heatsink temperature at T = 15^{o}C. Fig. 5.87shows an RF spectrum line with the optical spectrum shown in the inset. The pulse width of the device could not be measured as the output power of the device was too low, or mode-locking was too unstable.

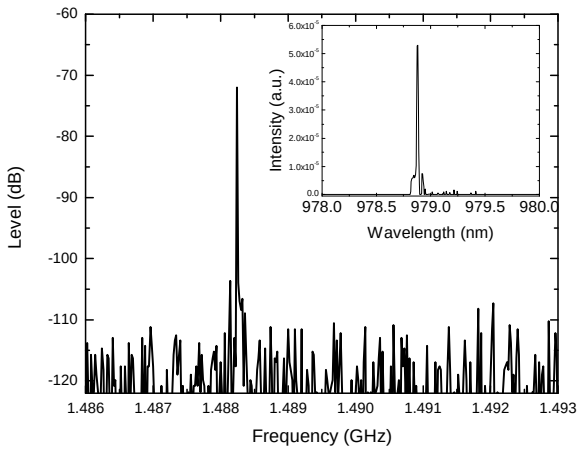

Fig. 5.87. RF spectrum indicating pulsed operation of the device. The optical spectrum is shown in the inset.

5.4. Chapter conclusions

To sum up, a set of EP-VECSELs was received from project partners for experimental testing. The devices were first tested in the cw configuration. The highest output powers achieved from such devices were up to 60 mW and devices with 100 µm diameter ring aperture demonstrated the best performance. Devices were then tested in mode-locking experiments. Pulsed operation was observed from the devices. The measurements indicated

270 ps pulse width with 8mW average output power at 1.9 GHz repetition rate. The underlying reason of such long pulses is still not clear. All devices operated at 980 nm.

Although devices were demonstrated to operate, their performance still falls far behind the levels demonstrated by previous reports [3]. Thus a lot of effort is put into design and growth in order to improve the performance of such devices, to make them more attractive for a wide range of applications. A high output power (up to 1 W) in fundamental transverse mode and single frequency is necessary to achieve. This would also allow a much better performance in mode-locked operation. The realization of such devices would be successful as a compact short pulse VECSEL could still provide comparably high power with good beam quality, but with direct electrical pumping and wafer scale manufacturability.

Additional efforts are also needed to achieve operation of QD based EP-VECSELs which would allow the exploration of their unique properties in such laser configurations. In order to achieve such a milestone, two main parameters should be improved. The gain of the QDs should be increased and the growth and fabrication of extremely low optical loss devices should be achieved.

References

[1] J. Chilla, Q. Z. Shu, H. L. Zhou, E. Weiss, M. Reed, and L. Spinelli, "Recent advances in optically pumped semiconductor lasers - art. no. 645109," in *Solid State Lasers XVI: Technology and Devices*. vol. 6451, H. J. Hoffman, R. K. Shori, and N. Hodgson, Eds., Bellingham: SPIE-Int. Soc. Optical Engineering, pp. 45109-45109, 2007.

[2] M. Butkus, K. G. Wilcox, J. Rautiainen, O. G. Okhotnikov, S. S. Mikhrin, I. L. Krestnikov, A. R. Kovsh, M. Hoffmann, T. Sudmeyer, U. Keller, and E. U. Rafailov, "High-power quantum-dot-based semiconductor disk laser," *Optics Letters*, vol. 34, pp. 1672-1674, 2009.

[3] J. G. McInerney, A. Mooradian, A. Lewis, A. Shchegrov, E. M. Strzelecka, D. Lee, J. P. Watson, A. Liebman, G. P. Carey, B. D. Cantos, W. R. Hitchens, and D. Heald, "High-power surface emitting semiconductor laser with extended vertical compound cavity," *Electronics Letters*, vol. 39, pp. 523-525, 2003.

[4] G. McInerney, A. Mooradian, A. Lewis, A. V. Shchegrov, E. M. Strzelecka, D. Lee, J. P. Watson, M. Liebman, G. P. Carey, A. Umbrasas, C. Amsden, B. D. Cantos, W. R. Hitchens, D. Heald, and V. V. Doan, "Novel 980 nm and 490 nm light sources using vertical cavity lasers with extended coupled cavities," in *Vertical-Cavity Surface-Emitting Lasers VII*. vol. 4994, C. Lei and S. P. Kilcoyne, Eds., Bellingham: SPIE-Int. Soc. Optical Engineering, pp. 21-31, 2003.

[5] Q. A. Zhang, K. Jasim, A. V. Nurmikko, A. Mooradian, G. Carey, W. Ha, and E. Ippen, "Operation of a passively mode-locked extended-cavity surface-emitting diode laser in multi-GHz regime," *IEEE Photonics Technology Letters*, vol. 16, pp. 885-887, 2004.

[6] K. Jasim, Q. Zhang, A. V. Nurmikko, E. Ippen, A. Mooradian, G. Carey, and W. Ha, "Picosecond pulse generation from passively modelocked vertical cavity diode laser at up to 15 GHz pulse repetition rate," *Electronics Letters,* vol. 40, pp. 34-36, 2004.

[7] E. U. Rafailov, W. Sibbett, A. Mooradian, J. G. McInerney, H. Karlsson, S. Wang, and F. Laurell, "Efficient frequency doubling of a vertical-extended-cavity surface-emitting laser diode by use of a periodically poled KTP crystal," *Optics Letters,* vol. 28, pp. 2091-2093, 2003.

[8] A. Bousseksou, S. Bouchoule, M. El Kurdi, M. Strassner, I. Sagnes, P. Crozat, and J. Jacquet, "Fabrication and characterization of 1.55 µm single transverse mode large diameter electrically pumped VECSEL," *Optical and Quantum Electronics,* vol. 38, pp. 1269-1278, 2006.

[9] A. Harkonen, A. Bachmann, S. Arafin, K. Haring, J. Viheriala, M. Guina, and M.-C. Amann, "2.34 µm electrically-pumped VECSEL with buried tunnel junction," in *Semiconductor Lasers and Laser Dynamics IV*. vol. 7720, R. Panajotov, Ed., 2010.

[10] P. Kreuter, B. Witzigmann, D. Maas, Y. Barbarin, T. Sudmeyer, and U. Keller, "On the design of electrically pumped vertical-external-cavity surface-emitting lasers," *Applied Physics B-Lasers and Optics*, vol. 91, pp. 257-264, 2008.

[11] D. T. D. Childs, J. R. Orchard, D. Williams, L. C. Lin, B. J. Stevens, J. S. Roberts, R. A. Hogg, “Trade-offs in the realization of electrically pumped vertical external cavity surface emitting lasers,” IEEE International Semiconductor Laser Conference, Kyoto, Japan, 2010.

[12] J. R. Orchard, D. T. D. Childs, L. C. Lin, B. J. Stevens, D. M. Williams, and R. A. Hogg, "Design rules and characterisation of electrically pumped vertical external

cavity surface emitting lasers," *Japanese Journal of Applied Physics*, vol. 50, 04DG05, 2011.

[13] Novalux. Inc, "Manufacturable high-power, single-mode surface emitting lasers," *III-Vs Review*, vol. 14, pp. 38-40, 2001.

6. Conclusions and future work

The last chapter of the thesis gives a short summary of the presented work and discusses the relevant future work in the area.

The work presented in the thesis was focussed on the development and testing of semiconductor disk lasers based on novel quantum dot structures. The QDs were based on InGaAs/GaAs semiconductor materials formed using the Stranski-Krastanow growth method. The use of a QD material allowed extension of the spectral coverage by the SDL into 1-1.3 µm region [1]. Devices with emission wavelengths of 1040, 1180 and 1260 nm were developed in our work. QD based SDLs were tested in various configurations. Experiments were done to test the maximum achievable output power in the continuous wave regime. Laser intracavity techniques like second harmonic generation and wavelength tuneability were performed. Finally, mode-locked SDL using a QD based saturable absorber was demonstrated. Part of the work was also devoted to exploring an alternative electrical pumping scheme for quantum well based SDLs.

Power scaling up to 6 W was achieved for 1040 nm, 2.25 W for 1180 nm and 1.6 W for 1260 nm devices. Excited state transition in QDs was shown to be more efficient for high power QD SDLs as compared with ground state transition. New spectral regions were covered by QD SDLs using frequency doubling into the visible region with green, orange and red light emission with output powers of 2 W, 2.5 W and 0.34 W respectively. The broad gain bandwidth of the quantum dot material was explored and wavelength tuneability up to 60 nm around 1040 nm, 69 nm around 1180 nm, and 25 nm around 1260 nm was demonstrated.

A QD based saturable absorber was used to mode-lock the quantum well SDL, resulting in the first such type of laser with sub-picosecond pulse durations. Pulses with duration of 870 fs at a repetition rate of 896 MHz and wavelength of 1028.5 nm were demonstrated. Pulses were 1.14 times Fourier limited and an average output power of 46 mW was achieved.

Finally, quantum well based VECSELs with electrical pumping schemes were tested. The devices were first tested in the cw configuration. Highest output powers up to 60 mW were achieved from such devices. Devices were then tested in mode-locking experiments. Pulsed operation was observed and the measurements indicated 270 ps width pulses with 8 mW average output power at 1.9 GHz repetition rate. All devices operated at 980 nm.

The results presented in this thesis contributed to the development of QD SDLs. However, this area was under intense scientific and commercial interest for only the last five years. Thus, it is still in an early development state and more efforts are needed to fully explore the advantages of QD based materials. This will include wider research concerning the thermal sensitivity and operational stability of QD based lasers. Deeper knowledge of these properties would allow more precise design of the devices resulting in more efficient operation.

Additional work is needed to be done to explore the wide gain bandwidth of QD materials. Extensive experiments will be performed to explore laser tuneability and mode-locking. Potentially, tuneable QD SDLs with a spectral range up to 100 nm around 1 μm emission wavelength should be possible after solving the issue of limited DBR stop bandwidth. Also, efforts will be made towards tuneable laser sources in pulsed operation or in the visible light range through second harmonic generation. This would enable a powerful tool for spectroscopic applications [2].

Also, additional work is required for the development of mode-locked SDLs. High performance all QD based mode-locked SDLs have already been demonstrated [3]. However, devices working at room temperature need to be developed. Also, QD based SESAMs will be developed further as they have already proven to be a powerful tool for mode-locking various types of lasers [4, 5]. QD SDL mode-locking tests using p-n junction SESAMs also are part of the on-going work.

A lot of efforts will be devoted to further development of electrically pumped SDLs. This should result in high output power (few hundred mW to W level), low threshold or mode-locked compact devices featuring the benefits of SDL configuration [6].

Finally, the applications of SDLs will be explored. Part of the on-going work is devoted for THz frequency generation using intracavity difference frequency generation [7].

References

[1] M. Butkus, J. Rautiainen, O. G. Okhotnikov, C. J. Hamilton, G. P. A. Malcolm, S. S. Mikhrin, I. L. Krestnikov, D. A. Livshits, and E. U. Rafailov, "Quantum dot based semiconductor disk lasers for 1-1.3 um," *IEEE Journal of Quantum Electronics*, vol. 17, pp. 1763-1771, 2011.

[2] R. Aviles-Espinosa, G. Filippidis, C. Hamilton, G. Malcolm, K. J. Weingarten, T. Sudmeyer, Y. Barbarin, U. Keller, S. I. C. O. Santos, D. Artigas, and P. Loza-Alvarez, "Compact ultrafast semiconductor disk laser: targeting GFP based nonlinear applications in living organisms," *Biomedical optics express*, vol. 2, pp. 739-47, 2011.

[3] M. Hoffmann, O. D. Sieber, V. J. Wittwer, I. L. Krestnikov, D. A. Livshits, Y. Barbarin, T. Sudmeyer, and U. Keller, "Femtosecond high-power quantum dot vertical external cavity surface emitting laser," *Optics Express*, vol. 19, pp. 8108-8116, 2011.

[4] A. A. Lagatsky, C. G. Leburn, C. T. A. Brown, W. Sibbett, S. A. Zolotovskaya, and E. U. Rafailov, "Ultrashort-pulse lasers passively mode locked by quantum-dot-based saturable absorbers," *Progress in Quantum Electronics*, vol. 34, pp. 1-45, 2010.

[5] E. U. Rafailov, S. A. Zolotovskaya, and M. Butkus, "QD-based saturable absorbers for utrafast lasers," *Vertical External Cavity Surface Emitting Lasers*. vol. 7919, U. Keller, Ed., Bellingham: SPIE-Int. Soc. Optical Engineering, 2011.

[6] J. R. Orchard, D. T. Childs, L. C. Lin, B. J. Stevens, D. M. Williams, R. A. Hogg, M. Butkus, E. U. Rafailov, S. Gronenborn, J. Kolb, H. Moench, M. Miller, M. Hoffmann, Y. Barbarin, W. P. Pallmann, D. H. Maas, P. Kreuter, B. Witzigmann, M. C. Golling, T.

Sudmeyer, and U. Keller, "Development of EP-VECSELs for mode locking applications," *SPIE Photonics West*, San Francisco, US, pp. 8242-11, 2012.

[7] M. Scheller, J. M. Yarborough, J. V. Moloney, M. Fallahi, M. Koch, and S. W. Koch, "Room temperature continuous wave milliwatt terahertz source," *Optics Express*, vol. 18, pp. 27112-27117, 2010.